ISWEC: a Gyroscopic Wave Energy Converter

POLITECNICO DI TORINO

SCUOLA DI DOTTORATO
Dottorato in Ingegneria Meccanica – XXII ciclo

Tesi di Dottorato

ISWEC: a Gyroscopic Wave Energy Converter

Giovanni Bracco
matr. 144039

Tutore
Prof. Massimo Sorli

Coordinatore del corso di dottorato
Prof. Graziano Curti

May 2010

Summary

ISWEC (Inertial Sea Wave Energy Converter) is a Wave Energy Converter transforming the wave-induced rocking motion of a buoy into electrical power by means of the gyroscopic effects produced from a spinning flywheel carried inside the buoy.

One of the main advantages of ISWEC with respect to most of the existing converters is that externally it is composed only of a floating body without moving parts working into sea water or spray, thus achieving a better reliability and lower maintenance costs.

In this Thesis firstly the converter dynamics is analyzed in order to obtain a mathematical model of its performances. A design procedure has been obtained thanks to the linearization of the model and a small scale prototype with rated power 2.2 W has been built in order to work in the wave tank present at the Institute for Energy Systems of the University of Edinburgh. Before the tank tests, the prototype has been tested on a wave simulation rig built at the Department of Mechanics at Politecnico di Torino in order to validate the numerical model and the prototype performances. In July 2009 the prototype has been tested at the wave tank in Edinburgh: it produced the rated power but only if equipped with a wider float. Back in Torino an improved float has been designed, built and tested in the flume present at the Department of Hydraulics. The tests highlighted the need of a float with considerable dimensions, but even that the rated power can be achieved with a smaller angular velocity of the gyro: a good news making the device cheaper than expected.

In the final part of the Thesis a bigger device with rated power 213 W has been designed thanks to the experimental results obtained both in the tank and in the flume. This prototype is going to be tested in December 2010 at the wave tank of the University Federico II in Naples.

In the ninth chapter the expected performances of a full scale ISWEC are compared with one of the most famous WECs, the Pelamis. The comparison shows that so far the two systems have almost the same performances.

In order to assess the economics of the ISWEC device, in the tenth chapter an economical analysis has been carried out to understand possible market scenarios. A market for both a grid connected and for a stand-alone system were evaluated.

A company able to exploit those markets was designed in order to be as lean and quick as possible. Eventually an estimate of the cost of energy for a 5 kW rated power ISWEC was given at 0.34 €/kWh with a device life of 20 years.

Contents

List of Tables

List of Figures

Chapter 1

Introduction

Wave Power has been investigated in Europe since the Seventies. In 1974 at the University of Edinburgh Prof. Stephen Salter proposed one of the first Wave Energy Converters (WEC) he called Duck [1]. Since then a lot of devices have been proposed and a few of them have been commercialized. In this chapter a brief introduction on the wave energy resource is provided and some of the most famous WECs are described.

1.1 The wave energy resource

Sea waves are generated by wind passing over stretches of water. The mechanics of waves creation is complex and not completely understood, however it can be summarized in three main steps [2].

1. The wind exerts a tangential stress on the water surface inducing and increasing the formation of waves

2. Turbulent air flow creates pressure and shear stresses fluctuations that, if phased with the existing waves, generates more waves

3. When the waves have reached a certain size, the wind exerts a stronger force on the up-wind face of the wave and make it grow further.

Wave energy is generated from wind energy that originally is created from the sun, so sea waves can be considered a storage of solar energy. Solar power density is of the order of 100 W/m^2 (daily average) [3] and can be transformed eventually in wave power densities of over 100 kW per metre of crest length. Waves are a very efficient way to transport energy: *storm waves* are generated locally and can travel long distances producing *swell waves*. The size of a wave is determined by three

factors: wind speed, duration and the *fetch*, the distance over which the wind blows transferring energy to the water.

A regular wave can be described by its height H, period T and wavelength λ. The wave height H is the vertical distance between crest and through, the wavelength λ is the horizontal distance along the wave direction between two crests and the wave period T is the time needed from two successive crests to pass through a fixed point. The shape of a regular wave is sinusoidal and it is described from the (1.1) where x is the coordinate orientated along the wave direction and z is the wave elevation with respect to the still water level. The angular frequency $\omega = 2\pi/T$ and the wave number $K = 2\pi/\lambda$ define the periodicity in time and space. The crest velocity v is evaluable by dividing the wavelength λ over the wave period T.

$$z(x,t) = \frac{H}{2}\sin(\omega t - Kx) \tag{1.1}$$

According to the Linear Wave Theory [4], [5], [6] and [7], the power density of a sinusoidal wave is evaluable by the (1.2). If P_D is expressed in kW per metre of crest length it is approximately equal to the square of the wave height multiplied by the wave period.

$$P_D = \frac{\rho g^2}{32\pi} H^2 T \frac{W}{m} \simeq H^2 T \frac{kW}{m} \tag{1.2}$$

In the (1.2) ρ is the water density and g is the acceleration due to gravity.

The water depth influences the wave main parameters. A wave is considered traveling in deep water conditions if the water depth d is greater than half the wavelength λ. On the other hand the wave travels in shallow water when the ratio $d/\lambda < 1/20$. Between the two cases, the wave travels in intermediate water. Table 1.1 shows the wave main relations with respect to the water depth.

Wave property	Shallow Water $d/\lambda < \frac{1}{20}$	Intermediate Water $\frac{1}{2} < d/\lambda < \frac{1}{20}$	Deep Water $d/\lambda > \frac{1}{2}$
Dispersion relation	$\omega^2 = gK^2 d$	$\omega^2 = gK \tanh Kd$	$\omega^2 = gK$
λ - T relation	$\lambda = T\sqrt{gd}$	$\lambda = \frac{g}{2\pi}T^2 \tanh\frac{2\pi d}{\lambda}$	$\lambda = \frac{g}{2\pi}T^2 \simeq 1.56T^2$
Group velocity	$c_g = c$	$c_g = \frac{1}{2}c(1 + \frac{2kd}{\sinh 2kd})$	$c_g = \frac{1}{2}c$

Table 1.1. Linear wave theory - small review.

The real sea waves are composed of many different regular components with different height, period and direction of traveling. In order to estimate the wave characteristics a wave measurement sensor is deployed to the sea. The sensor can be a wave rider buoy or a submersed system using SONAR and high precision pressure gages to detect the surface elevation.

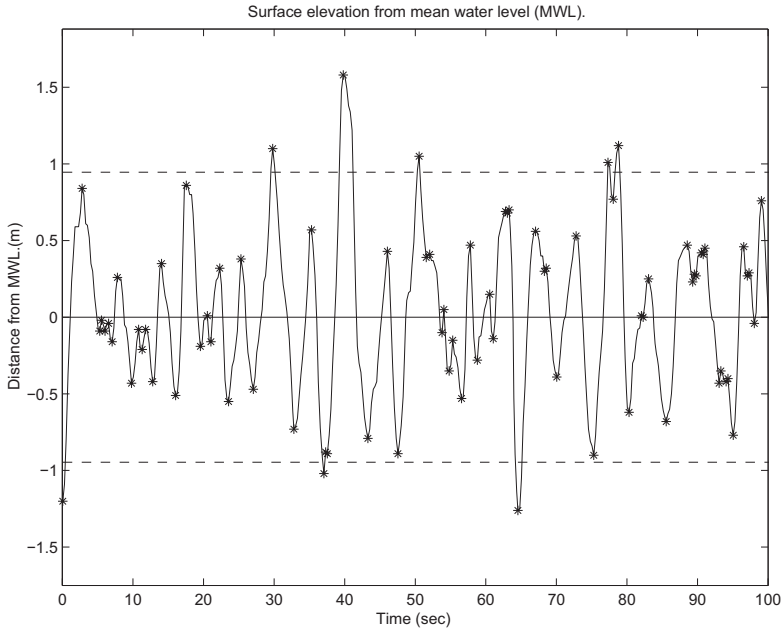

Figure 1.1. Wave height time record.

From the wave height time record (figure 1.1 shows a sample time record extracted from WAFO User Guide [8]) two parameters among the others can be extracted: the significant wave height H_s, evaluable as four time the rms value of the surface elevation respect to the mean water level, and the energy period T_e[1]. The wave power density can be evaluated as follows.

$$P_D = \frac{cH_s^2T_e}{16} \simeq \frac{H_s^2T_e}{2} \tag{1.3}$$

The wave power density is very variable around the world and its highest values are detected in the Oceans between the latitudes of $\sim 30°$ and $\sim 60°$ on both hemispheres (see figures 1.2 and 1.3 [9]). In Europe the West coasts of the U.K. and Ireland along with Norway and Portugal receive the highest power densities.

[1]For a real example of this process refer to section 7.6.2

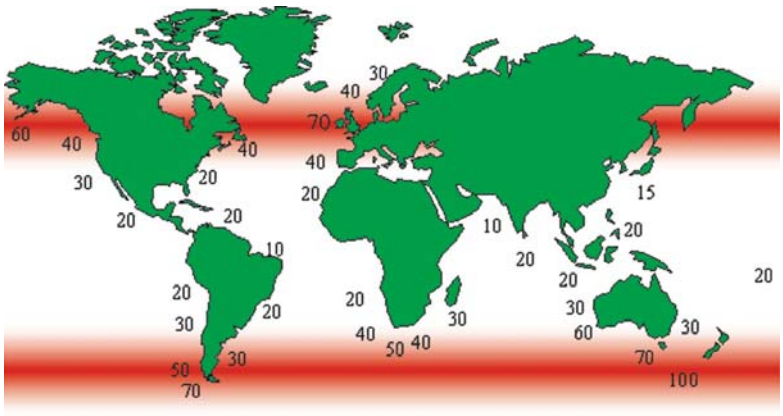

Figure 1.2. Wave power density World map (yearly average values in kW/m).

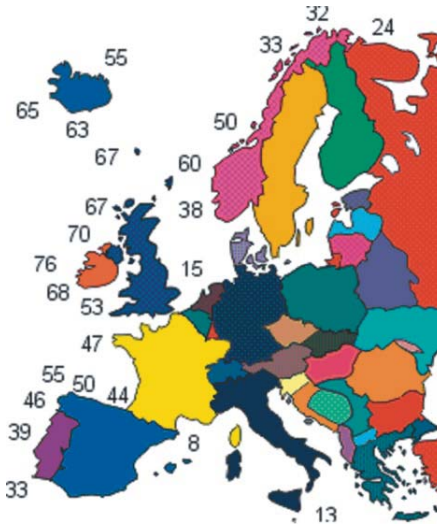

Figure 1.3. Wave power density Europe map (yearly average values in kW/m).

1.2 Wave Energy Converters

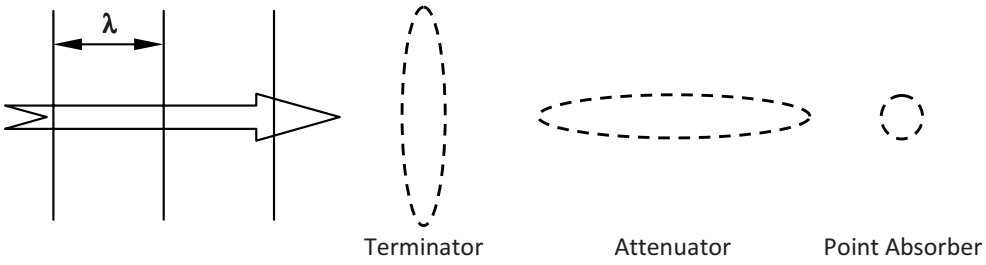

Figure 1.4. One of the WECs classification scheme.

Wave Energy Converters can be classified in function of their dimensions and orientation respect to the incoming wave [10]. A *Point Absorber* is a device with horizontal dimensions negligible with respect to the wavelength. A Point Absorber can absorb power from a width much bigger than its physical width (the theoretical maximum absorption width is $\frac{\lambda}{2\pi}$). *Terminators* and *Attenuators* have definite dimensions with respect to the wave and usually a dominant horizontal dimension. Terminators physically intercept the incoming wave whereas attenuators extract energy as the wave passes through their length.

WECs can be classified also respect to their location:

- fixed to the seabed (generally in shallow water)
- floating offshore (in deep water)
- tethered in intermediate water

During the last four decades several WECs have been developed. In the next pages a brief review of some of the most famous devices is given [9], [11] and [12].

1.2.1 Oscillating Water Column

The Oscillating Water Column (OWC) is a device composed mainly of an air chamber and a turbine. The air chamber is partially submerged and open below the waterline thus the heave motion of the sea surface forces the air contained in the chamber through the turbine. Due to the oscillatory nature of waves, the air is pushed or pulled through the turbine, resulting in an alternate flow. In order to use this alternate flow, the Wells turbine is used because of its capacity to rotate continuously in one direction in spite of the direction of the air flow. It uses symmetrical

airfoils with their planes of symmetry in the plane of rotation and perpendicular to the air stream and for this reason the turbine works with a lower efficiency with respect to 'normal' turbines using asymmetric airfoils.

The OWC air chamber can be integrated in a breakwater in shoreline devices, as shown in figure 1.5, or it can be included in a buoy floating in shallow water, like the OSPREY device [9]. The two main examples of OWC in Europe are the European Pilot Plant on the Pico Island in the Azores [13] [14] [15] and the Limpet in the United Kingdom [16]. The former is a 400 kW plant providing a part of the island's energy need whereas the latter is a 75 kW prototype constructed in the island of Islay in Scotland in 1991.

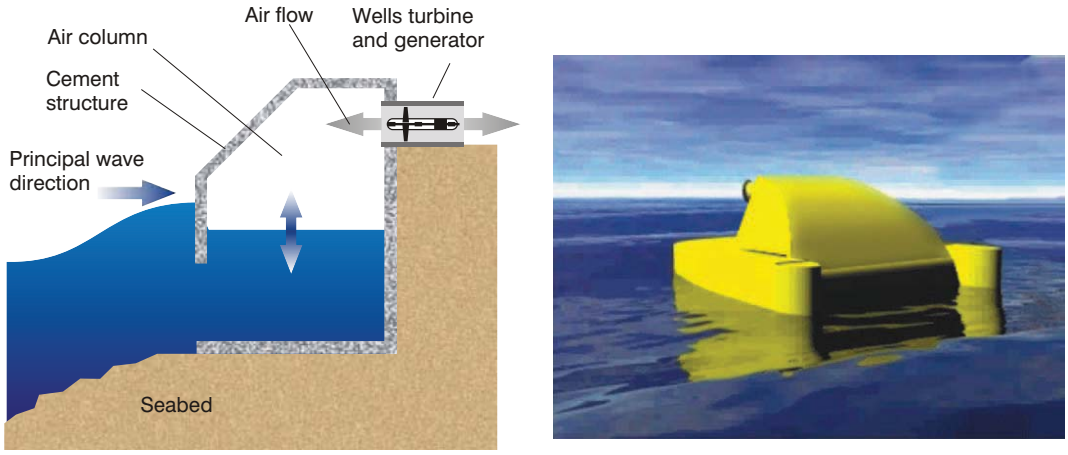

(a) Fixed OWC. (b) OSPREY.

Figure 1.5. OWC schemes.

1.2.2 Archimedes Wave Swing

The Archimedes Wave Swing (AWS) [17], [18] and [19] is a submerged air-filled piston expanding and contracting in response to wave pressure. Figure 1.6 [20] shows the external appearance and internal mechanism. The relative motion between the external moving part and the internal part fixed to the seabed is converted in electrical energy directly by a linear generator included in the water-tight air chamber. This converter is closed to a mass-spring-damper system and thus it can be put in resonance with the incoming wave to capture the maximum power.

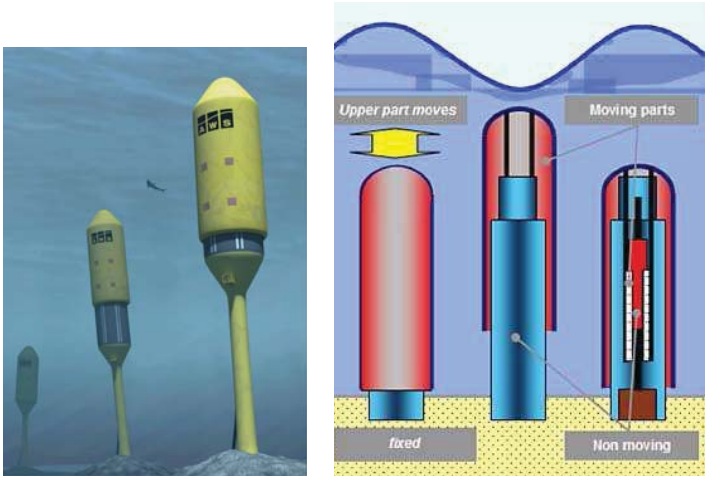

(a) Concept. (b) Cross section.

Figure 1.6. AWS concept and cross section.

1.2.3 Pelamis

Figure 1.7. A picture of the Pelamis WEC.

The Pelamis is a semi-submerged articulated structure composed of cylindrical sections hinged together by special joints [21], [22] and [23]. Each joint is equipped with hydraulic rams working as pumps and converting the relative motion between the sections in hydraulic power. The pressurized oil is sent to smoothing accumulators from which it is drained to supply an hydraulic motor coupled with an electric generator. The hydraulic circuit is equipped with an oil-to-water heat exchanger dumping the excess of power in the most powerful sea state and providing a thermal

load in the event of loss of the grid. The P-750 version is 150 m long composed of four sections and three joints. The rated power is 750 kW obtained when the wave power density is 55 kW/m [24]. Figures 1.7 and 1.8 [20] [24] show a prototype of the Pelamis WEC deployed to the ocean and the device working principle.

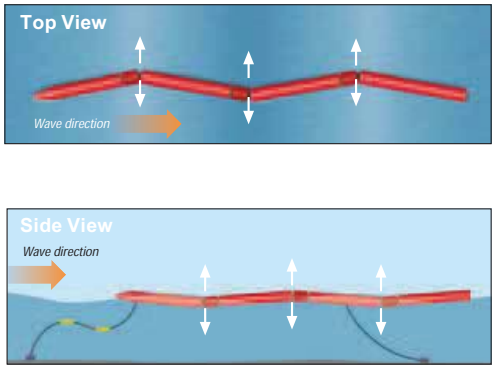

Figure 1.8. Pelamis working principle.

1.2.4 Duck

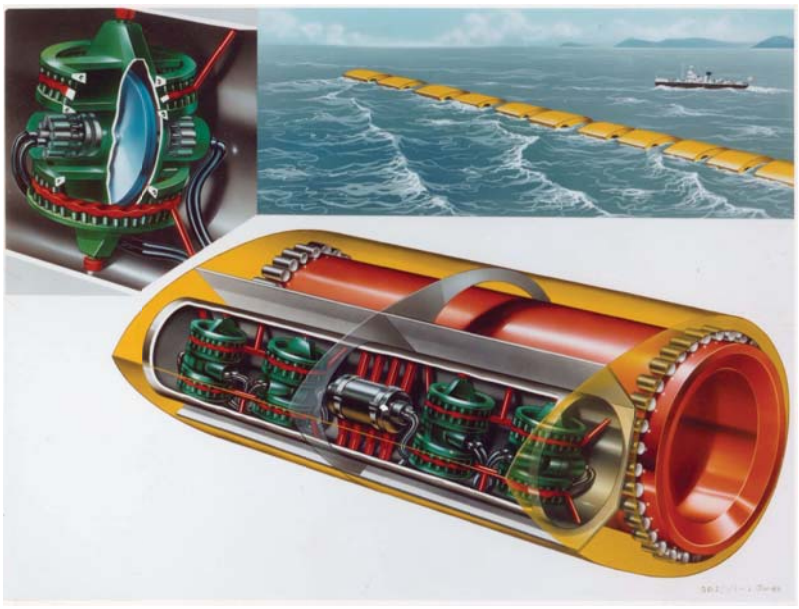

Figure 1.9. An artist impression of the Duck using gyros to extract energy (source: ETSU/University of Edinburgh).

The Duck was proposed from Salter in 1974 and it is one of the first WECs studied in Europe [1] [25] [26] [27]. The Duck is a nodding, asymmetric, slack-moored, floating, deep water, wave energy converter. Each Duck can rotate along a spine connecting all the devices. Since each Duck is positioned differently respect to the incoming waves, the resulting nodding motions are differently phased between each other obtaining an average null torque on the (torsionally stiff) spine. The spine should allow flexure to relieve the extreme stresses and to provide secondary means of power extraction too. The array of Ducks can be classified as a terminator.

As it can be seen in figure 1.9, in one of its proposed forms the duck uses a 'gyro canister' technology to transform the rocking motion into electrical power [28] [29] [30]. The canister contains four large gyroscopes acting in pairs: in each pair the two gyros precess in opposing direction in response to the Duck rocking motion and driving high-pressure oil ring-cam pumps. The high pressure oil is sent to high-speed hydraulic motors driving the electrical generators. The clever use of the gyro canister avoids the need for means of torque transmission between spine and Duck.

The concept of using the gyroscopic effects to transform the tilting motion of a floating body into electrical power is continued with some differences in the ISWEC.

Chapter 2

System dynamics

ISWEC (Inertial Sea Wave Energy Converter) is a gyroscopic system able to convert wave power into electrical power. In this chapter the device is supposed to work with bi-dimensional regular waves [31] [32] [33]. Starting from this assumption a mechanical analysis of the gyroscopic system and the expression of the extractable power is given.

2.1 ISWEC working principle

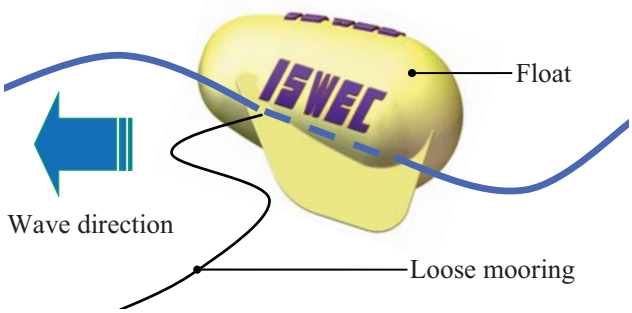

Figure 2.1. ISWEC: external appearance (concept).

As shown in figures 2.1 and 2.2, the ISWEC device is composed mainly of a floating body slack moored to the seabed. The waves tilt the buoy with a rocking motion that is transmitted to the gyroscopic system inside the buoy. The gyroscopic system is composed of a spinning flywheel carried on a platform allowing the flywheel to rotate along the y_1 axis. As the device works, the gyroscopic effects born from the combination of the flywheel spinning velocity $\dot{\varphi}$ and the wave induced rocking velocity $\dot{\delta}$ create a torque along the ε coordinate. Using this torque to drive an

electrical generator the extraction of energy from the system -and therefore from the waves- is possible.

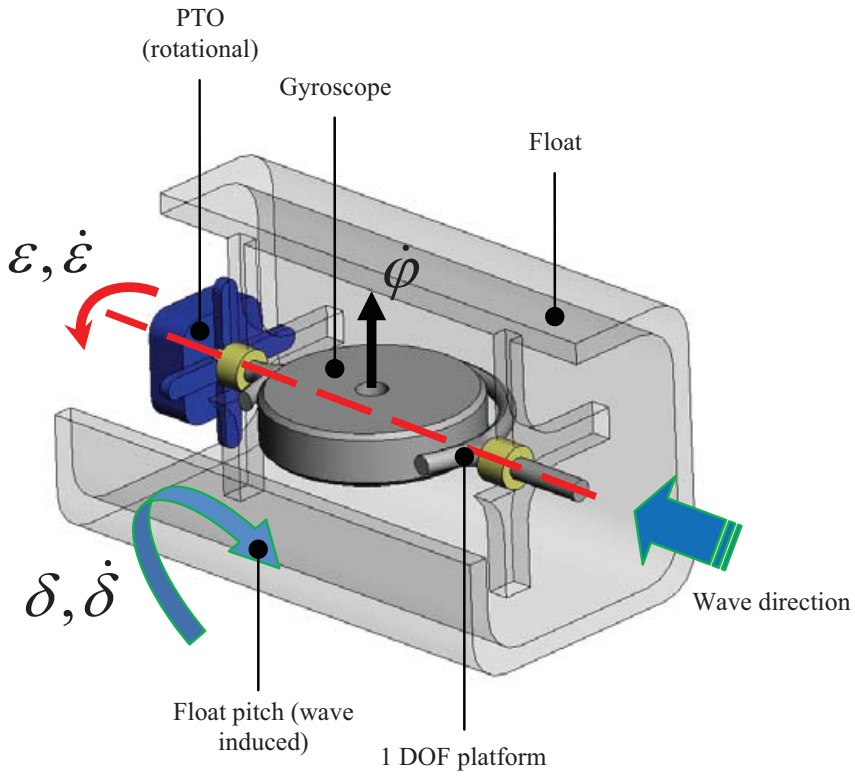

Figure 2.2. ISWEC: gyroscopic system.

2.2 Mechanical equations

The reference frames used in the analysis of the system are shown in figure 2.3. A mobile reference frame $x_1y_1z_1$ is obtained respect to the inertial reference frame xyz with two subsequential rotations δ and ε[1].

The mechanical behavior of the system can be easily explained by starting from the initial position in which $\delta = 0$ and $\varepsilon = 0$, there are no waves and the flywheel rotates around the axis z_1 with constant angular velocity $\dot{\varphi}$. As a effect of the first incoming wave, the system is tilted along the pitch direction δ gaining a certain

[1]Since the centre of gravity of the system lays exactly in the origin of the reference frames, the reference frame xyz can be either inertial or translating into the space, as the real device does.

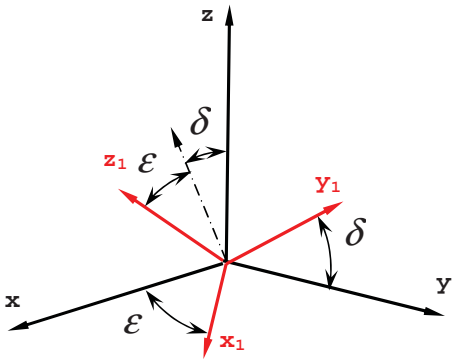

Figure 2.3. Reference frames.

angular velocity $\dot{\delta}$ along the x axes. The flywheel is so subjected to the two angular velocities $\dot{\varphi}$ and $\dot{\delta}$ and the gyroscopic effects produce a torque on the direction y_1 that is perpendicular to both the velocities. If the gyroscope is free to rotate along the y_1 direction with rotation ε, its behavior is governed just from the inertia and being the system conservative there is no mechanical power available for generation. The extraction of energy from the system can be performed by damping the motion along the ε coordinate. In this situation the gyroscope acts as a *motor* on the rotary damper and the energy extracted from the system by the damper is available for power generation. The damper can be for instance an electric generator directly coupled on the ε shaft. During the evolution of the system -damped or undamped- a gyroscopic torque arises on the buoyant too. In fact the two angular velocities $\dot{\varphi}$ and $\dot{\varepsilon}$ combined together produce a gyroscopic reaction on the buoyant along the δ coordinate opposing the wave induced pitching motion. And a second reaction torque is similarly induced on the z_1 axis by the combination of the $\dot{\delta}$ and $\dot{\varepsilon}$ angular velocities. These two reaction torques are to be taken into account when sizing respectively the buoyant and the motor driving the flywheel.

The angular velocity $\vec{\omega}_1$ of the mobile reference frame $x_1y_1z_1$ and the flywheel angular velocity $\vec{\omega}_G$ are both written with respect to the mobile reference frame - assuming $\vec{i}_1\vec{j}_1\vec{k}_1$ the versors associated to the mobile reference frame $x_1y_1z_1$.

$$\vec{\omega}_1 = \dot{\delta}\cos\varepsilon \cdot \vec{i}_1 + \dot{\varepsilon} \cdot \vec{j}_1 + \dot{\delta}\sin\varepsilon \cdot \vec{k}_1 \tag{2.1}$$

$$\vec{\omega}_G = \dot{\delta}\cos\varepsilon \cdot \vec{i}_1 + \dot{\varepsilon} \cdot \vec{j}_1 + (\dot{\delta}\sin\varepsilon + \dot{\varphi}) \cdot \vec{k}_1 \tag{2.2}$$

$$\vec{M}_e = \frac{d\vec{K}_G}{dt} \tag{2.3}$$

The (2.3) expresses the conservation of the angular momentum written with respect to the centre of gravity of the system. The equation describes the rotational equilibrium a mechanical system, asserting that the variation with respect to time of the angular momentum is equal to the applied external torque. In this analysis J is the moment of inertia of the flywheel around its axis of spinning z_1 and I represents the two moments of inertia of the flywheel with respect to the axes perpendicular to z_1.

$$\vec{K}_G = \vec{I} \cdot \vec{\omega}_G = I\dot{\delta}\cos\varepsilon \cdot \vec{i}_1 + I\dot{\varepsilon} \cdot \vec{j}_1 + J(\dot{\delta}\sin\varepsilon + \dot{\varphi}) \cdot \vec{k}_1 \tag{2.4}$$

Time deriving the angular momentum leads to time derive even the three versors $\vec{i}_1\vec{j}_1\vec{k}_1$ and at the end of all the mathematical passages, the equilibrium of the system is described by the vectorial equation (2.6).

$$\begin{array}{c} \frac{d\vec{i}_1}{dt} = \vec{\omega}_1 \times \vec{i}_1 = \dot{\delta}\sin\varepsilon \cdot \vec{j}_1 - \dot{\varepsilon} \cdot \vec{k}_1 \\ \frac{d\vec{j}_1}{dt} = \vec{\omega}_1 \times \vec{j}_1 = -\dot{\delta}\sin\varepsilon \cdot \vec{i}_1 + \dot{\delta}\cos\varepsilon \cdot \vec{k}_1 \\ \frac{d\vec{k}_1}{dt} = \vec{\omega}_1 \times \vec{j}_1 = \dot{\varepsilon} \cdot \vec{i}_1 - \dot{\delta}\cos\varepsilon \cdot \vec{j}_1 \end{array} \tag{2.5}$$

$$\vec{M}_e = \left\{ \begin{array}{c} I\ddot{\delta}\cos\varepsilon + (J-2I)\dot{\varepsilon}\dot{\delta}\sin\varepsilon + J\dot{\varepsilon}\dot{\varphi} \\ I\ddot{\varepsilon} + (I-J)\dot{\delta}^2\sin\varepsilon\cos\varepsilon - J\dot{\varphi}\dot{\delta}\cos\varepsilon \\ J(\ddot{\delta}\sin\varepsilon + \dot{\varepsilon}\dot{\delta}\cos\varepsilon + \ddot{\varphi}) \end{array} \right\} \tag{2.6}$$

The torque on the PTO T_ε and the torque on the motor driving the flywheel T_φ are given respectively by the second and the third scalar equation of the (2.6).

$$T_\varepsilon = I\ddot{\varepsilon} + (I-J)\dot{\delta}^2\sin\varepsilon\cos\varepsilon - J\dot{\varphi}\dot{\delta}\cos\varepsilon \tag{2.7}$$

$$T_\varphi = J(\ddot{\delta}\sin\varepsilon + \dot{\varepsilon}\dot{\delta}\cos\varepsilon + \ddot{\varphi}) \tag{2.8}$$

As the device works, an inertial torque T_δ is discharged from the gyroscopic system to the floating body along the pitching direction δ. T_δ can be evaluated projecting $\vec{M}_e$ along the x direction.

$$\begin{aligned} T_\delta &= \vec{M}_e \cdot \vec{i} \\ &= \vec{M}_e \cdot (\cos\varepsilon \cdot \vec{i}_1 + \sin\varepsilon \cdot \vec{k}_1) \\ &= (J\sin^2\varepsilon + I\cos^2\varepsilon)\ddot{\delta} + J\ddot{\varphi}\sin\varepsilon + J\dot{\varepsilon}\dot{\varphi}\cos\varepsilon + 2(J-I)\dot{\delta}\dot{\varepsilon}\sin\varepsilon\cos\varepsilon \end{aligned} \tag{2.9}$$

2.3 Linearization

The equations representing the system are nonlinear and coupled together. They can be implemented numerically in order to evaluate the time evolution of the system, but in order to design the device there is the need for linearization. The linearization point is the device steady condition $\varepsilon = 0$. The linearized parameters are pinpointed with a tilde.

$$\begin{Bmatrix} \tilde{T}_\delta \\ \tilde{T}_\varepsilon \\ \tilde{T}_\varphi \end{Bmatrix} = \begin{Bmatrix} (J\varepsilon^2 + I(1-\varepsilon^2)\ddot{\delta} + J\ddot{\varphi}\varepsilon + J\dot{\varepsilon}\dot{\varphi} + 2(J-I)\dot{\delta}\dot{\varepsilon}\varepsilon \\ I\ddot{\varepsilon} + (I-J)\dot{\delta}^2\varepsilon - J\dot{\varphi}\dot{\delta} \\ J(\ddot{\delta}\varepsilon + \dot{\varepsilon}\dot{\delta} + \ddot{\varphi}) \end{Bmatrix} \tag{2.10}$$

In the (2.10) I represents the sum of the moments of inertia around y_1 due to flywheel, platform and rotor of the PTO. As shown in chapter 3, it's almost natural to build a device featuring $I \simeq J$. Furthermore we can assume that the gyroscope is driven at constant speed. Thanks to these two assumptions the (2.10) can be simplified in the (2.11).

$$\begin{Bmatrix} \tilde{T}_\delta \\ \tilde{T}_\varepsilon \\ \tilde{T}_\varphi \end{Bmatrix} = J \begin{Bmatrix} \ddot{\delta} + \dot{\varepsilon}\dot{\varphi} \\ \ddot{\varepsilon} - \dot{\varphi}\dot{\delta} \\ \ddot{\delta}\varepsilon + \dot{\varepsilon}\dot{\delta} \end{Bmatrix} \tag{2.11}$$

If the PTO can be controlled to behave as a spring - damper group with stiffness k and damping factor c, the second equation of the (2.11) changes as follows.

$$-k\varepsilon - c\dot{\varepsilon} = J\ddot{\varepsilon} - J\dot{\varphi}\dot{\delta}$$

$$J\ddot{\varepsilon} + c\dot{\varepsilon} + k\varepsilon = J\dot{\varphi}\dot{\delta} \tag{2.12}$$

The (2.12) is the equation describing a linear second order system in which the forcing function is the gyroscopic effect. A linear analysis is then performed, giving to the system a sinusoidal input δ and observing the output ε.

$$\begin{aligned} \delta &= \delta_0 \cdot e^{\jmath\omega t} \\ \dot{\delta} &= \jmath\omega\delta_0 \cdot e^{\jmath\omega t} \\ \ddot{\delta} &= -\omega^2\delta_0 \cdot e^{\jmath\omega t} \end{aligned}$$

$$\begin{aligned} \varepsilon &= \varepsilon_0 \cdot e^{\jmath\omega t} \\ \dot{\varepsilon} &= \jmath\omega\varepsilon_0 \cdot e^{\jmath\omega t} \\ \ddot{\varepsilon} &= -\omega^2\varepsilon_0 \cdot e^{\jmath\omega t} \end{aligned}$$

$$\left(-J\omega^2 + c\jmath\omega + k\right)\varepsilon_0 = J\dot{\varphi}\jmath\omega\delta_0 \tag{2.13}$$

$$\varepsilon_0 = \frac{J\dot{\varphi}\jmath\omega}{-J\omega^2 + c\jmath\omega + k}\delta_0 \tag{2.14}$$

Defining the natural frequency $\omega_n^2 = k/J$, the complex amplitude ε_0 and the average power absorbed from the system by the damper P_d are written. The power extracted by the damper is considered available for electricity production.

$$\varepsilon_0 = \frac{J\dot{\varphi}\jmath\omega}{J(\omega_n^2 - \omega^2) + c\jmath\omega}\delta_0 \tag{2.15}$$

$$P_d = \frac{c}{2}\omega^2\varepsilon_0^2 = \frac{c}{2}\frac{(J\dot{\varphi}\jmath\omega^2\delta_0)^2}{J^2(\omega_n^2 - \omega^2)^2 + c^2\omega^2} \tag{2.16}$$

The linearized torques on the float, on the PTO and on the gyro axis are shown below.

$$\begin{Bmatrix} \tilde{T}_\delta \\ \tilde{T}_\varepsilon \\ \tilde{T}_\varphi \end{Bmatrix} = J\delta_0 \begin{Bmatrix} [-\omega^2 - \frac{J\dot{\varphi}^2\omega^2}{J(\omega_n^2-\omega^2)+c\jmath\omega}] \cdot e^{\jmath\omega t} \\ (k + \jmath\omega c)\frac{J\dot{\varphi}\jmath\omega}{J(\omega_n^2-\omega^2)+c\jmath\omega} \cdot e^{\jmath\omega t} \\ -\delta_0 \frac{J\dot{\varphi}\jmath\omega^3}{J(\omega_n^2-\omega^2)+c\jmath\omega} \cdot e^{2\jmath\omega t} \end{Bmatrix} \tag{2.17}$$

For a better understanding of the system dynamics and sensitivity to its main quantities, refer to chapter 4.

2.4 Extractable power

The (2.16) shows that the maximum extractable power is achieved in the resonating conditions ($\omega = \omega_n$). In the hypothesis of having a wave resonating mechanical system or a PTO controlled in order to make the device resonating with the incoming wave, equation (2.18) can be derived.

$$P_d = \frac{(J\dot{\varphi}\omega\delta_0)^2}{2c} \tag{2.18}$$

From the (2.16), the damping coefficient c can be written as follows.

$$c = \frac{2P_d}{\omega^2\varepsilon_0^2}$$

Substituting c in the (2.18), equation (2.19) appears.

$$P_d = \frac{(J\dot{\varphi}\omega\delta_0)^2}{2\frac{2P_d}{\omega^2\varepsilon_0^2}} \Rightarrow P_d = \sqrt{\frac{(J\dot{\varphi}\omega^2\delta_0\varepsilon_0)^2}{4}}$$

$$P_d = \frac{1}{2}(J\dot{\varphi})\omega^2\delta_0\varepsilon_0 \tag{2.19}$$

Thus from the linear analysis descends that in order to increase the extracted power of a wave resonating ISWEC, we need to increase the angular momentum, the pitching amplitude of the float δ and the ε amplitude on the PTO shaft. Furthermore the device can produce more if the incoming wave has a shorter period.

2.4.1 On the motor torque

Considering a flywheel driven at constant speed, a theoretical demonstration that the power absorbed by the motor driving the flywheel is null can be obtained rewriting the (2.8) in the following shape.

$$T_\varphi = \frac{d}{dt}(\dot{\delta}\sin\varepsilon) \tag{2.20}$$

The energy provided by the motor in a time interval $[t_0,t_1]$ to drive the gyroscope at $\dot{\varphi} = const$ is the integral of the instantaneous power.

$$\int_{t_0}^{t_1} P_M dt = J\dot{\varphi}|\dot{\delta}\sin\varepsilon|_{t_0}^{t_1} \tag{2.21}$$

The (2.21) creates a link between the energy provided by the motor and the state of the system. Let's imagine at $t = t_0$ the system is in the position $\varepsilon = 0$, whatever chosen time $t = t_1$ in which the system comes back to the same position (for instance the sequence: dead calm ($t = t_0$) - waves - dead calm ($t = t_1$), or just a half-cycle with two passages at $\varepsilon = 0$), the total energy provided by the motor to win the gyroscopic effects on the φ axes in $[t_0,t_1]$ is null. This relation stands for the full non-linear system.

Chapter 3

Design of a small scale prototype

In this chapter a prototype model of ISWEC is designed thanks to the linear system analysis performed in chapter 2. The model is designed to work at the curved wave tank in Edinburgh with a 1 Hz and 100 mm wave .

3.1 The Edinburgh curved wave tank

Figure 3.1. Picture of the curved wave tank.

The curved wave tank present at the University of Edinburgh [34] is shown in figures 3.1 and 3.2. The tank is designed to work at the nominal scale of 1/100 compared

with North-East Atlantic waves, and therefore the wave heights are relatively small (maximum around 110 mm) and the frequency range quite high (principally between 0.5 and 1.6Hz). The 'design frequency' for the tank is 1 Hz and so the reference regular wave chosen for the prototype model is at 1 Hz with a height of 100 mm.

$$\lambda = \frac{2\pi}{g}T^2 = \frac{2\pi}{9.81}1^2 = 1.56m \tag{3.1}$$

As the (3.1) shows, at 1 Hz the wavelength is 1.56 m. The tank depth is 1.2 m and as this is much greater than half of the design wavelength, the waves can be considered to be in deep water.

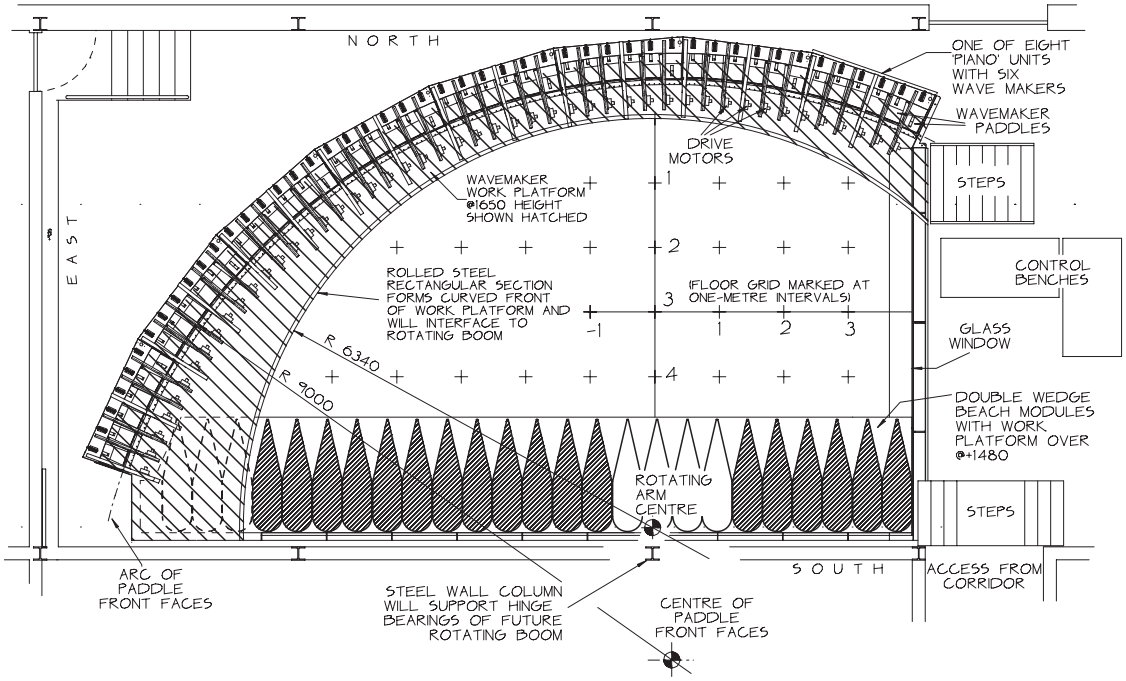

Figure 3.2. Wave tank plain view.

3.2 Design parameters

In order to establish the physical parameters of the prototype model there is the need to make some assumptions. The first is that the device must be tilted from the waves in order to perturb the gyroscope and produce energy by the PTO, so the shape should be unstable with respect to the waves. The wave generated at the

design point of the tank has wavelength 1.56 m: in order to have a float able to follow the shape of the wave, the dimension of the float in the direction of the wave propagation should be smaller than half the wavelength. This first consideration puts a limit of maximum length of the float in the direction of the axis equal to 780 mm. The maximum wave steepness for a regular wave can be evaluated with the (3.2)

$$\lambda_s = \arctan \frac{\pi H}{\lambda} \tag{3.2}$$

For the wave at the design point, λ_s is 11.4 deg. In order to avoid dealing with hydrodynamics, in a first approach we assume that under the action of the wave the float pitches with an oscillation of $\pm$ 2 deg. Due to the nature of the linearization, the linear system approximates the real device up to an angle ε smaller than 90 deg (modulus). Over this value the linear model has no physical meaning. The third assumption is that at the design point ε_0 is equal to 70 deg. Even though the system has been linearized around $\varepsilon = 0$ and 70 deg seems to be far from the linearization point, we will see in the comparison with the nonlinear model in paragraph 3.4 that this assumption still leads to good results. From the results of previous prototype models tested at the wave tank of the University of Edinburgh [35] the relative capture width (the ratio between absorbed power and incident power) for some point absorbers is around 50%. Since we don't know exactly this value for the ISWEC prototype, we decide to assume it equal to 100%, making the device able to deal with bigger power. The last assumption made is to have a gyroscopic system resonating at the wave frequency in order to extract the maximum power - refer to the equation (2.16).

The design parameters are summarized in Table 3.1.

Wave height	0.1 m
Wave frequency	1 Hz
Max. length of the device along the wave direction	780 mm
δ_0	2 deg
ε_0	70 deg
elative capture width	100 %
ω_n	1 Hz

Table 3.1. Design parameters.

3.3 Design procedure

The prototype model must be watertight and easy to assemble and disassemble. Furthermore it should be as cheap as possible. From these considerations we decided to make the external shape of the device from an acrylic (in the UK often referred to by the trade-name Perspex) tube sealed at the ends with acrylic caps with O-rings. The choice of acrylic makes the device light and transparent, helping to understand what's happening inside and to show the working principles of the device. PTO, gyro and sensors must be mounted on the same axis (ε) giving a preferential dimension of the device and making natural the choice of aligning the axis ε with the axis of the tube. Hence the tube is aligned to the wave direction: from the first consideration descends that the maximum length of the tube is 780 mm. The design procedure starts evaluating the nominal incident power. The power density of the 'design wave' is evaluated.

$$P_D = \frac{\pi\rho g}{32} T \cdot H^2 = \frac{\pi \cdot 1000 \cdot 9.81}{32} 1 \cdot 0.1^2 = 9.63 \frac{W}{m} \tag{3.3}$$

From previous experience at the University of Edinburgh we decided to choose the nominal width (the diameter of the tube) equal to 200 mm. Thus, the rated power of the device is

$$P_R = P_D \cdot D = 9.63 \cdot 0.2 = 1.92W \tag{3.4}$$

Being the relative capture width 100 %, P_R is equal to the average power absorbed from the device and so must be the average power absorbed by the damping component of the PTO. From Eq. (2.16) it's possible to obtain directly the damping factor of the device.

$$c = \frac{2 \cdot P_d}{(\omega\varepsilon_0)^2} = \frac{2 \cdot 1.92}{(\frac{2\cdot\pi}{1}\frac{70\pi}{180})^2} = 6.53 \cdot 10^{-2} \frac{Nm \cdot s}{rad} \tag{3.5}$$

Eq. (2.18) defines the needed angular momentum.

$$J\dot{\varphi} = \frac{c\varepsilon_0}{\delta_0} = \frac{6.53 \cdot 10^{-2} \cdot \frac{70\pi}{180}}{\frac{2\pi}{180}} = 2.28 kgm^2 \frac{rad}{s} \tag{3.6}$$

The electric actuator driving the gyroscope must be at constant speed since the 'motor' of the device is the angular momentum and the performance of the device is proportional to it. Desiring a fixed inertia system (easy to build and manage), by adjusting the angular velocity of the gyro it's possible to change the angular momentum continuously and 'switch off' the device by switching off the motor of the gyro. Furthermore it's possible to start up the device with a smaller angular velocity, observe the system behavior, and in case of stable working increase the

angular momentum up to the desired value. In order to maintain the system light and simple, the motor can be coupled directly to the gyro. Due to the amount of the torque ripple on the gyroscope shaft and the value of the inertia momentum, closed loop speed control is not required on this ISWEC prototype -see later in paragraph 3.7. By fixing the angular velocity of the motor at 4000 rpm it's possible to evaluate the gyroscope inertia J.

$$J = \frac{2.28}{\frac{2\pi}{60}4000} = 5.46 \cdot 10^{-3} kgm^s \tag{3.7}$$

The value of J puts another technological boundary because I must be the same in order to accomplish the simplification made on Eq. (2.11). The stiffness of the spring can be evaluated by means of the natural frequency of the system ω_n.

$$k = I \cdot \omega_n^2 = 0.216 Nm/rad \tag{3.8}$$

The last boundary to be satisfied is buoyancy: at least the device must not sink. However there is another condition, because the tube should float being half submerged in order to have the maximum hydrostatic stiffness. By means of drawing the system in a 3D CAD environment and estimating the total mass, we can see that in this case the system is too heavy: the tube must be longer than 780 mm to float half-submerged. The external diameter is then increased to the next commercial dimension, 230 mm, and the whole procedure is repeated. By increasing the external diameter of the tube there is the double advantage of getting a higher buoyancy and a smaller mass of the gyro for the required inertia. These two gains compensates the increase of mass and inertia due to the increase of power absorbed. The parameters of the final version of the prototype are shown in table 3.2 while its performances are summarized table 3.3.

3.4 Comparison with non linear model

The design procedure exploited with the linear model gives first trial values for the system. Then a non-linear simulation in the environment Matlab - Simulink© to verify the linear model is launched. Since the modulus of the forcing function decreases when the system abandons the initial position $\varepsilon = 0$, the linearized model overestimates the value of the real average power. So the inertia of the gyro and all the other parameters have been slightly increased in order to make the real system catch the 100% of the incoming power.

The condition called here Cfg. A has been obtained by looking for a device designed with the linear system and verified with the non-linear model which is able (in the full nonlinear conditions) to produce the rated power. The device is designed to oscillate with $\varepsilon_0 = 70 deg$ but the real system oscillates of $60.7 deg$. By decreasing

J	$1.74 \cdot 10^{-2}\ kgm^2$
I	$1.66 \cdot 10^{-2}\ kgm^2$
$\dot{\varphi}$	2000 rpm
k	0.656 Nm/rad
c	$0.106\ Nm \cdot s/rad$
External diameter and length	230 mm x 560 mm
Total mass	12.3 kg

Table 3.2. Prototype parameters.

the damping coefficient it is possible to make the device oscillate at $70deg$ and according to the 2.18 catch a bigger power. By gradually decreasing the damping coefficient on the non-linear model, the $\varepsilon_0 = 70deg$ configuration is achieved with $c = 0.084Nm{\cdot}s/rad$. This last configuration is called Cfg. B. The final version of the prototype model assumes the features summarized in Table 3.3 [1] and a comparison between the time domain behaviors of the system is shown in Figures 3.3, 3.4 and 3.5.

		Linear model	Non-linear model (A)	Non-linear (B)
ε_0	$[deg]$	69.4	60.7	70.2
$\dot{\varepsilon}_0$	$[rad/s]$	7.6	7.0	8.4
P_R	[W]	3	2.2	2.4
T_{ε_0}	[Nm]	0.89	0.83	0.84
rcw	[%]	130	96	109

Table 3.3. Linear vs. Non-linear.

[1] As table 3.3 shows, $\dot{\varphi}$ is equal to 2000 rpm despite previously it was decided for 4000 rpm. Actually the 4000 rpm flywheel has been built and tested, but when I drove the flywheel over 3500 rpm, the system started to vibrate excessively and safety problems arose. So the flywheel speed was halved and the inertia doubled. The stiffness has been doubled too in order to maintain the natural frequency at 1 Hz. In the calculations the PTO inertia on axis ε is neglected since it is at least three orders of magnitude smaller than J (see Table 3.11).

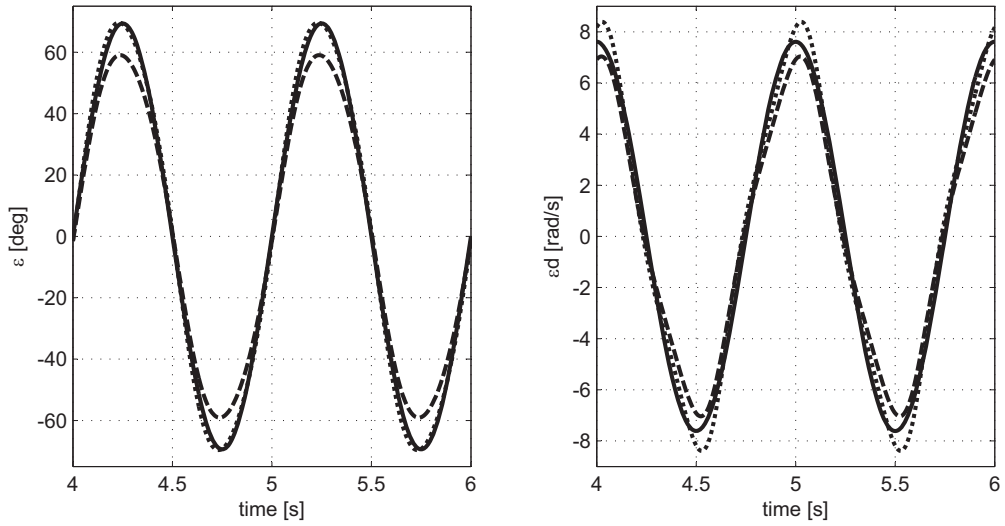

Figure 3.3. Angular position and velocity around axes ε (continuous line: linearized system, dashed line: non linear system -A-, dotted line: non linear system -B-).

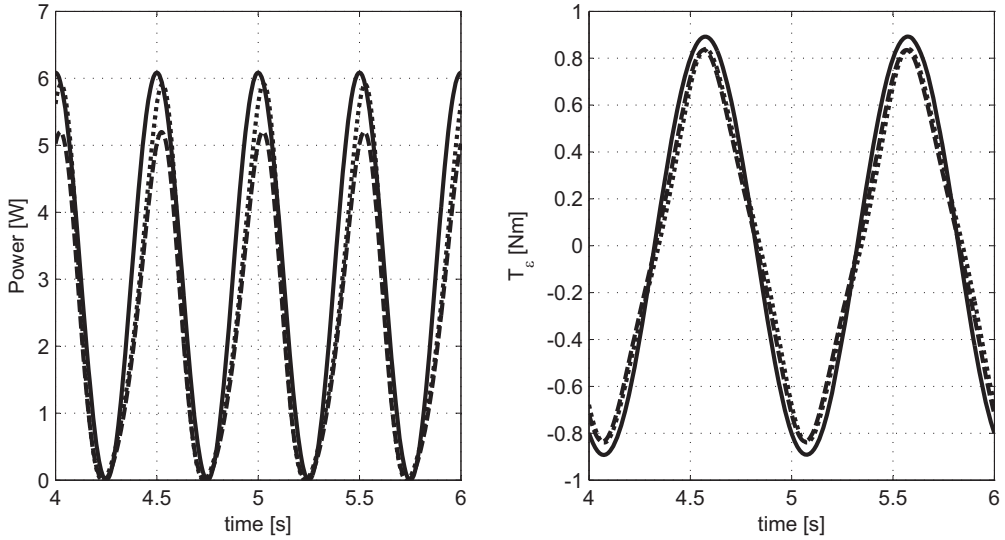

Figure 3.4. Power absorbed by the damper and torque on the PTO (stiffness + damping).

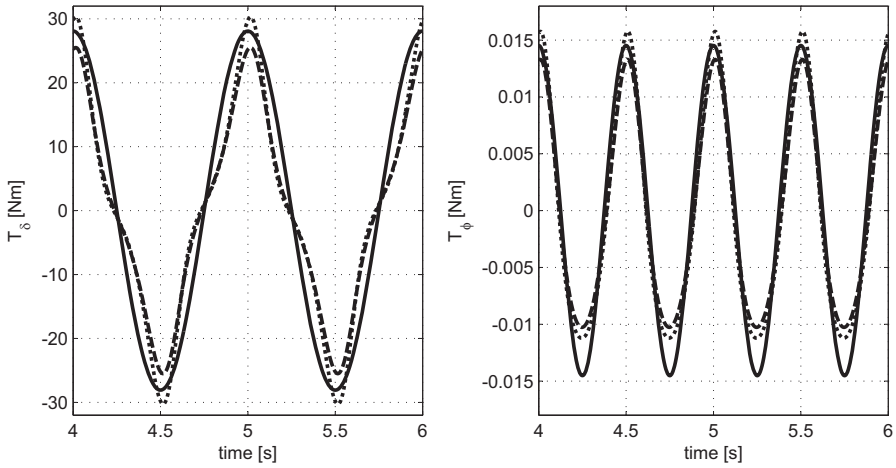

Figure 3.5. Torque along the δ and φ axis.

3.5 Mechanical design

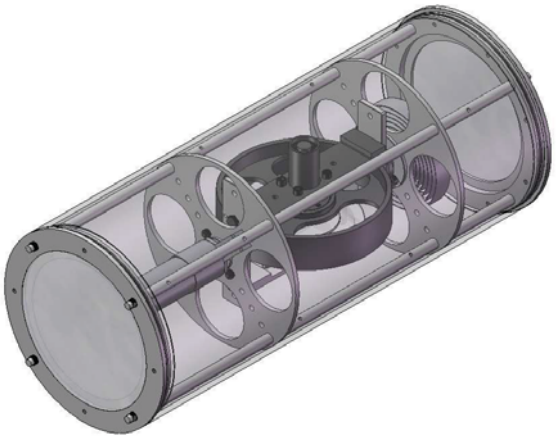

Figure 3.6. ISWEC prototype axonometry.

The internal mechanism is suspended inside the acrylic tube by an aluminum structure made using plates held in their relative position with rods put at the extremity of the plates. The resultant structure is cheap, easy to machine, stiff and flexible to change. Between the two central plates there is the structure carrying the gyroscope

along the rotation ε. This structure mounts a flat DC electric motor and two bearings to drive the gyroscope. The gyroscope is placed in the middle of the structure in order to exploit all the internal available radial space: this consideration leads to place the bearings and the DC flat motor at the two extremities. The two shafts protruding from the structure and coupling with the bearings on axis ε are hollow in order to allow the cables direct to the DC motor to pass through. Figures 3.6 and 3.7 show the layout of the prototype model.

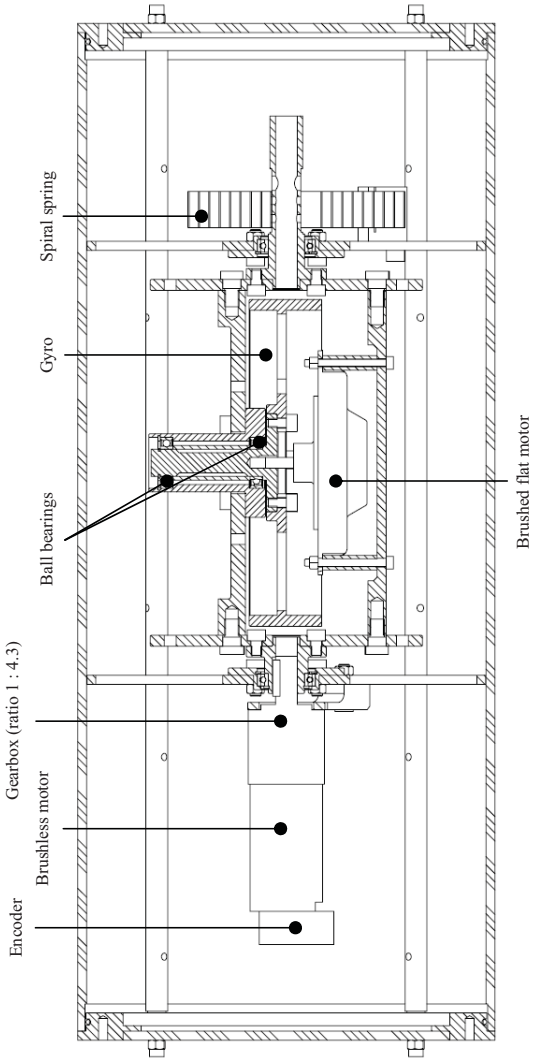

Figure 3.7. ISWEC prototype cross section.

Since T_ε is transmitted from the gyro platform via the PTO to the Plexiglas tube, if it is not constrained along the ε axis, the tube begins to oscillate around its axis damped only by the viscous forces with water. Moreover, if the centre of gravity of the overall system lays close to the axis of the Plexiglas tube, there is not an equilibrium position granting the steady position of the system. This can be solved in different ways: by inserting a mass on the bottom of the tube, by arranging the mooring line or by putting external floats to eliminate the system axial-symmetry. In this project the third solution has been chosen integrating thus the device with the indexable system of arms and floats shown in figure 3.8

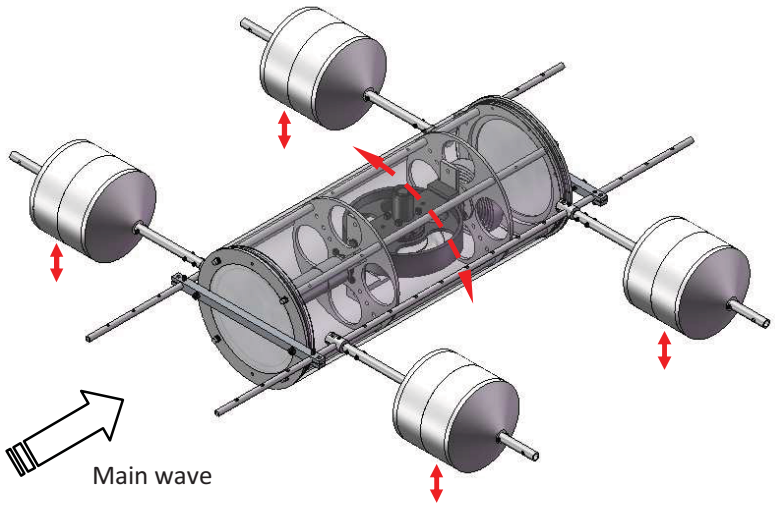

Figure 3.8. The device with side floats.

3.6 PTO

The rotational PTO system is composed of a brushless motor coupled through an high efficiency planetary gear head to the gyroscope structure. This solution allows an increase in the motor shaft speed and a reduction in the motor size and weight in order to satisfy the buoyancy requirement for the whole device. Moreover the higher motor speed allows the use of commercial low torque low voltage servo motor avoiding, at this step of the prototyping activity, a purposely designed (or re-winded) motor. The PTO brushless motor is equipped with an incremental encoder both for control and monitoring purposes. The supply converters for the PTO and for the gyroscope rotor and the energy storage system are located off the ISWEC and connected to the buoy by cables. Even if the PTO brushless motor can be controlled

in order to supply both the damping torque and the elastic torque, some space has been reserved inside the ISWEC for a spiral spring on the PTO shaft. In order to allow complete rotations of the PTO the possibility to carry the electric supply to the PTO brushless motor and to the gyroscope by a slip ring connector has been taken into account during the ISWEC design.

As a general statement, since the power density of the wave is small, the power produced from the prototype is small, too. Thus particular care should be placed in the choice of high efficiency components.

Figure 3.9. The PTO (motor, gearbox and encoder).

The brushless motor should have a speed constant large enough to grant acceptable voltages at the low speeds on its shaft. After a search among the providers commercially available, the Maxon© seems to be the most suitable: a EC 40 brushless motor, a HEDL 5540 encoder and GP 42 C gearbox have been identified as the components of the PTO (see the Appendix for factory datasheets). The PTO can work continuously with the torque in Cfg. A since the rms of that torque reported to the motor shaft (gearbox efficiency = 90%, the maximum value from the datasheet) is smaller than the nominal torque.

$$T_{m,rms} \simeq \frac{T_{\varepsilon 0}}{\sqrt{2}} \cdot \frac{1}{\tau} \cdot \eta = \frac{0.83}{\sqrt{2}} \cdot \frac{1}{\frac{13}{3}} \cdot 0.9 = 0.122Nm < 0.129Nm$$

			118901
Motor Data			
	Values at nominal voltage		
1	Nominal voltage	V	48.0
2	No load speed	rpm	2020
3	No load current	mA	24.4
4	Nominal speed	rpm	893
5	Nominal torque (max. continuous torque)	mNm	129
6	Nominal current (max. continuous current)	A	0.599
7	Stall torque	mNm	237
8	Starting current	A	1.07
9	Max. efficiency	%	72
	Characteristics		
10	Terminal resistance phase to phase	Ω	44.8
11	Terminal inductance phase to phase	mH	10.7
12	Torque constant	mNm / A	221
13	Speed constant	rpm / V	43.2
14	Speed / torque gradient	rpm / mNm	8.75
15	Mechanical time constant	ms	7.78
16	Rotor inertia	gcm²	85.0

Figure 3.10. Brushless motor parameters (extract from the Maxon© datasheet).

	Order Number		203114
1	Reduction		4.3 : 1
2	Reduction absolute		$^{13}/_{3}$
3	Mass inertia	gcm²	9.1
4	Max. motor shaft diameter	mm	8

Figure 3.11. Gearbox parameters (extract from the Maxon© datasheet).

Counts per turn	500
Number of channels	3
Max. operating frequency (kHz)	100
Max. speed (rpm)	12000
Shaft diameter (mm)	3

Figure 3.12. Encoder parameters (extract from the Maxon© datasheet).

3.6.1 Achieving damping

By connecting to the motor a Y bridge made of resistors the motor behaves as a linear damper. The mono phase equivalent circuit of the brushless motor is shown in figure 3.13 and the equations evaluating the damping coefficient are written below.

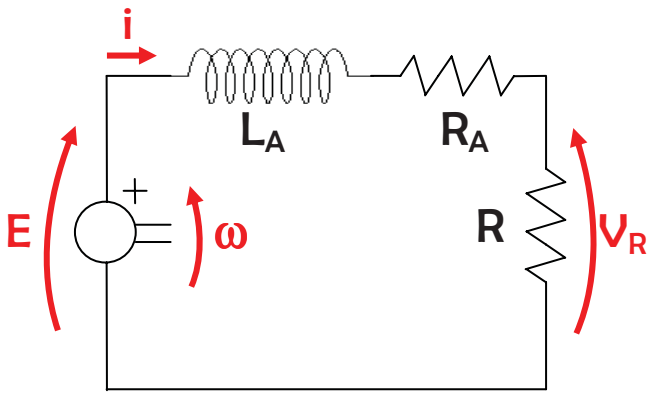

Figure 3.13. Monophase equivalent circuit.

$$\begin{aligned} E &= k_e \cdot \omega \\ E &= (R_a + R) \cdot i + L_a \tfrac{di}{dt} \\ T_m &= k_T \cdot i \end{aligned} \tag{3.9}$$

Since the pole of the electrical system is at $\frac{1}{2 \cdot \pi \cdot \tau} = \frac{R}{2 \cdot \pi \cdot L} = 670$ Hz and the PTO shaft oscillates at 1Hz, the effect of the inductance can be neglected. By adapting the (3.9) to the application and considering an ideal gearbox with drive ratio τ ($\omega = \tau \cdot \dot{\varepsilon}$), the damping coefficient can be written.

$$\begin{aligned} T_\varepsilon &= c \cdot \dot{\varepsilon} \\ T_m \cdot \tau &= c \cdot \tfrac{\omega}{\tau} \\ k_T \cdot i \cdot \tau &= c \cdot \tfrac{E \cdot k_E}{\tau} \\ k_T \cdot \tfrac{E}{R_a + R} \cdot \tau^2 &= c \cdot E \cdot k_E \end{aligned}$$

$$c = \frac{k_T}{k_E} \frac{\tau^2}{R_a + R} \tag{3.10}$$

The maximum damping coefficient is achieved when $R = 0$.

$$c_{max} = \frac{221 \cdot 10^{-3}}{\frac{43.2 \cdot 2 \cdot \pi}{60}} \frac{(\frac{13}{3})^2}{22.4} = 0.041 \frac{Nm \cdot s}{rad}$$

The required damping factor is 0.106 $\frac{Nm \cdot s}{rad}$ and the (3.10) shows that it can't be achieved putting external resistors. Among the electric motors that have been considered suitable to this application, the system described above has been retained the best choice, so by changing it with an equivalent between the motors selected, the situation doesn't improve. The situation can be improved by increasing the gear ratio τ, but the next available gearbox for this motor has a high drive ratio $\tau =$

$\frac{49}{4} \simeq 12$ that can generate efficiency and reversibility problems. Therefore we settled for this motor+gearbox configuration and decided to use an electronic driver to set up a torque control. The chosen driver is the EPOS2 50/5 controller, recommended for the Maxon © EC 40 series. The power extracted from the gyroscopic system is evaluated measuring the torque and the angular velocity on the motor shaft.

3.7 Electric motor

The flywheel must be accelerated to the desired speed and then maintained in rotation. Due to the architecture, the motor driving the flywheel should be short enough to stay into the four bars structure. This boundary narrows the possible choice to the pancake motors that are radially big but axially short. The chosen motor is the brushed DC motor GPM9 purchasable from RS Components Ltd. The motor is shown in figure 3.14 and its main parameters are reported in table 3.4. Due to the strict geometry boundaries, few motors were suitable and the GPM9 was the cheapest. A check on the startup time has been performed neglecting the motor inertia and the air drag. The equations (3.11) show the transfer function and, in case the acceleration is made at $T_m = T_n$, the time behavior of $\dot{\varphi}$. Figure 3.15 shows that the motor accelerates the flywheel in 31 s.

$$\begin{aligned} \bar{T}_m - T_f &= (c_m + sJ)\bar{\dot{\varphi}} \\ \dot{\varphi}(t)|_{T_m=T_n} &= \frac{T_n - T_f}{c_m} \cdot e^{-\frac{t}{J/c_m}} \end{aligned} \tag{3.11}$$

Figure 3.14. The pancake motor, RS Components Ltd.

rated torque	T_r	Nm	0.131
rated speed	ω_r	rpm	3000
rated voltage	V_r	V	14.5
rated current	i_r	A	6.9
rated power	P_r	W	41
voltage constant	k_E	$\frac{V}{rad/s}$	$2.2 \cdot 10^{-2}$
torque constant	k_t	$\frac{Nm}{A}$	$2.2 \cdot 10^{-2}$
terminal resistance	R_a	Ω	1.1
viscous friction	c_m	$\frac{Nm \cdot s}{rad}$	$2.86 \cdot 10^{-5}$
static friction	T_f	Nm	0.012

Table 3.4. GPM9 motor parameters.

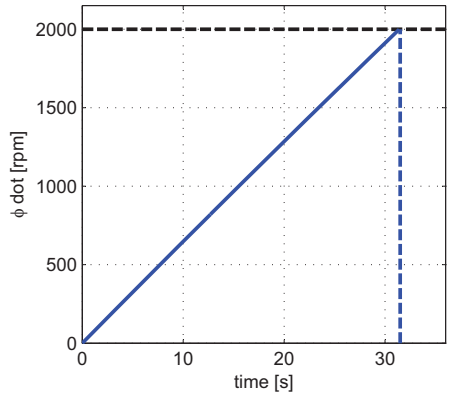

Figure 3.15. Flywheel startup.

As assessed in paragraph 3.4, the torque acting on the gyroscope due to the inertial effects is roughly a sine wave with amplitude 0.015 Nm and frequency 2 Hz. A Simulink © model of the motor + flywheel system has been built in order to evaluate the velocity ripple due to the torque and decide if a speed controller on the φ axis was needed. If the motor is driven at constant voltage (by connecting it directly to a power supply) a ripple of $\pm$ 0.7 rpm has been estimated. The flywheel inertia and the motor are filtering the incoming torque noise and therefore there is no need of a controller to stabilize $\dot{\varphi}$.

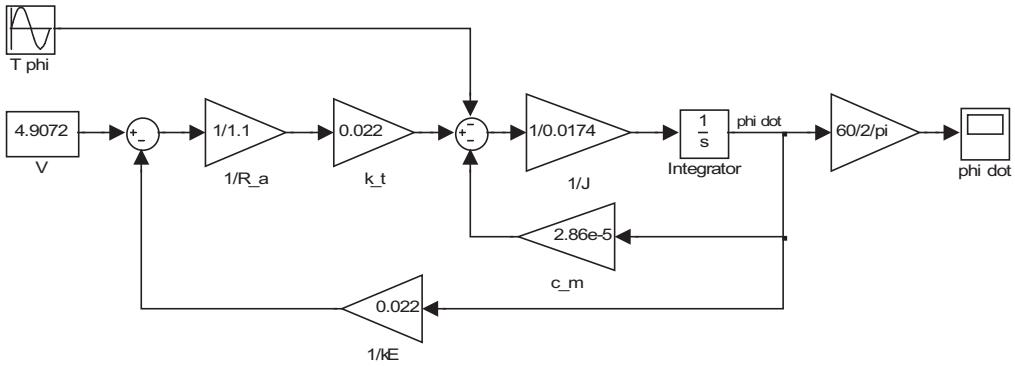

Figure 3.16. Simulink model - constant voltage.

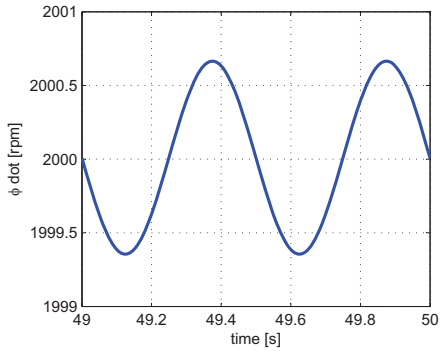

Figure 3.17. $\dot{\varphi}$ ripple.

The assessment on the variation of $\dot{\varphi}$ has been carried out without taking into account the effect the variation of $J\dot{\varphi}$ induces on the gyroscopic system. Theoretically the model of the device should include the model of the electric motor, but as shown before, the ripple of T_φ - evaluated with $\dot{\varphi} = const$ - induces a variation of $J\dot{\varphi}$ equal to $\pm\frac{0.7}{2000} = \pm 0.035\%$ that reasonably, at this stage of the activity, doesn't create any relevant effect on the dynamics of the gyroscopic system.

Chapter 4

Parametric analysis

In this chapter the influence on the absorbed power of a variation of the system main parameters is analyzed. The linear and the non-linear (Cfg. A) systems are compared both in absolute terms and in relative terms with respect to the rated parameters. The aim of this chapter is to understand what can be done to improve the system and if the linear model can be used with confidence to predict the system response to a variation of the parameters.

4.1 PTO stiffness

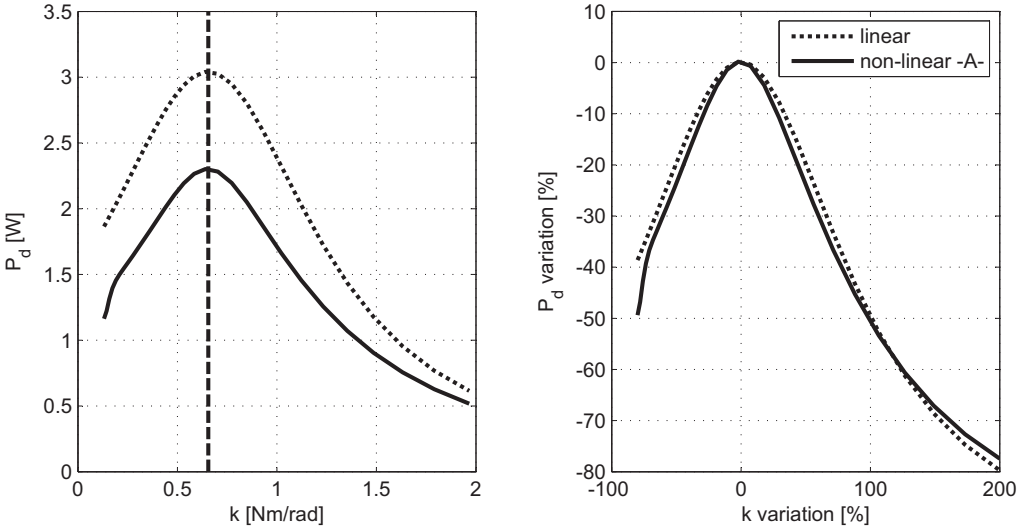

Figure 4.1. The influence of the PTO stiffness.

Figure 4.1 shows the influence of the PTO stiffness on the absorbed power. The vertical dashed line represents the stiffness making the device wave resonant. The stiffness varies from one fifth to the triple of the initial value. According to the 2.16, the more the stiffness changes from the wave resonant value, the more the power absorbed by the damper decreases. This happens both in the linear and in the non-linear system. The graph on the right in figure 4.1 has been built by dividing the two power curves on the left to their value at the rated stiffness (see tables 3.2 and 3.3). The x-axis represents the variation of stiffness with respect to the rated stiffness. The importance of choosing a wave-resonant stiffness is highlighted: for instance by doubling k, P_d halves. Furthermore the linear model represents a good estimator of the real system with respect to a PTO stiffness variation.

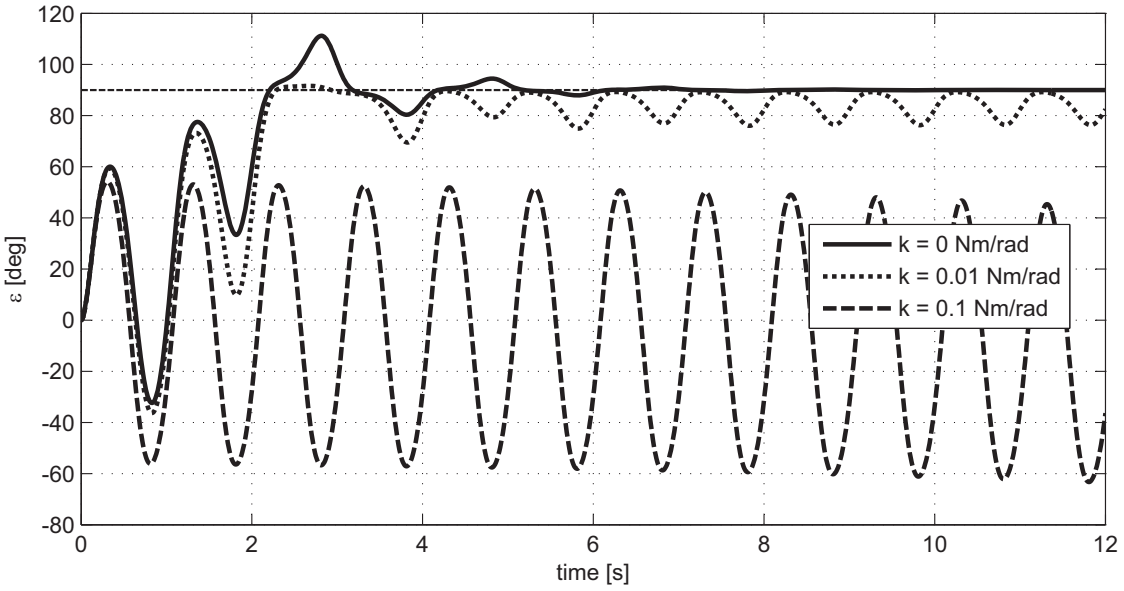

Figure 4.2. Time behavior at null and small stiffness.

As figure 4.2 shows, if the PTO has no stiffness the systems settles with a damped oscillation to the condition $\varepsilon = 90deg$ because in that position the gyroscopic effects disappear and therefore the torque on the PTO is null. The more the stiffness increases the more the system oscillation tends to have mean value $\varepsilon = 0deg$, as in the rated conditions. If the input δ is given to the system opposite in sign, the system settles at $\varepsilon = -90deg$ and generally the time behavior is a mirror of figure 4.2 with respect to the x-axis. On the other hand if the stiffness is too big, the system is constrained to the position $\varepsilon = 0$ and, since this decreases the amplitude

of oscillation, the absorbed power decreases as well.

4.2 PTO damping coefficient

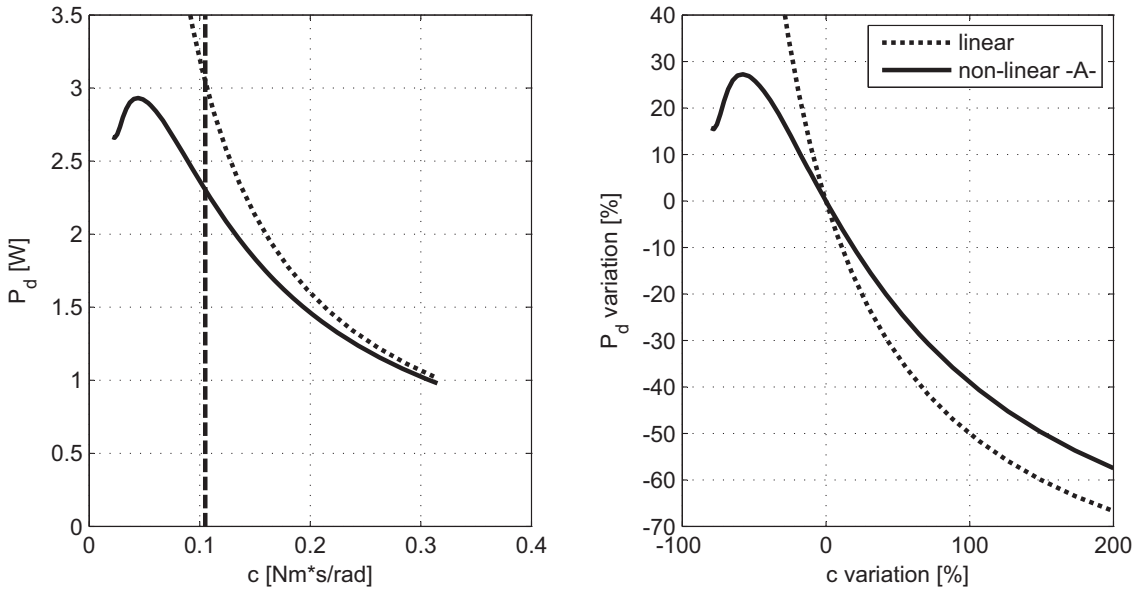

Figure 4.3. The influence of the PTO damping coefficient.

The linearized equation (2.18) suggests that decreasing the damping coefficient, the power extracted from the damper increases (because the amplitude of oscillation ε_0 increases, see (2.16)). Figure 4.3 shows that this suggestion is correct in a small field, because the (2.18) has been written by neglecting the term $\cos\varepsilon$. In fact if $|\varepsilon > 90deg|$ the gyroscopic torque on the PTO shaft changes its sign, by trying to push the gyro back to the condition $|\varepsilon < 90deg|$. The amplitude of motion is therefore reduced with respect to the linear amplitude and the power absorbed by the damper too (see figure 4.4).

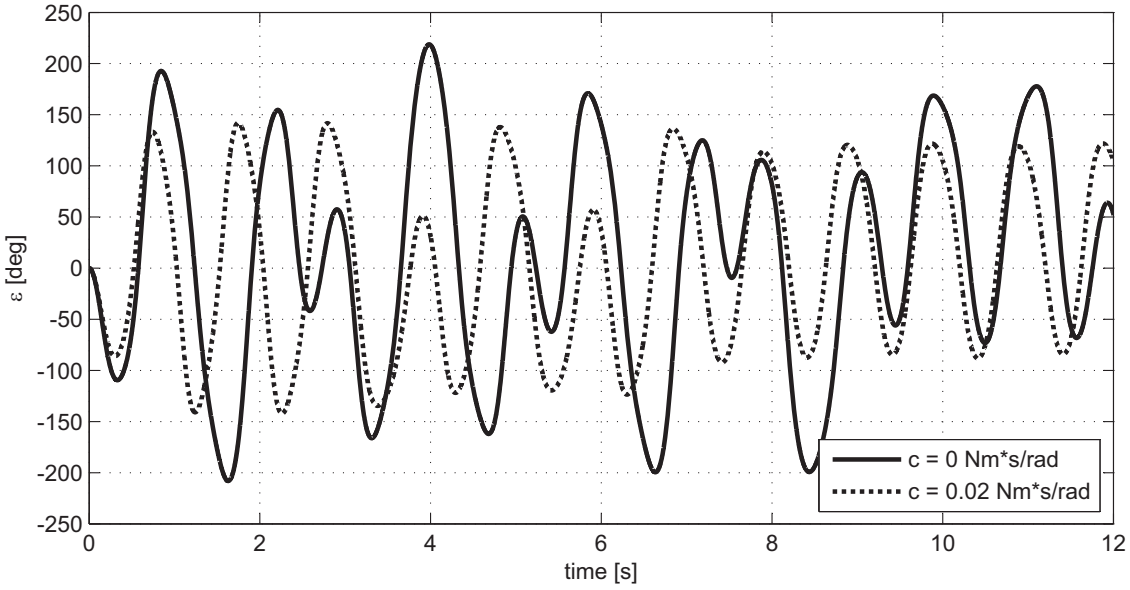

Figure 4.4. Time behavior at null and small damping (ε).

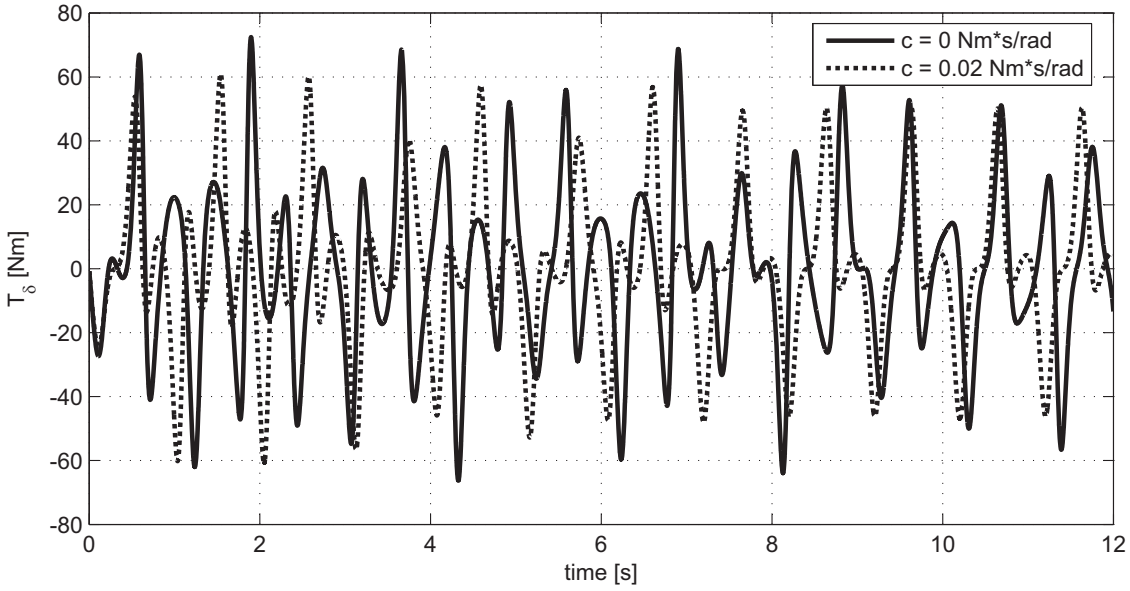

Figure 4.5. Time behavior at null and small damping (T_δ).

Figure 4.5 shows the torque on the float along the pitching direction: T_δ reaches values that are double with respect to the rated point. So a particular care should be taken if the PTO looses its damping action but not the stiffness (e.g. the stiffness is provided by a mechanical spring and not directly from the PTO) because of the torque induced on the whole structure along the δ coordinate. A possible action in this situation is the reduction of $\dot{\varphi}$ and, if that's too slow to do, an emergency brake on the ε axes. The linear model in this case doesn't predict the system performance for small damping coefficient whereas for higher damping it underestimates the absorbed power.

4.3 Flywheel speed and angle of pitch

In this section the system behavior due to variations of $\dot{\varphi}$ or δ_0 is analyzed. The modulus of the forcing function in the (2.14) is proportional to both these parameters and so a variation of the former or the latter produces the same effect on the system. Theoretically increasing $\dot{\varphi}$ or δ_0 the absorbed power increases without limits, but the non-linear system puts a boundary at about three times the rated power. If the absorbed power increases, so does the torque along the pitching direction. The linear model is a good estimator only when decreasing the two parameters (as usual because the amplitude ε_0 decreases).

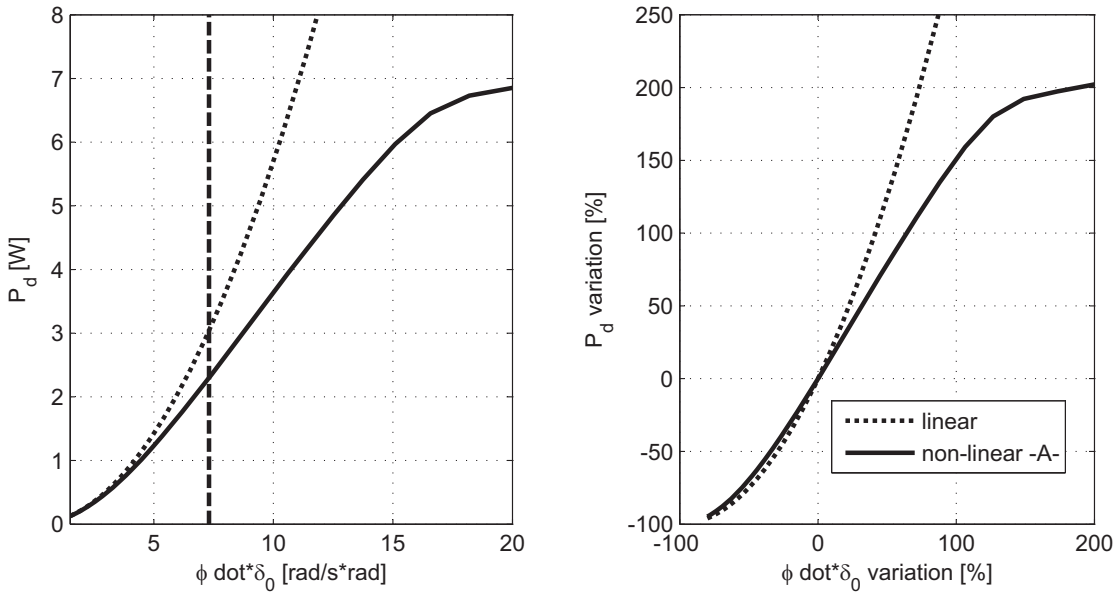

Figure 4.6. The influence of $\dot{\varphi}$ and δ_0.

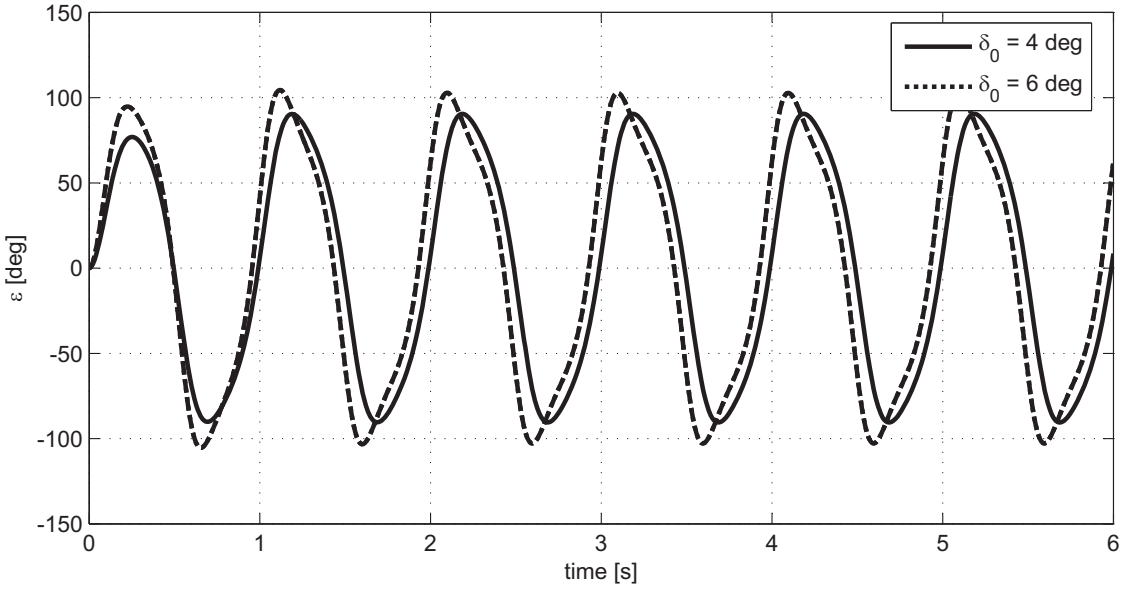

Figure 4.7. Time behavior increasing δ_0 (ε).

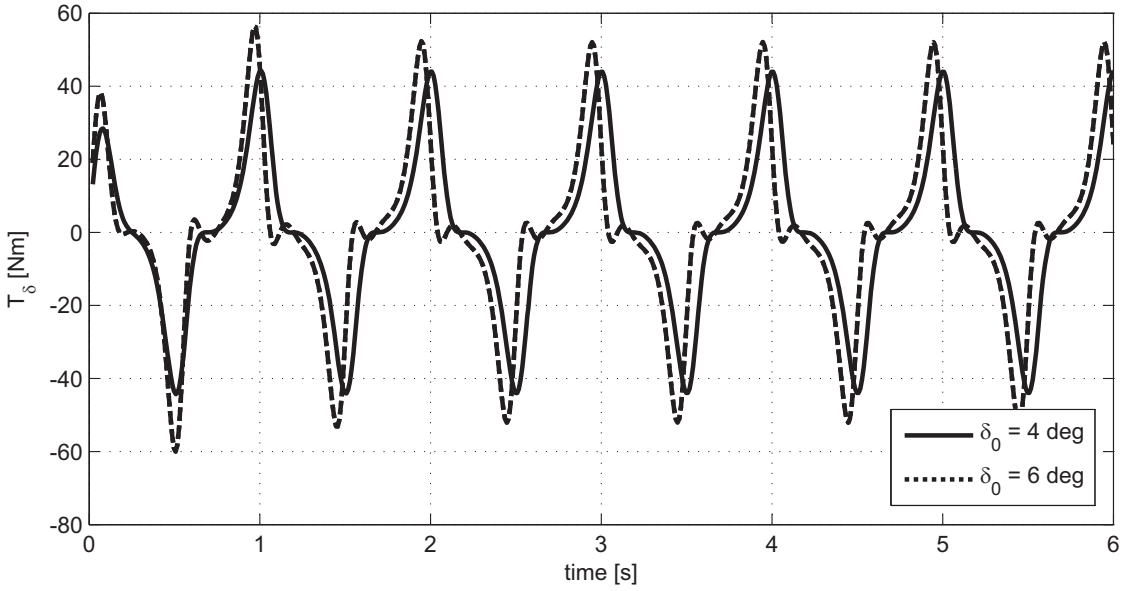

Figure 4.8. Time behavior increasing δ_0 (T_δ).

4.4 Wave frequency

This section shows the frequency response of the system. ISWEC behaves very differently if it is tuned or not with the incoming wave. Figure 4.9 shows the absorbed power with respect to the wave frequency: as the frequency decreases the absorbed power decreases, if the frequency increases, the power slightly increases up to a limit of about +30%. The linear model predicts well just the part of smaller frequencies. If the device is resonant with the incoming wave the power absorbed from the damper increases without limits and the linear model is almost a perfect estimator (see Figures 4.10 and 4.11)[1]. As figure 4.11 shows, in any condition the non-linear tuned system produces more power than the non-linear system with constant stiffness.

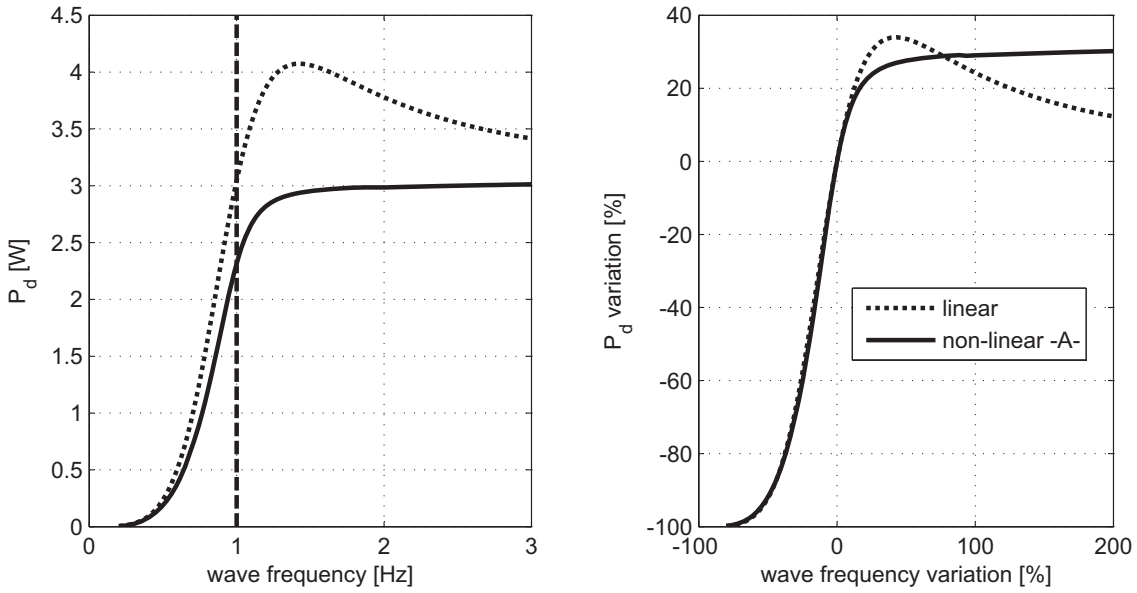

Figure 4.9. The influence of the wave frequency ω (k = const).

[1]The frequency response doesn't take into account that as the power produced by ISWEC increases, T_δ increases opposing more damping (T_δ and $\dot{\delta}$ are phased in resonance) on the float and, depending on the hydrodynamics, the float oscillates less.

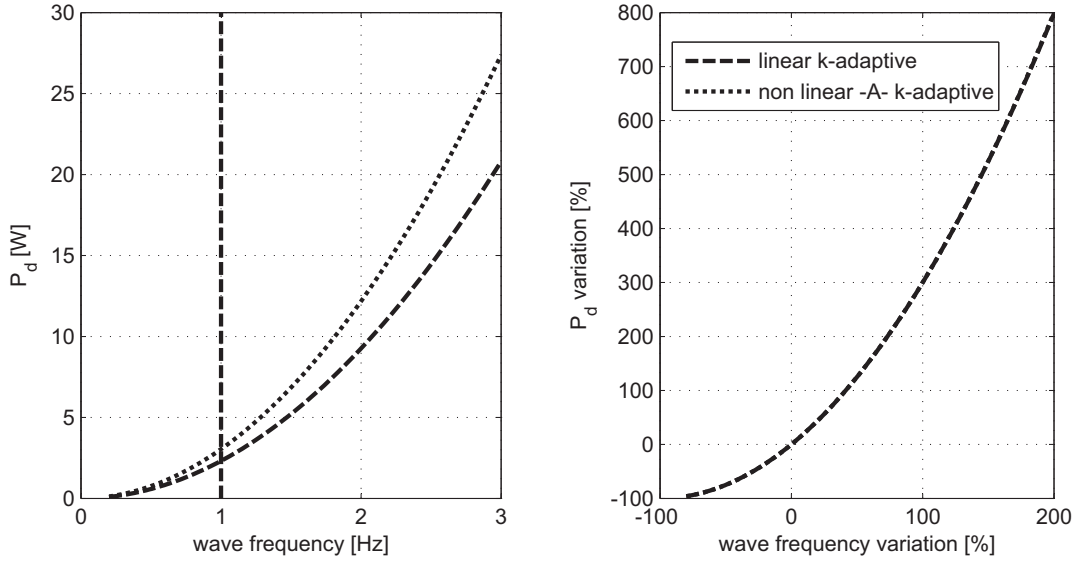

Figure 4.10. The influence of the wave frequency ω (k tuned).

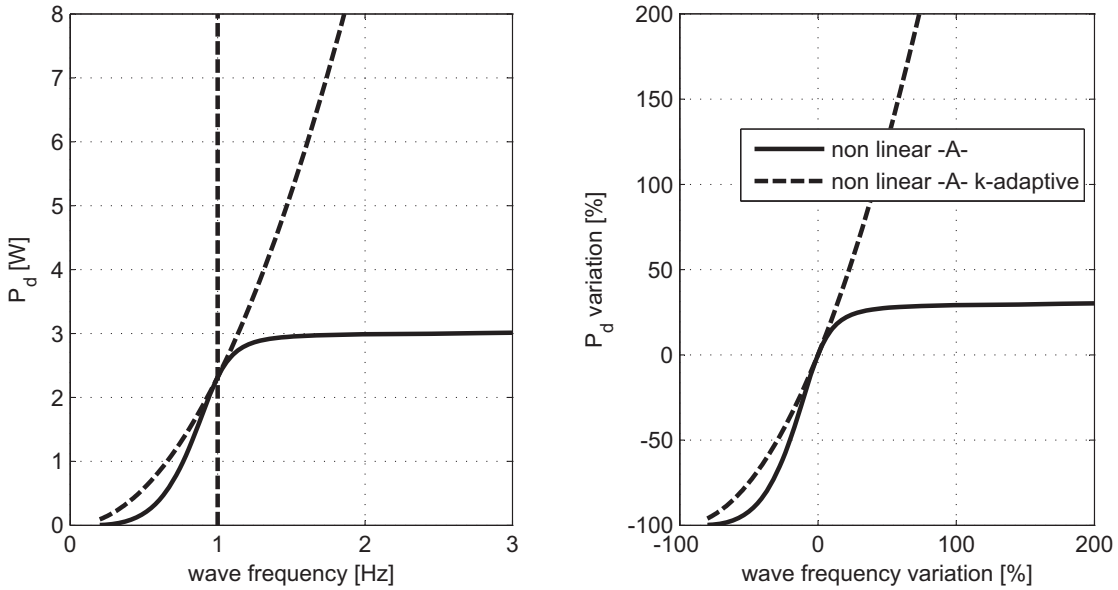

Figure 4.11. The influence of the wave frequency ω (comparison among the tuned and the not tuned system).

4.5 Chapter remarks

In this chapter a parametric analysis has been performed on the ISWEC prototype model. The analysis is related to the power generation capacity of the mechanical system whereas the buoyant dynamics is not considered at this stage. The results show mainly that ISWEC works at its best when tuned with the incoming wave. The flywheel velocity can be used to regulate the power absorption, for instance if the incoming wave generates a pitching angle too big, $\dot{\varphi}$ can be reduced to absorb the rated power even if the waves are too much powerful. If the waves are so big to be dangerous, then the flywheel can be arrested shutting down the gyroscopic effects and, if the PTO is locked, making the buoy behave like a dead body.

The linear model has proved to be reliable in estimating the system behavior with respect to a variation of stiffness and generally with respect to changes making ε decreasing. In the other cases and for small variations, it gives a rough estimation but a non-linear simulation is needed to assess correctly the behavior of the system.

Finally figure 4.12 shows a plot with respect to the wave period of the absorbed power P_d of the tuned ISWEC (dashed line). The dotted line represents the power density P_D of the incoming wave. The wave power density is proportional to the wave period while the power absorption capacity decreases with the wave period. So when there is a bigger power ISWEC can absorb less and viceversa. This leads to two considerations: ISWEC is more suitable to exploit short waves and probably, since short waves carry a smaller power, ISWEC will not be a device with a high rated power.

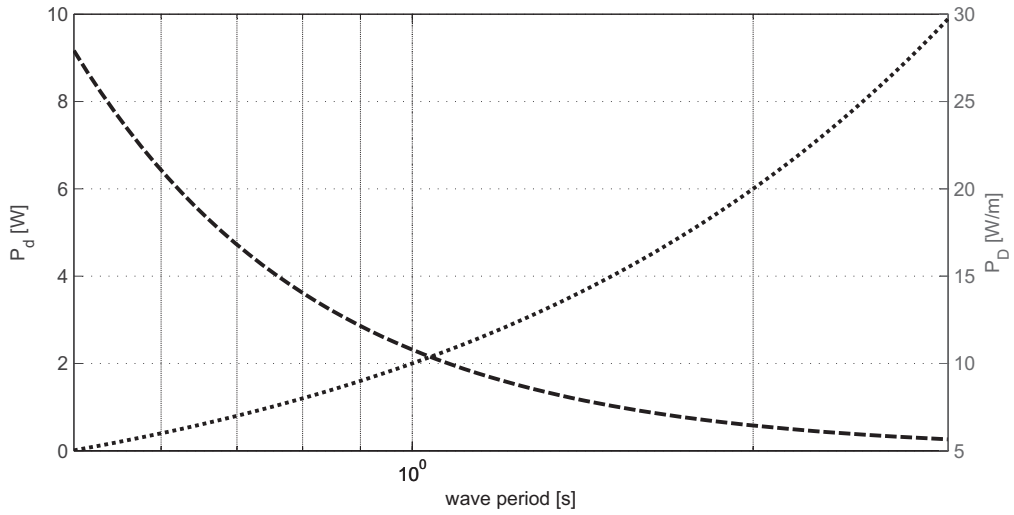

Figure 4.12. Tuned system - dashed line - vs. power density - dotted line - with respect to wave period.

Chapter 5

Dry test

A series of dry tests has been performed on a wave simulation rig before going to the Edinburgh wave tank. The tests were meant to assess the prototype capabilities and to validate the numerical model of ISWEC.

5.1 The wave simulation rig

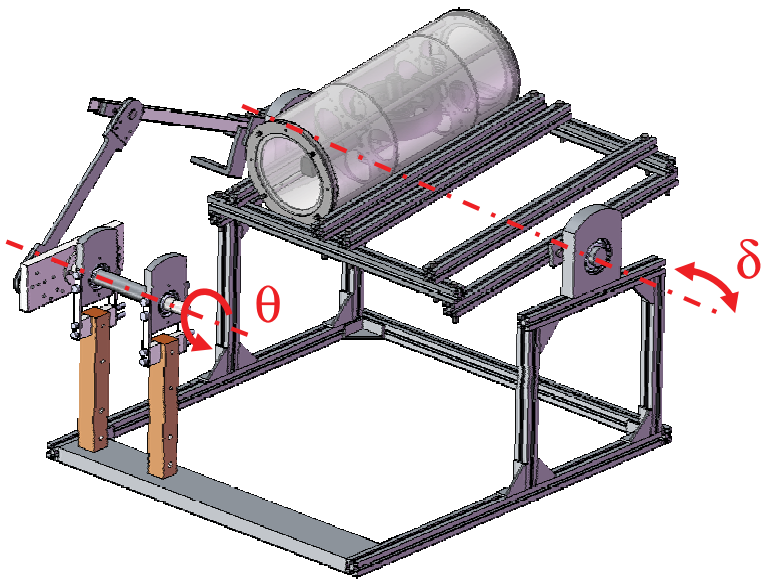

Figure 5.1. Axonometry of the wave simulation rig.

The wave simulation rig is composed mainly by an articulated quadrilateral mechanism able to generate a regular sinusoidal motion δ on a rocking platform from a continuous rotation θ given through a brushed dc motor. Being the amplitude of oscillation δ small and if the motor is driven at $\dot{\theta} = const$, δ results almost in an ideal sinusoid.

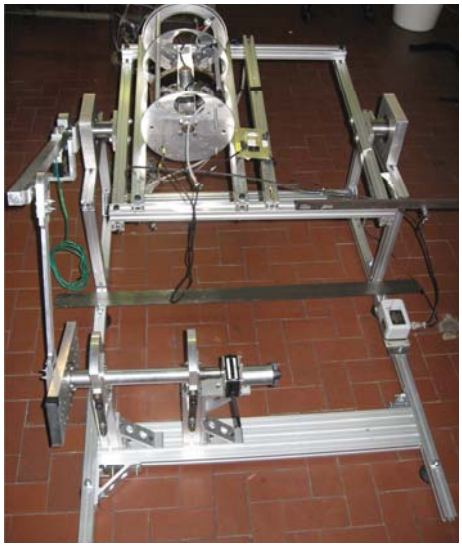

Figure 5.2. Picture of the wave simulation rig.

The wave simulation rig can vary the amplitude δ_0 in the span $1.5 \div 15$ deg with step 0.5 deg by changing the distance a (see Figure 5.3). The wave frequency is regulated by changing the supply voltage of the dc motor. The dc motor is coupled with a high ratio gearbox reducing the effect on the motor of the disturb torque T_δ produced from the ISWEC prototype on the rocking platform and granting a quasi constant velocity $\dot{\theta}$.

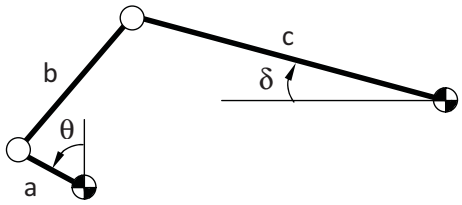

Figure 5.3. Kinematic scheme (a = variable ($10 \div 140$ mm), b = 400 mm, c = 600 mm).

5.2 Transducers

In order to assess the prototype performances and to validate the numerical model, during the dry tests the system was monitored by acquiring ε, δ and T_ε. The position ε is measured by the encoder of the PTO (see 3.12) and the velocity $\dot{\varepsilon}$ is evaluated time deriving the encoder signal. The torque on the PTO is measured using a load cell mounted with a lever arm on the PTO stator whereas the motion δ is measured with a wire transducer (the gray little box on the right in Figure 5.2). The angular velocity $\dot{\varphi}$ of the gyro is measured with an inductive pick-up giving a + 5V TTL signal every time one of the three rays of the flywheel passes in correspondence of the sensor. By measuring the frequency of the square wave coming from the pickup and dividing it by three, $\dot{\varphi}$ is evaluated.

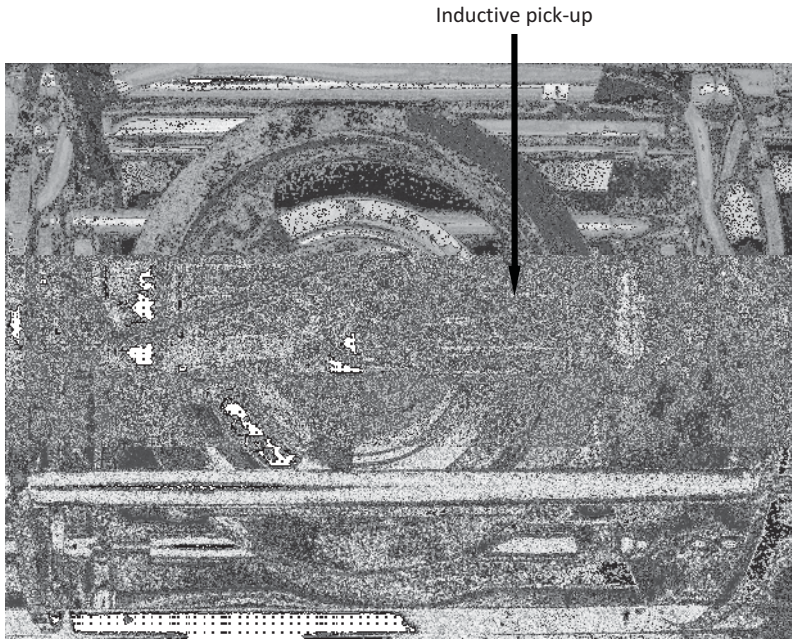

Figure 5.4. The inductive pick-up to measure the flywheel speed.

5.2.1 Load cell

The load cell DACELL UU-K5 has been mounted as shown in Figures 5.5 and 5.6. The load cell has been suspended with two spherical joints SKF SIKB6F on the extremities in order to measure the force without bending torques. The torque on the PTO is obtained measuring the voltage produced by the cell knowing the cell gain and the lever arm.

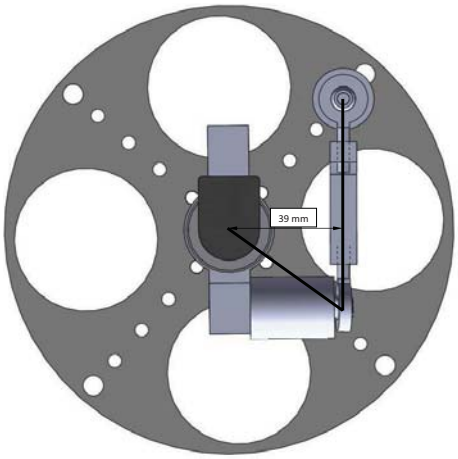

Figure 5.5. Torque measurement scheme.

Figure 5.6. The PTO equipped with the load cell to measure the damping torque.

5.3 Data acquisition system

In order to acquire the signals from the transducers the system has been equipped with a data acquisition card National Instruments USB-6259 connected via USB to a laptop. On the laptop the Labview 8.60 software runs with a program visualizing

Rated capacity(R.C.)	5kgf
Rated output(R.O.)	2.0mV/V1%
Nonlinearity	0.03% of R.O.
Hysteresis	0.03% of R.O.
Repeatability	0.03% of R.O.
Temperature effect (on R.O.)	0.05% of load /10 C
Temperature range, compensated	-10 ÷ 60 deg
Excitation recommended	10V
Safe overload	150% R.C

Table 5.1. Extract of the load cell DACELL UU-K5 datasheet.

and logging the data at 100 Hz (the main phenomenon is at 1 Hz, so 100 samples per cycle is enough to get the system dynamics).

Figure 5.7. The National Instruments USB-6259 DAQ card in the middle, connected with a BNC 2120 connector block on the left and a SCC 68 screw terminal on the right.

Analog Inuput	
Number of channels	16 differential or 32 single ended
A/D converter resolution	16 bits
Sampling rate	1.25 MS/s single channel
	1.00 MS/s multi-channel (aggregate)
Input range	±10 V, ±5 V, ±2 V, ±1 V, ±0.5 V, ±0.2 V, ±0.1 V
Input impedance (device on)	>10 GΩ in parallel with 100 pF
Analog Output	
Number of channels	4
A/D converter resolution	16 bits
Maximum update rate	
1 channel	2.86 MS/s
2 channel	2.00 MS/s
3 channel	1.54 MS/s
4 channel	1.25 MS/s
Output range	±10 V, ±5 V
Output impedance	0.2Ω
Output current drive	±5 mA
Digital I/O	
Number of channels	32
Type of signal	TTL
Counters/Timers	
Number of counters/timers	2
Resolution	32 bits
Internal base clocks	80 MHz, 20 MHz, 0.1 MHz

Table 5.2. Main features of the NI USB 6259 DAQ card.

5.3.1 Filtering

Except for the encoder all the acquired signals are analog, thus bringing with them an extra-amount of noise due to the antenna-effect of the cables. In order to get rid of the noise, the acquired data have been filtered with a low-pass 6^{th} order Butterworth filter with cut-off frequency at 10 Hz, one decade over the main frequency in the phenomenon.

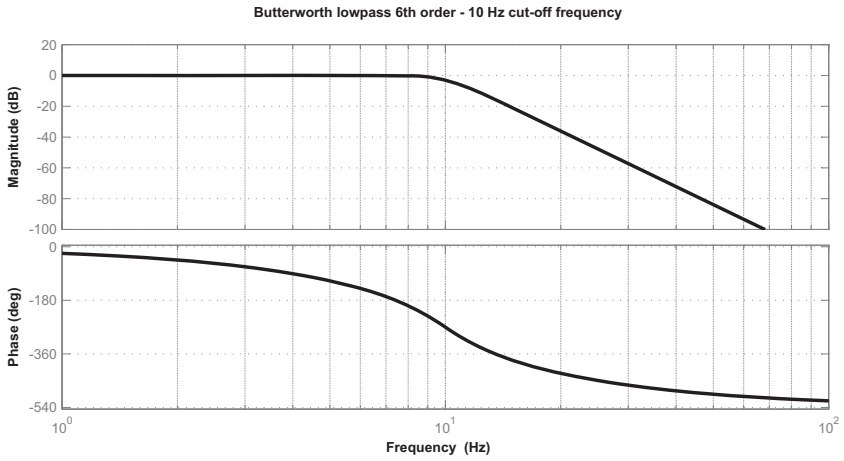

Figure 5.8. Bode plot of the Butterworth filter.

As shown in figure 5.8, the filter induces a phase lag on the input data. To avoid this effect, the time history has been filtered, reversed, re-filtered and eventually reversed to the original direction. The whole process is implemented by the Matlab function `filtfilt`. Figure 5.9 shows a comparison between raw and filtered data.

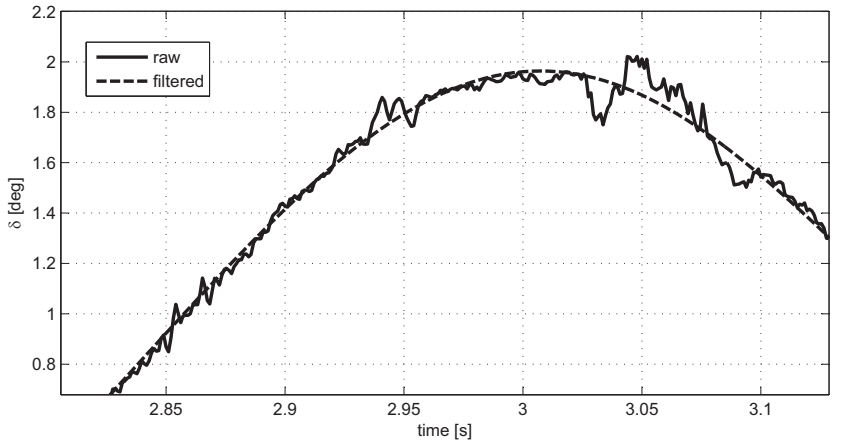

Figure 5.9. Effect on the data of the Butterworth filter implemented with the Matlab function `filtfilt`.

If not differently specified, henceforth all the experimental data are filtered using the previous procedure.

5.4 The damping coefficient

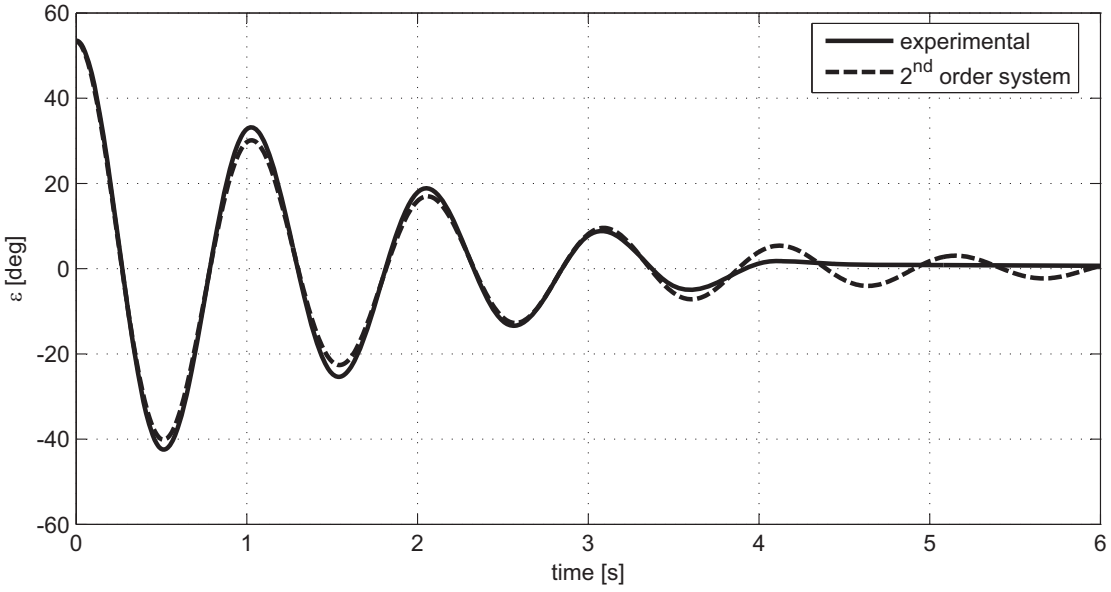

Figure 5.10. The test executed to evaluate the damping coefficient due to friction on the ε axes.

The spring and the damping action on the ε axes are provided from the PTO. The EPOS2 controller can be set to the torque control mode granting in this way a torque proportional to an external analog reference given to the EPOS2. The reference signal is generated through one of the analog output channels available on the NI USB 6259 DAQ card. The signal coming out from the encoder is sent to both the EPOS2 controller and to the data acquisition card. The software managing the acquisition, is integrated with a loop taking the position ε from the encoder, time-deriving it to obtain $\dot{\varepsilon}$ and writing to the analog output 0 a voltage proportional to $T_\varepsilon = k\varepsilon + c\dot{\varepsilon}$. The EPOS2 uses a PWM modulation at 30 V peak and 50 kHz whereas the internal control loop works at 10 kHz in the current mode. Eventually, as shown in 3.6.1, the electric constant of the motor is 670 Hz. So the electrical part of the system is really faster than the 1 Hz of the main phenomenon frequency. On the other hand the Labview software transforming the encoder signal to the torque reference runs under the O.S. Microsoft Windows which is a non deterministic environment. After some tests it has been noticed that the acquisition and reference generation software can run in a maximum 8 ms cycle time when the working frequency is set

to 100 Hz[1]. This value can be drastically reduced[2] but in this case being 100 Hz two order of magnitude greater than the wave frequency, the system has been regarded as suitable to generate the torque reference signal. The data acquisition and the reference generation have been thus performed at 100 Hz and synchronized with the DAQ card physical clock running at 100 kHz.

The PTO in this configuration behaves as a damper and as spring with variable stiffness and avoiding therefore the need of a mechanical spring. The spring realized electronically has proved reliable: for instance if the PTO is set to behave just like a spring and its shaft is forced to move to an initial angle and then released, the shaft oscillates with the initial amplitude for dozens of cycles and more than a hundred cycles pass before it settles to the position $\varepsilon = 0$. However, since its realization is cheap and relatively quick, a mechanical spring composed by two linear springs mounted with a lever arm on the PTO axes has been realized. The spring system is tuned at 1 Hz and can be easily connected and disconnected on the PTO axes.

The damping coefficient on the ε axes for Cfg. A is 0.106 Nms/rad. This value is the sum of the damping coefficient provided by the PTO and the damping coefficient due to the friction on the bearings and with the air. If the gyro is switched off, the friction on the bearings is relatively small. However driving in rotation the flywheel at 2000 rpm, the total friction due to the 'fan' effect of the flywheel increases substantially the total friction torque on ε. In order to evaluate the damping coefficient due to the friction on the ε axes, the EPOS2 controller has been set to make the PTO behaving like a pure spring: the flywheel has been then driven at 2000 rpm and the structure carrying the flywheel has been manually forced to reach a position $\varepsilon_{initial}$ of about 50 deg and then released. The underdamped oscillation of the system coming back to the initial position is acquired from the encoder and shown in figure 5.10. The theoretical expression of such oscillation follows.

$$\varepsilon(t) = \varepsilon_{initial} \cdot e^{-\zeta\omega_n t} \cdot \cos(\omega_n \sqrt{1-\zeta^2} \cdot t + \Phi) \tag{5.1}$$

The three parameters ζ, ω_n and Φ are unknown and they have been evaluated with a Least Square curve fitting procedure. Technically this has been executed writing the norm of the error vector (the difference between the real position ε and the theoretical response) and using the Matlab function `fminsearch` to find the three parameters realizing the minimum of the norm of the error vector. Here it is the code, `out_epsilon` is the experimental response and `out_time` the sampled time coming from the acquisition process. The vector `x` represents the initial try for

[1]The software runs on a PC with an Intel Pentium IV processor at 2GHz, 2 GB of RAM and O.S. Windows XP Professional SP2.

[2]A twin PC was used in a different experimental context with the LabVIEW Real-Time module achieving 10 μs cycle time [36].

$[\zeta,\omega_n,\Phi]$.

```
myfun_gio=@(x)norm(out_epsilon-...
(out_epsilon(1)*exp(-x(1)*x(2)*out_time).*...
cos(x(2)*sqrt(1-x(1)^2)*out_time+x(3))));
x_def=fminsearch(myfun_gio,[1,2*pi*1 20/180*pi])
```

The output of `fminsearch` declares $\zeta = 0.0908$ and $\omega_n = 6.23 rad/s$. From the definition of ζ, c is evaluated

$$c_{friction} = \zeta \cdot 2 \cdot \sqrt{k \cdot I} = 0.0199 \frac{Nm \cdot s}{rad} \tag{5.2}$$

This value can't be neglected because it is roughly the 20% of the desired value. Therefore friction must be taken into account by decreasing of $0.02 \frac{Nm \cdot s}{rad}$ the damping on the PTO.

5.5 Dry test in the rated conditions (Cfg. A)

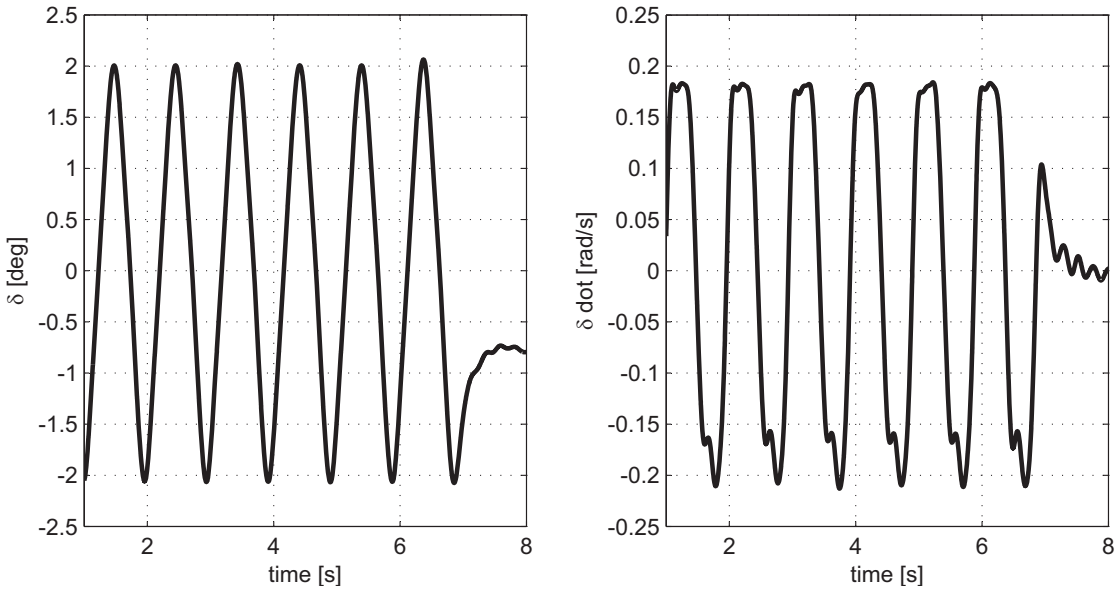

Figure 5.11. The input δ produced by the wave simulation rig with the ISWEC active in the rated conditions.

The ISWEC prototype has been set in Cfg. A (refer to paragraph 3.4) and then tested on the wave simulation rig. The wave simulation rig is set to give a sine wave

with amplitude 2 deg and frequency 1 Hz. During the working time the prototype exchanges T_δ with the mobile platform of the rig. The electric motor driving the rig is regulated in velocity by manually changing the supply voltage. Since the motor has not a speed control, the disturb T_δ makes $\dot{\theta}$ vary and thus δ is no more a sine wave. Figure 5.11 shows the time history of δ as the prototype works and figure 5.12 shows the comparison with the desired regular wave.

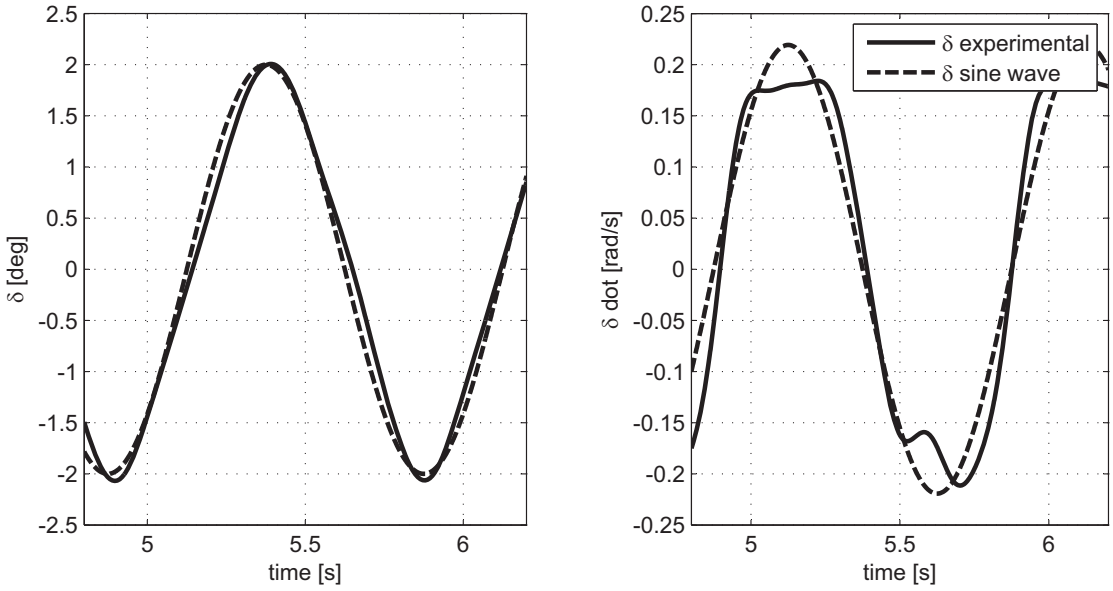

Figure 5.12. Comparison over δ between the experimental and the ideal sine wave.

The real δ has been given in input to the numerical model to make a comparison between the experimental results and the output of the numerical model - see figures 5.13 and 5.13. The torque and power plots relative to the experimental data are obtained by considering the contribution due to friction evaluated in section 5.4.

The average power P_d absorbed from the damper (PTO + friction) over 6 cycles is 2.22 W for the numerical model and 2.27 W (+2.2%) for the real system. There are small differences between the experimental measurements and the numerical model due to non exact geometry, sensors accuracy and measurements errors. Since the output of the numerical model is very close to the real system behavior, it's possible to affirm that for the analyzed case the numerical model is validated.

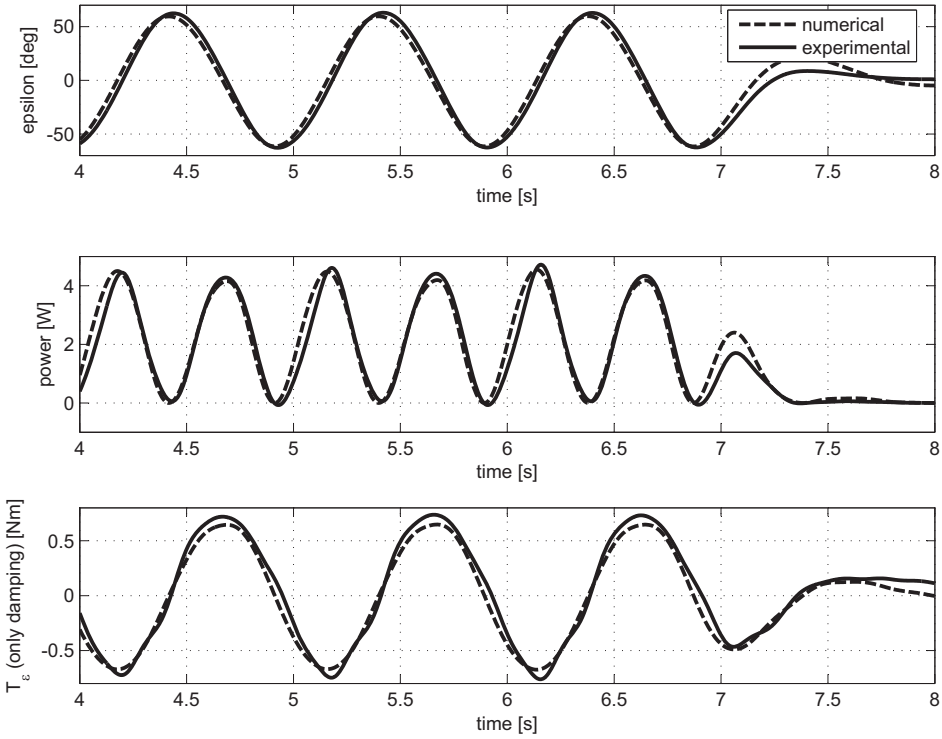

Figure 5.13. Experimental vs. numerical.

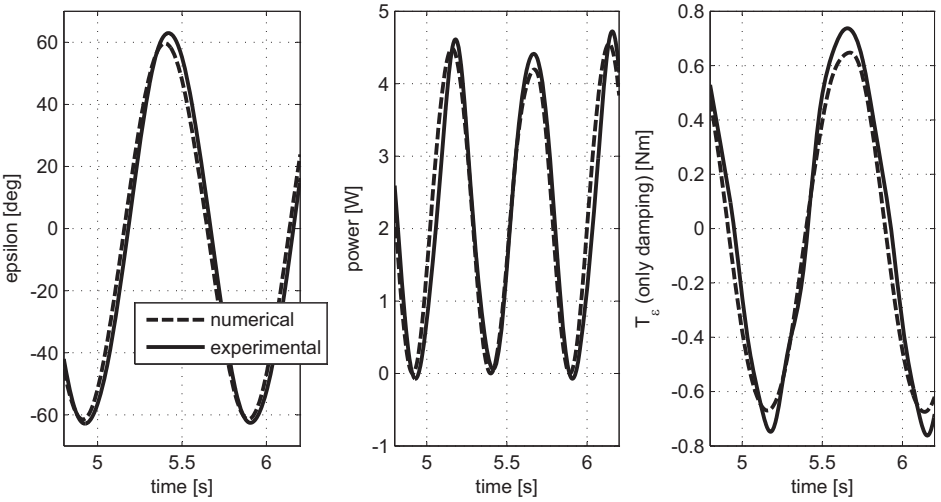

Figure 5.14. Experimental vs. numerical (zoom).

Chapter 6

Tank test

Between the 6^{th} and the 9^{th} of July 2009 the ISWEC device has been tested at the wave tank in Edinburgh. In this chapter the experimental setup, the test procedure and the obtained results are described.

6.1 The Edinburgh wave tank

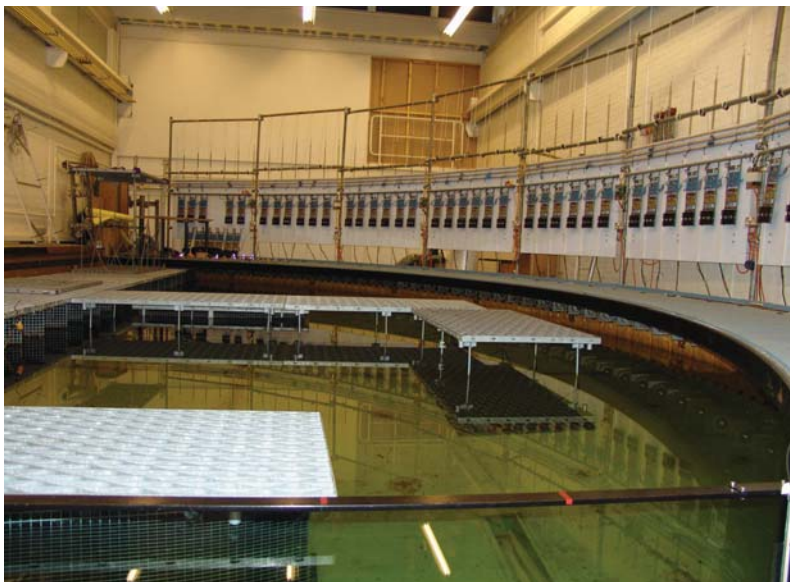

Figure 6.1. The Edinburgh curved wave tank.

The Edinburgh curved wave tank is designed to produce regular and irregular waves (see 3.1 and [34] for further details). The tank is designed to work at a nominal

scale of 1/100 compared with North-East Atlantic waves, and so the wave heights are relatively small (maximum around 110 mm) and the frequency range quite high (principally between 0.5 and 1.6Hz). In this project the tank was used to produce the 'nominal wave' with 1 Hz frequency, 1.56 m wavelength and 100 mm height used in chapter 3 to design the prototype. The tank depth is 1.2 m and since this value is much greater than half of the wavelength, the waves can be considered to be in deep water.

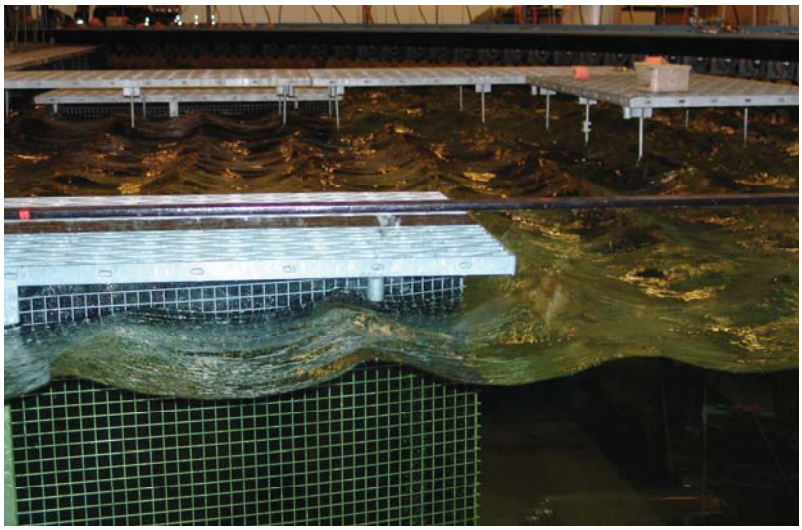

Figure 6.2. A bidimensional wave. The wave is generated from the wavemakers on the right and absorbed by the beaches on the left.

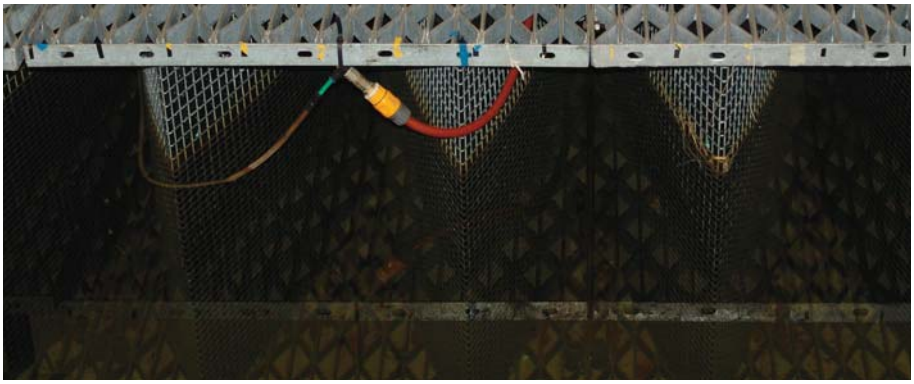

Figure 6.3. A particular of the beaches.

6.2 Experimental setup

The experimental setup (Daq card, software and equipment) used in Edinburgh is the same used for the dry test described in chapter 5. The acquired signals are the same too, except for the torque T_ε that has not been possible to acquire. In fact during the Daq system tuning, a problem on the encoder arose: due to a problem in a connector, the signal coming out from the encoder was corrupted carrying a lot of spikes. Time deriving the signal to obtain $T_\varepsilon = k\varepsilon + c\dot{\varepsilon}$ lead to a spiky torque set to the EPOS2 controller. This, combined with a not properly fixed load cell, caused hurts on the load cell from the PTO and a consequent miscalibration of the load cell. The whole process lasted only few seconds so it was not possible to act to save the system. However, knowing the EPOS2 setting, T_ε has been rebuilt mathematically afterwards.

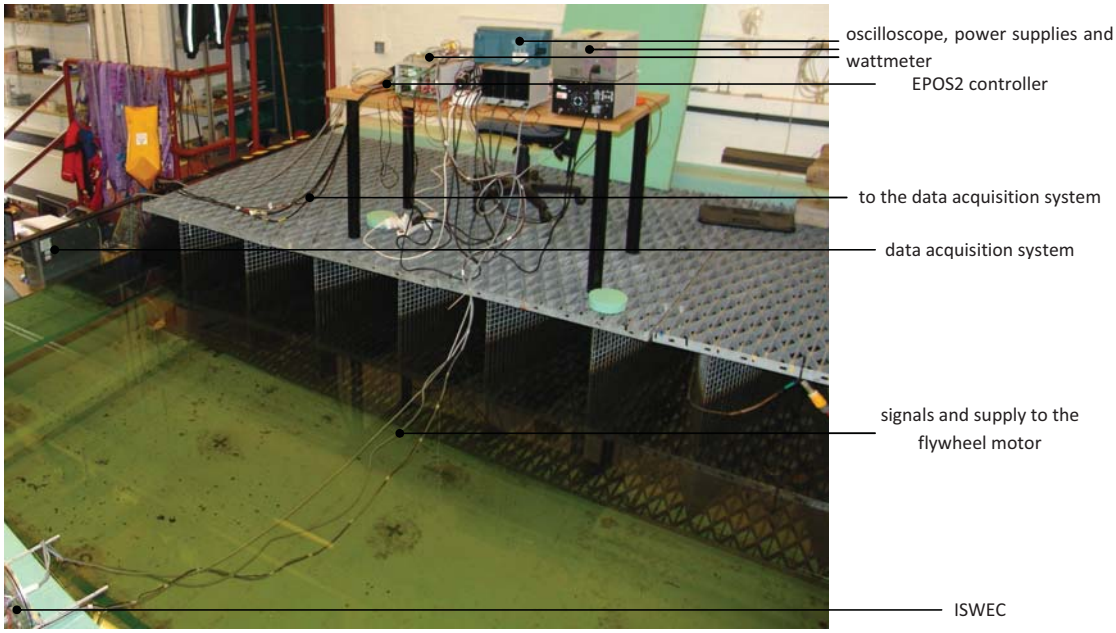

Figure 6.4. The ISWEC control desk.

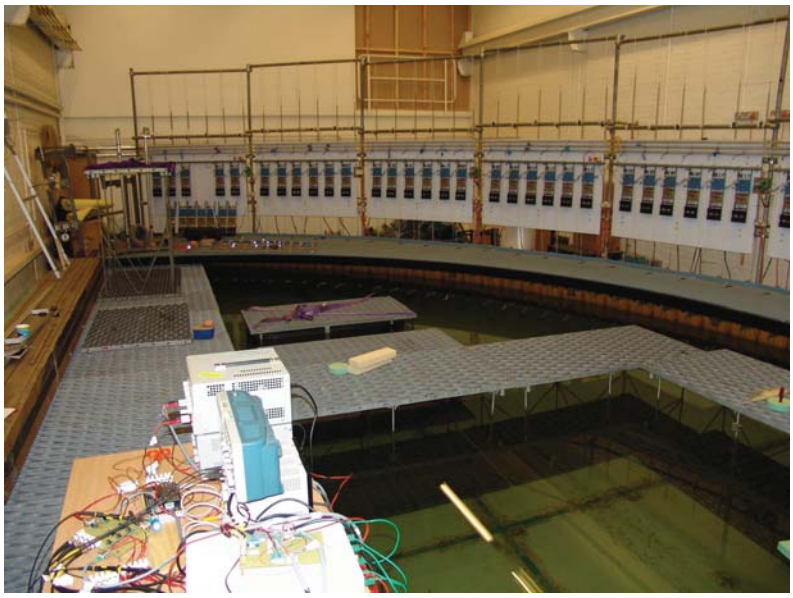

Figure 6.5. Another view of the wave tank along with the ISWEC control desk.

The ISWEC mooring has been implemented by using two mooring lines holding the forepart of the device, whereas in the back there was no need for mooring because the signals wires were stiff enough to maintain the device in position (and unfortunately influencing the system dynamics).

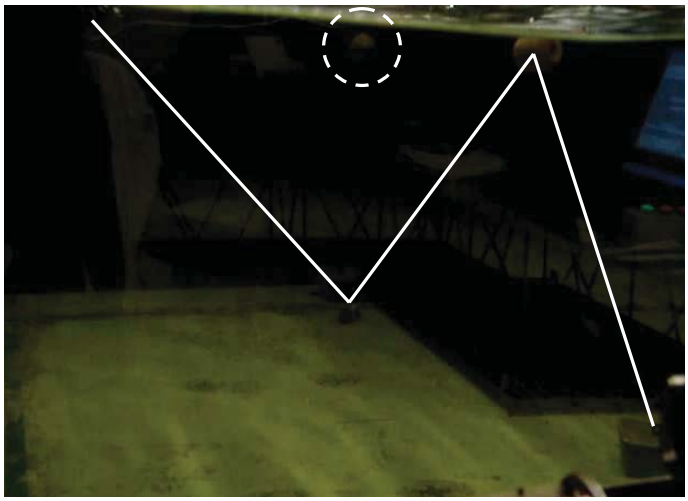

Figure 6.6. A view of a mooring lines (75 g sinker). The dashed circle highlights the float of the 2^{nd} line in background.

6.3 Main test

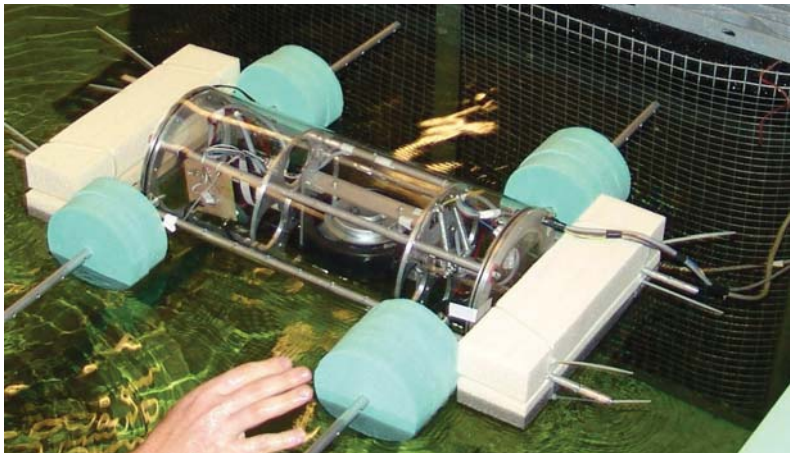

Figure 6.7. The device with side floats and extra floats at the extremities.

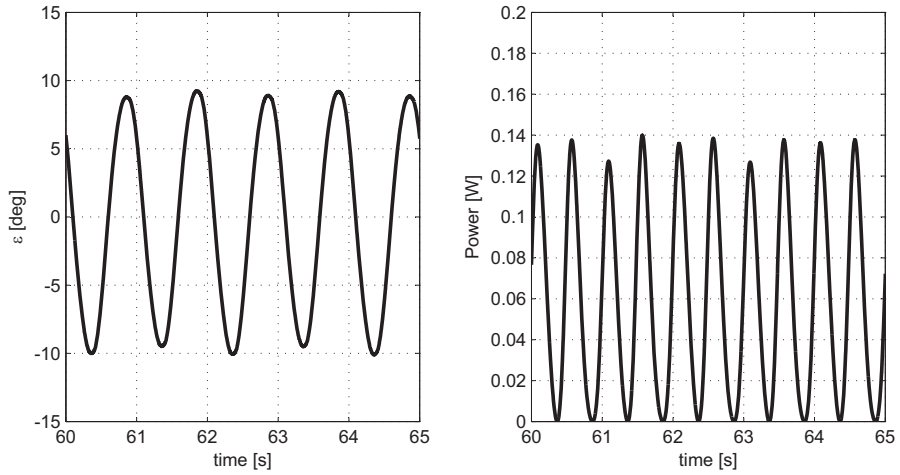

Figure 6.8. Time behavior of the system.

After some preliminary tests with small wave height, the 'nominal wave' was set on the tank controller. The device behaved as shown in figure 6.8: it was almost still. By switching off the gyro, the float was following almost perfectly the wave profile, but as soon as the gyro gained velocity, the stabilization action of the gyroscopic torque T_δ almost impeded the float to pitch. Being the float motion reduced, the average power absorbed by the device was also small, in this test 0.061 W.

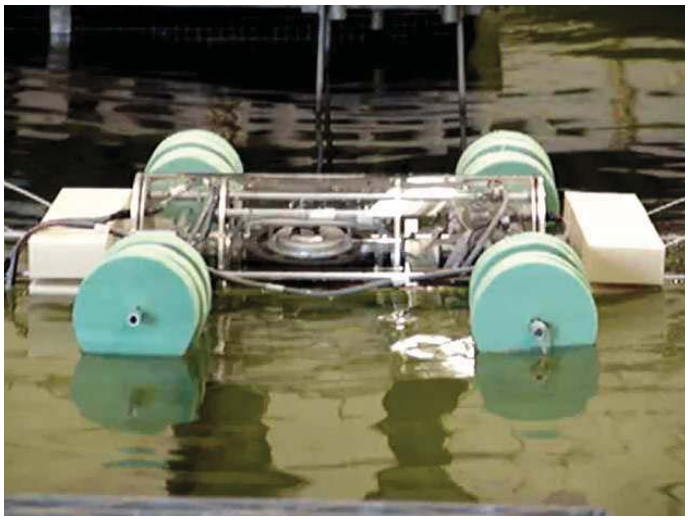

Figure 6.9. The device working with a small wave.

In order to make the float able to transfer the wave actions to the gyroscopic system, two extra-floats were introduced, but the situation only slightly improved: from 0.061 W the power capture passed to 0.12 W.

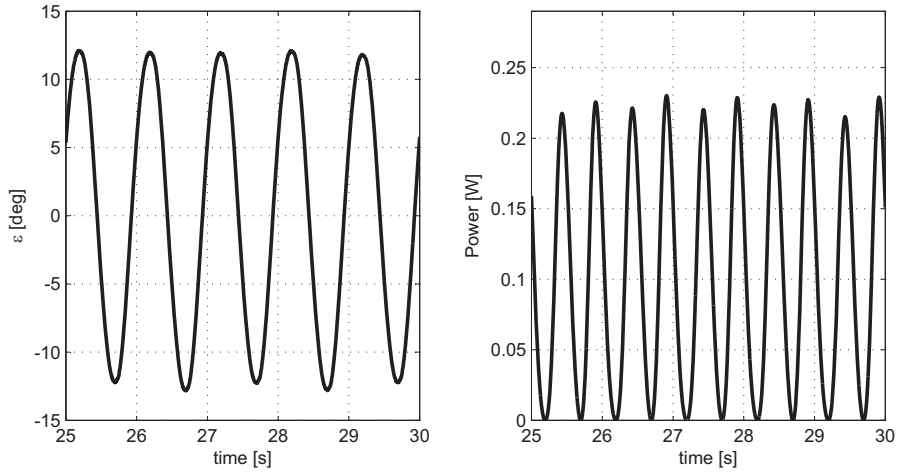

Figure 6.10. Time behavior of the system with extra floats.

The float demonstrated to be unable to transfer the needed pitching torque from the water to the gyro. Thus we decided to dramatically increase the float size: ISWEC was leant over a whole Divinycell slab 1200 mm wide 800 mm long 40 mm thick. Figure 6.11 shows the new plain float.

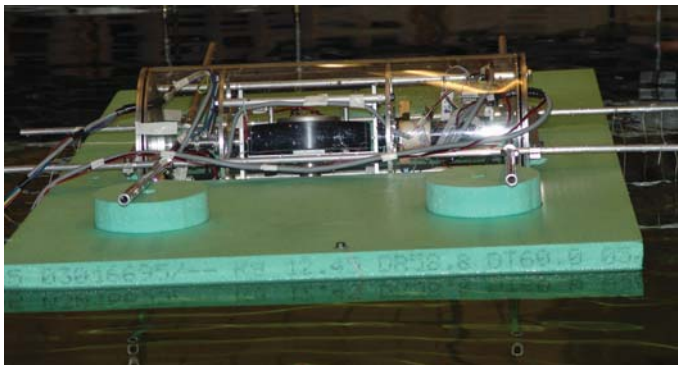

Figure 6.11. The plain float.

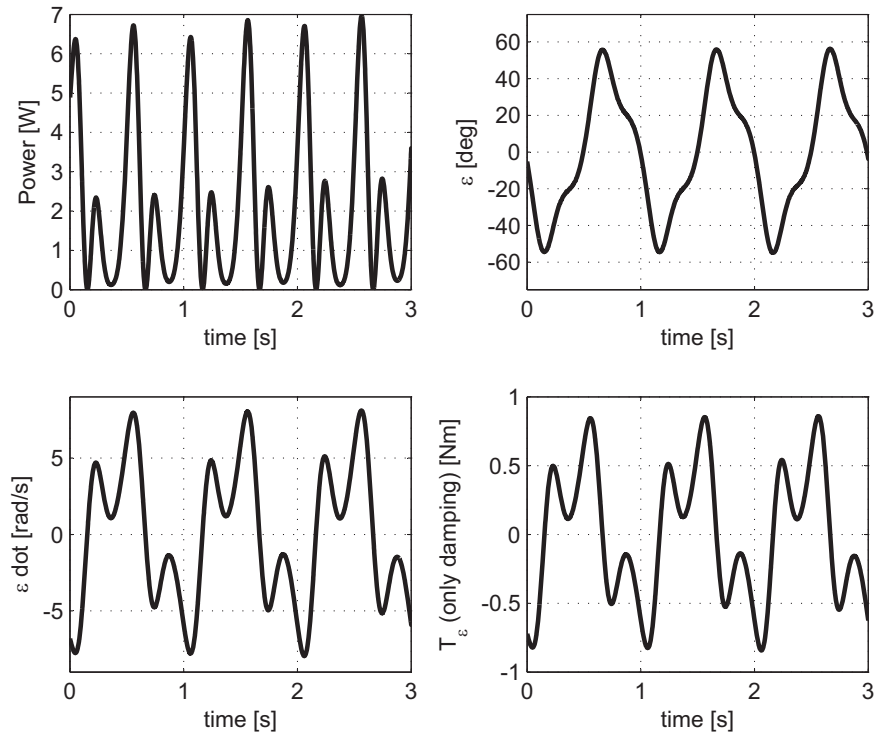

Figure 6.12. Time behavior of the system with the plain float.

In this case the behavior of ISWEC really improved: as figure 6.12 shows, the gyro oscillated with $\varepsilon_0 = \pm 56.3 deg$ nearly to the Cfg. A rated ε_0 60.7 deg. The average power extracted in these conditions was 2.06 W.

Figure 6.13. The system with the plain float.

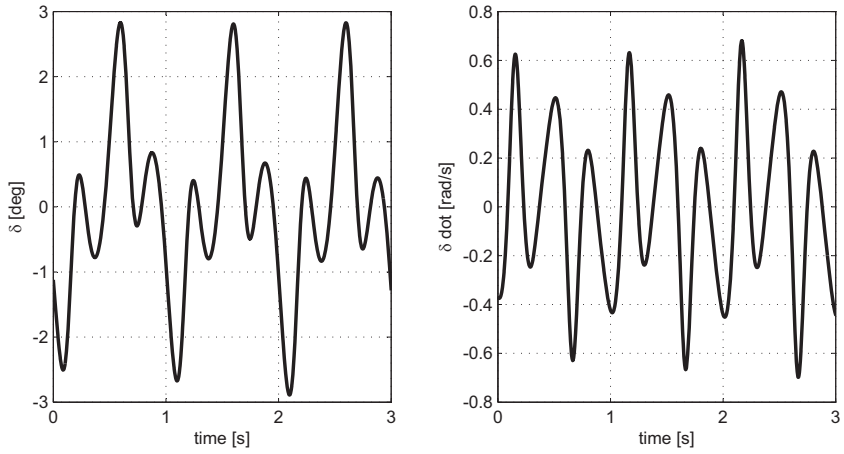

Figure 6.14. The float angle of pitching δ obtained through integration of the equation of motion.

The pitching rotation δ was not measured directly. In order to assess $\delta(t)$, it is recalled here the non linear equation of motion obtained in chapter 2 and then it is rewritten in order to separate $\dot{\delta}$.

$$I\ddot{\varepsilon} + c\dot{\varepsilon} + k\varepsilon = J\dot{\varphi}\dot{\delta}\cos\varepsilon \tag{6.1}$$

$$\dot{\delta} = \frac{I\ddot{\varepsilon} + c\dot{\varepsilon} + k\varepsilon}{J\dot{\varphi}\cos\varepsilon} \tag{6.2}$$

The velocity $\dot{\delta}$ is then integrated to obtain the float pitching angle δ. Even if this procedure could be not very accurate due to errors in the evaluation of the system main parameters, it allows to estimate that the float oscillated with an angle

comprised between 2 and 3 deg and therefore confirming the assumption on $\delta_0 = 2$ deg made in paragraph 3.2.

In order to get the exact float motion, in the test made in the flume present at the Department of Hydraulics of the Politecnico di Torino and described in the next chapter, the prototype has been equipped with an inertial sensor using three micro gyroscopic systems to measure the float orientation.

6.4 Wave power estimation

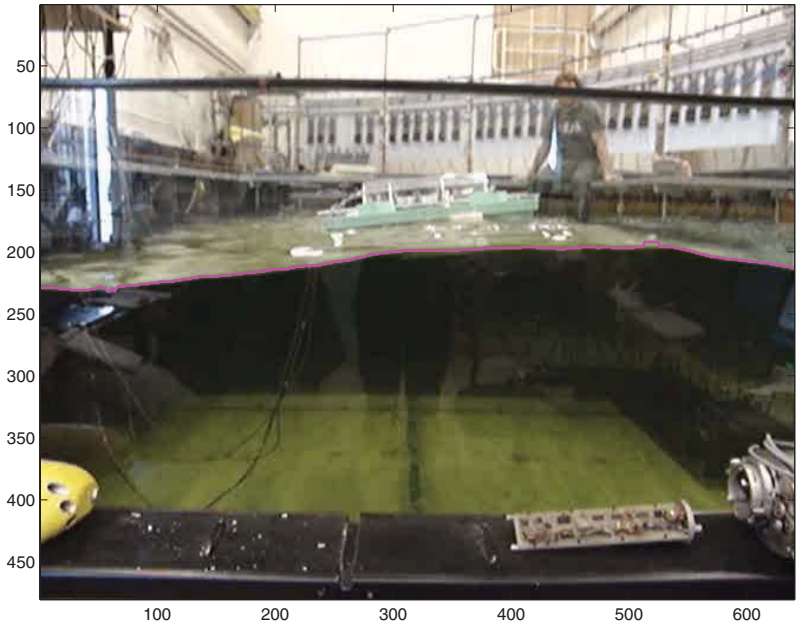

Figure 6.15. Image processing: wave profile identification (the purple line represents the captured profile).

During the test at the wave tank a video of the incoming wave through the glass has been recorded. As figure 6.15 shows, the video has been processed to capture the free surface and get the wave profile. Assuming the wave profile on the glass representative of the full wave and by approximating it with a regular sine wave[1], the power density is evaluated[2]. The video was shot at 25 frames per second and in

[1]The curve fitting procedure described in the paragraph 5.4 has been used to fit the data.

[2]This method has been improved for the flume tests described in chapter 7 where a high definition camcorder has been used to capture the wave. The tank can measure the wave height through resistive wave gages, but in this case unfortunately they have not been used because of the delay induced from the broken load cell on the test schedule.

relatively low resolution (640 x 480) so the resolution on the wave height is about 7 mm.

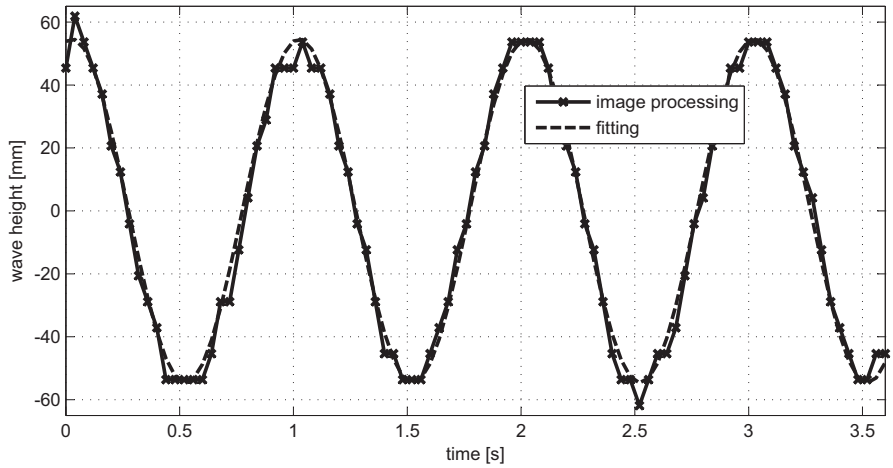

Figure 6.16. Wave height time plot.

$$P_D \simeq 1000H^2T = 1000 \cdot 0.1092^2 \cdot 1.003 = 11.96\frac{W}{m} \tag{6.3}$$

The fitted regular wave height is 109.2 mm whereas the period is 1.003 s. Such a wave carries a power density of 11.96 W/m. The nominal incident power is therefore:

$$P_D \cdot width = 11.96\frac{W}{m} \cdot 1.2m = 14.35W \tag{6.4}$$

The achieved relative capture width is $RCW = \frac{2.06}{14.35} = 14.3$ % and it is about six times smaller than the design value. However the procedure to evaluate both the absorbed power P_d and the wave power density P_D are not rigorous and the final value can be afffected from not negligible uncertainities. The wave tank tests at the University of Edinburgh were the first 'wet' tests the ISWEC prototype underwent and a first idea of the device performances has been obtained.

However, another campaign of test is needed.

Chapter 7

Flume test

The test in the wave tank at the University of Edinburgh allowed to estimate the prototype behavior with the regular wave at 1 Hz and 100 mm amplitude. Unfortunately due to data loss a complete understanding of the system has not been possible. The same wave has been created at the flume at the Department of Hydraulics of the Politecnico di Torino in order to assess more precisely the prototype dynamics. The system was integrated with a gyroscopic sensor able to measure the buoyant rotations.

7.1 The flume

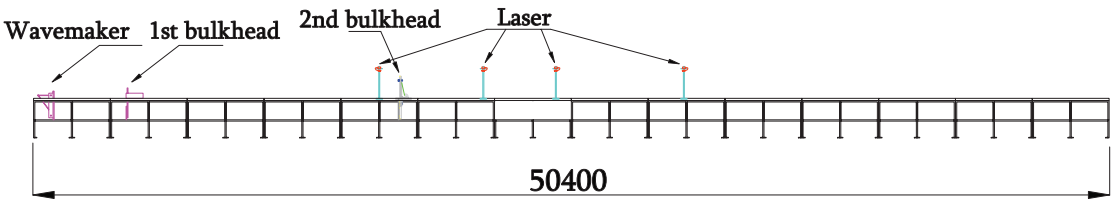

Figure 7.1. Flume scheme.

The wave making performances of the flume present at the Department of Hydraulics match the small scale ISWEC prototype wave requirement: the electrically driven wave maker can generate regular waves up to the frequency of 3 Hz and heights of about 150 mm when the flume is filled with 500 mm of water. The flume is 50.4 m long, 930 mm deep and 610 mm wide and its side walls are made of Plexiglas to observe the experimentation. It can be filled in few minutes thanks to a big duct

directly connecting a raised reservoir to the flume. The reservoir is filled from a underground channel flowing under the entire Hydraulics laboratory.

For this experiment the flume was equipped with a high definition (1920 x 1088) camcorder measuring the incoming wave through the lateral Plexiglas panel.

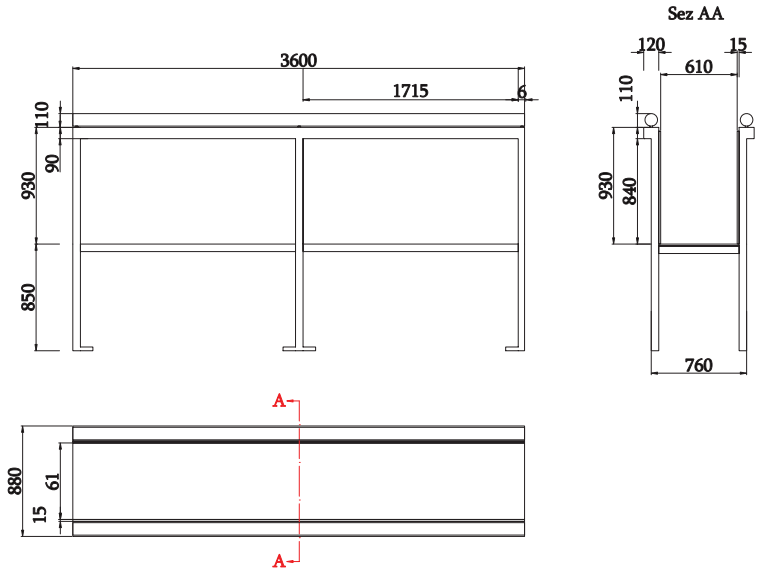

Figure 7.2. One of the 14 double sections composing the flume.

Figure 7.3. The wave maker.

7.2 Gyroscopic sensor

Figure 7.4. The MTi sensor (source: the XSens MTi and MTx User Manual and Technical Documentation).

The MTi sensor shown in figure 7.4 is a miniature, gyro-enhanced Attitude and Heading Reference System (AHRS). It carries internally a gyroscopic system able to assess the rate of turn of the sensor itself and a three directional accelerometer. Furthermore it mounts a 3D earth-magnetic field sensor to determine the orientation with respect to the earth. The sensor is USB-powered and thanks to the libraries provided with the sensor, it can be read directly from high-level softwares as Labview or Matlab. The low-power signal processor provides almost drift-free 3D orientation as well as 3D acceleration and 3D rate of turn (thanks to the gyros). The typical use for this sensor is to stabilize cameras, robots and vehicles. In this project it is used to measure the orientation of the float.

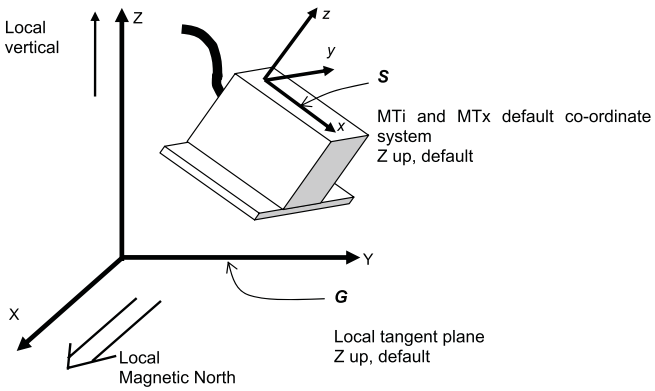

Figure 7.5. The MTi reference frame (source: the XSens MTi and MTx User Manual and Technical Documentation, G and S represent respectively the ground and the sensor reference frames).

		rate of turn	acceleration	magnetic field
Dimensions		3 axes	3 axes	3 axes
Full Scale		$\pm 300 deg/s$	$\pm 50 m/s^2$	$\pm 750 mGauss$
Linearity	[% of FS]	0.1	0.2	0.2
Alignment error	[deg]	0.1	0.1	0.1
Bandwidth	[Hz]	40	30	10
A/D resolution	[bits]	16	16	16
Sampling rate:		max. 120 Hz	max. 120 Hz	max. 120 Hz

Table 7.1. MTi main features.

7.2.1 Comparison with the wire transducer

In order to assess the performances of the MTi sensor it has been linked to the wave simulator during the normal working of the prototype, allowing this way a comparison between the wire transducer and the MTi sensor.

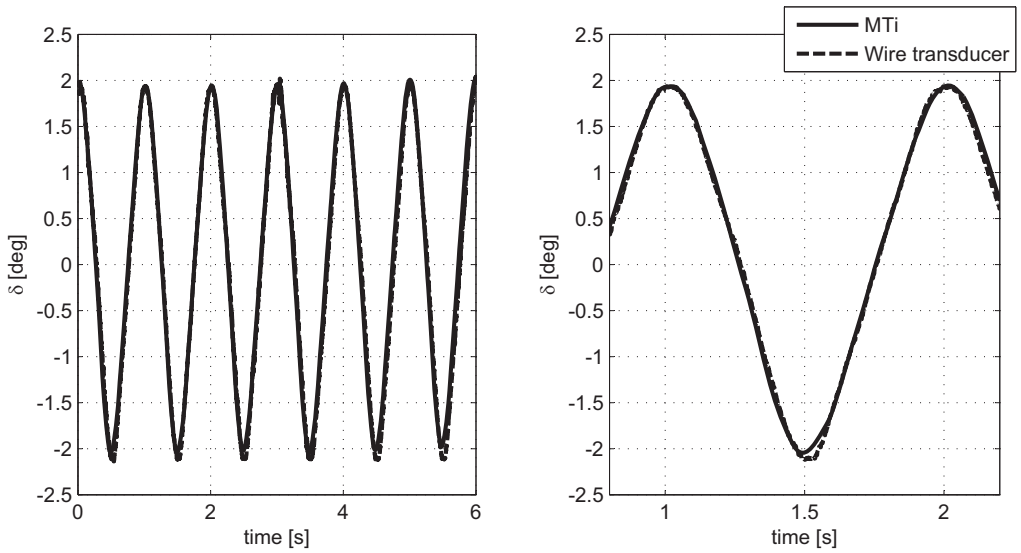

Figure 7.6. Comparison over δ between the wire transducer and the MTi sensor.

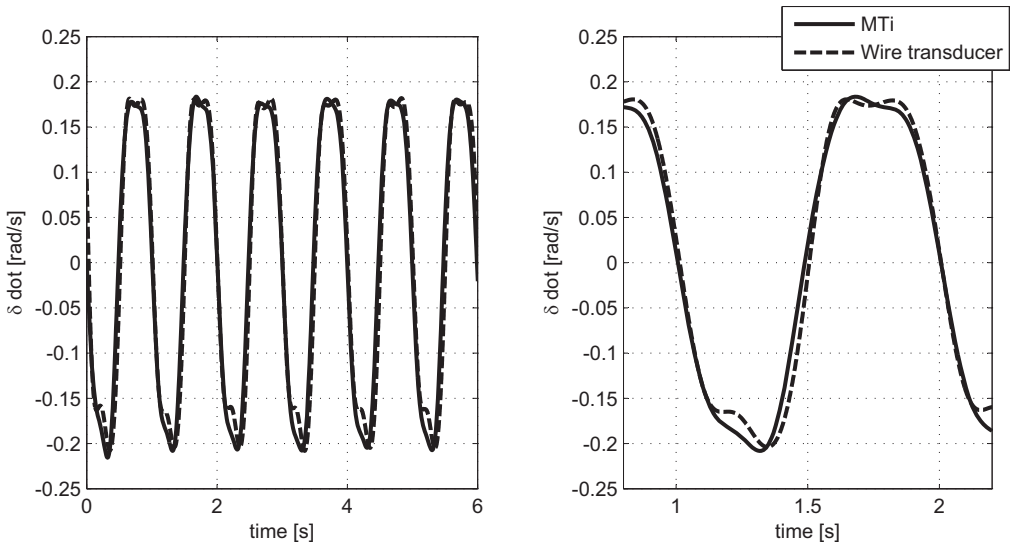

Figure 7.7. Comparison over $\dot{\delta}$ between the wire transducer and the MTi sensor.

7.3 The float

The prototype hull is improved with respect to the Divinycell slab used in the Edinburgh wave tank. In this case the hull is a 570 mm wide float with two fins deep into the water to stabilize the roll motion induced from the prototype . The bottom of the hull is shaped as shown in Figure 7.8. The top of the float presents a cylindrical hollow shape to accept the 230 mm diameter Plexiglas tube of the ISWEC prototype. The hull has been made in the following steps:

- construction of the internal wooden cage with the shaped bottom
- nailing of the Plexiglas sheet to the bottom of the cage
- positioning of the two external fins on the side of the cage (the fins were made using the 40 mm thick Divinycell slabs used in the Edinburgh tank)
- inserting the Polyurethane foam into the cage and putting the Plexiglas tube into the upper space before the foam dries
- once the foam is dry, the Plexiglas tube is removed and polished from the residual foam.

In this way a stiff buoyant with a perfect print of the external tube of the prototype is obtained, allowing a repeatable positioning of the prototype. The hull

is then completed by attaching two Teflon ribbons on the external faces of the fins in order to reduce friction with the walls of the flume as the device rocks.

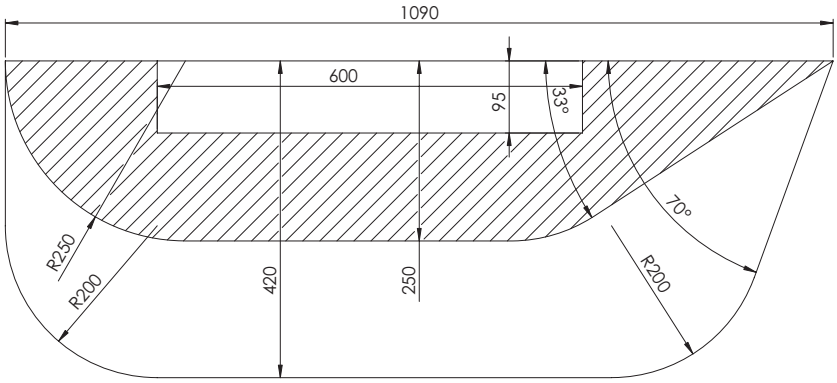

Figure 7.8. The hull used in the flume (wave coming from left to right).

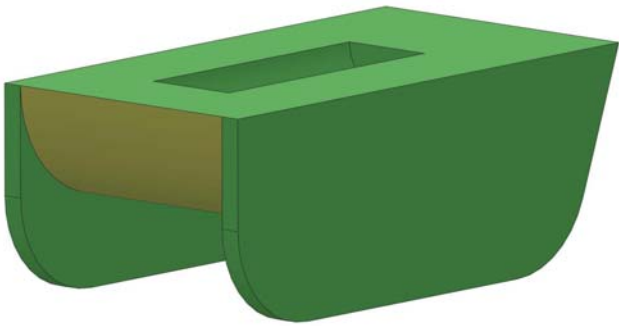

Figure 7.9. The hull used in the flume -3D representation.

7.4 Experimental setup

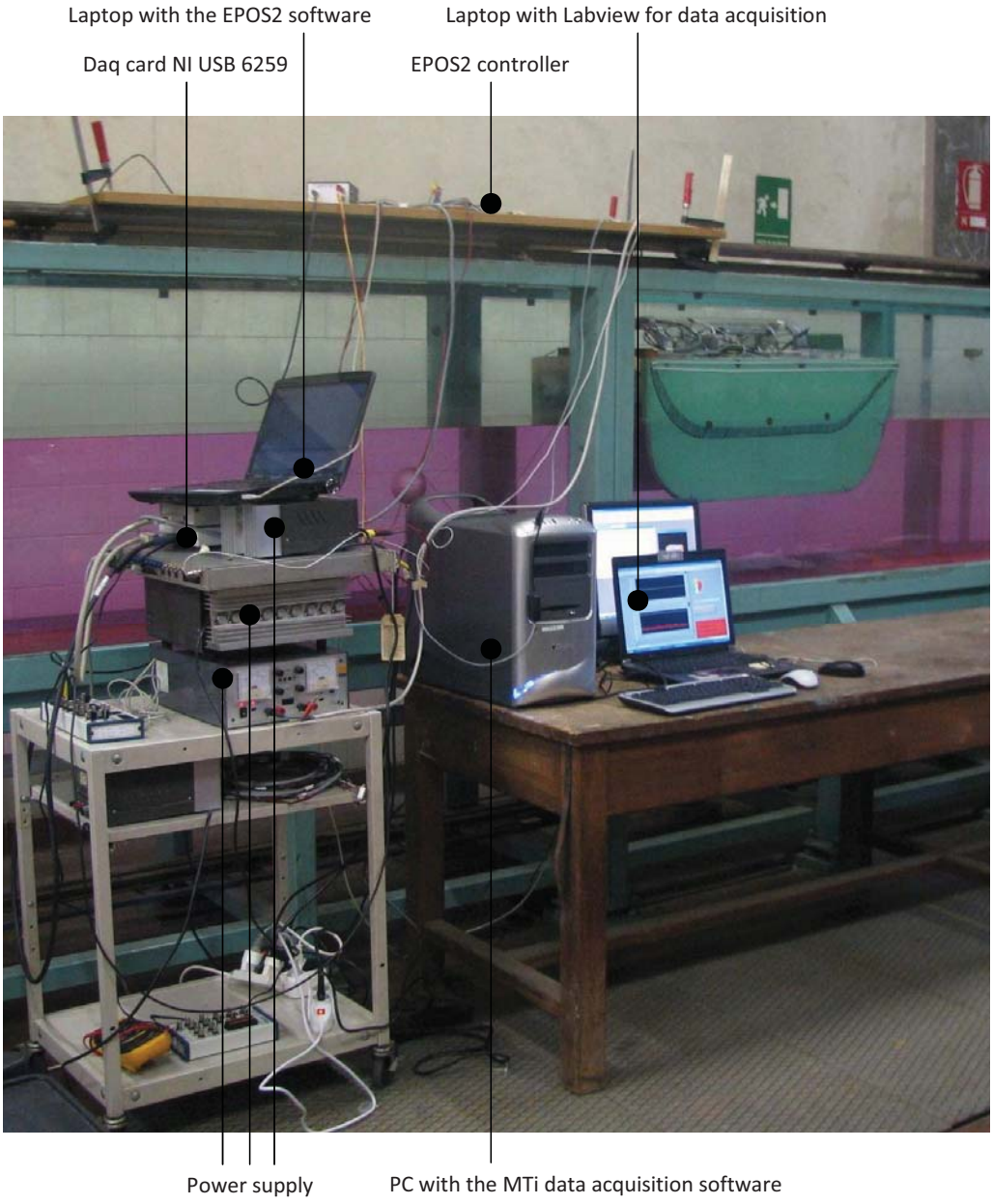

Figure 7.10. The experimental setup.

The prototype has been mounted on the float, connected to the data acquisition systems and to the power supplies and eventually put into the flume. A camcorder has been put upstream of the device to acquire the wave shape. The water has been hued with a pink biodegradable colouring allowing the camcorder to capture the wave. The PTO EPOS2 controller has been placed along with the load cell signal conditioner on a plaster plate on the top of the flume. The float has been moored to the bottom of the flume through the float and sinker chain as shown in figure 7.12.

The signals acquired are listed beneath.

National Instruments USB 6259 + Labview data acquisition system:

- angular position of the PTO shaft ε (counter input)
- load cell (analog input)
- z-oriented accelerometer - for synchronization purposes - (analog input)
- inductive pickup to measure $\dot{\varphi}$ (counter input)

MTi data acquisition system:

- float roll, pitch and yaw position (χ, δ and ψ) and velocity ($\dot{\chi}$, $\dot{\delta}$ and $\dot{\psi}$) of the hull
- z-axes acceleration - for synchronization purposes -

Figure 7.11. Close view of the prototype (the green case in the bottom right of the picture protects the MTi sensor from splashes).

A third PC has been used to program the EPOS2 controller. In this case we have no longer used a torque loop but a speed control. In fact by setting only the proportional gain of the PID controller of the velocity loop, the current in the motor (and so torque on the PTO shaft) is proportional to the velocity error. If the speed set point is zero, the system behaves as a linear damper. Thus there is no more need to externally acquire the encoder and calculate the torque set point to give it back to the analog input of the EPOS2 controller.

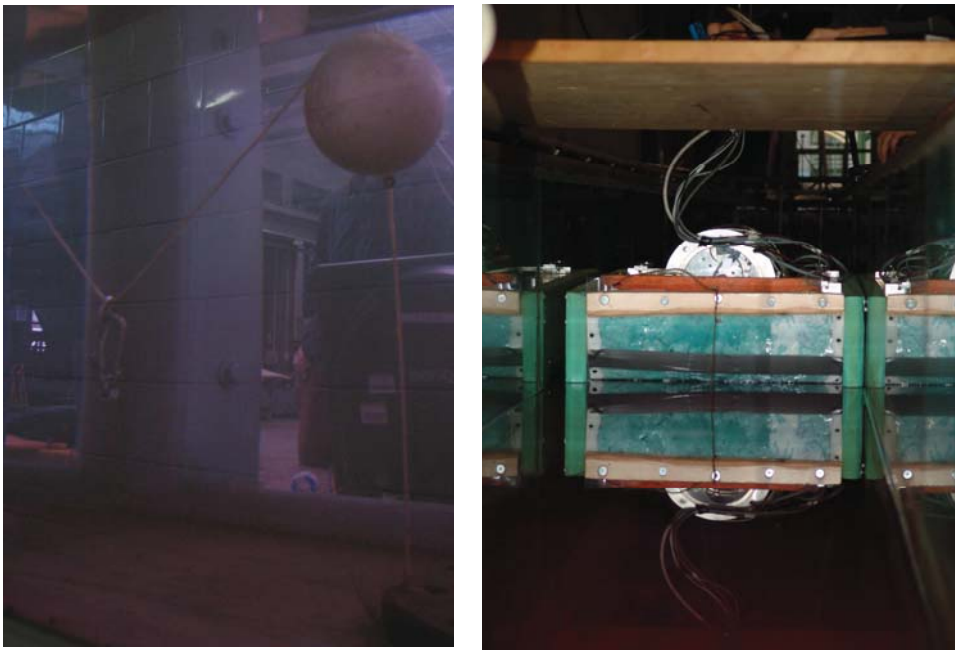

(a) The mooring line (43 g sinker). (b) Front view of the prototype.

Figure 7.12. Mooring line and flume front view.

7.5 Preliminary test: device switched off

In order to assess the float behavior, a first test with the wave at 100 mm and 1 Hz[1] and the flywheel angular velocity $\dot{\varphi} = 0$ has been performed. In this case the gyroscopic system behaves as an integral mass because the small friction due to the bearings on the ε axes impede the gyro to rotate. However to completely lock the ε axes, the EPOS2 controller has been set in the position control mode: giving a set point equal to zero, the controller maintains the gyro in the central position. Figure

[1]Since in the wavemaker control unit the wave frequency can be set only in pre-configured steps, the value closest to 1 Hz, 1.0194 Hz, has been selected.

7.13 shows the time-history of the buoy pitching angle δ, revealing an amplitude of motion δ_0 equal to about 10 deg.

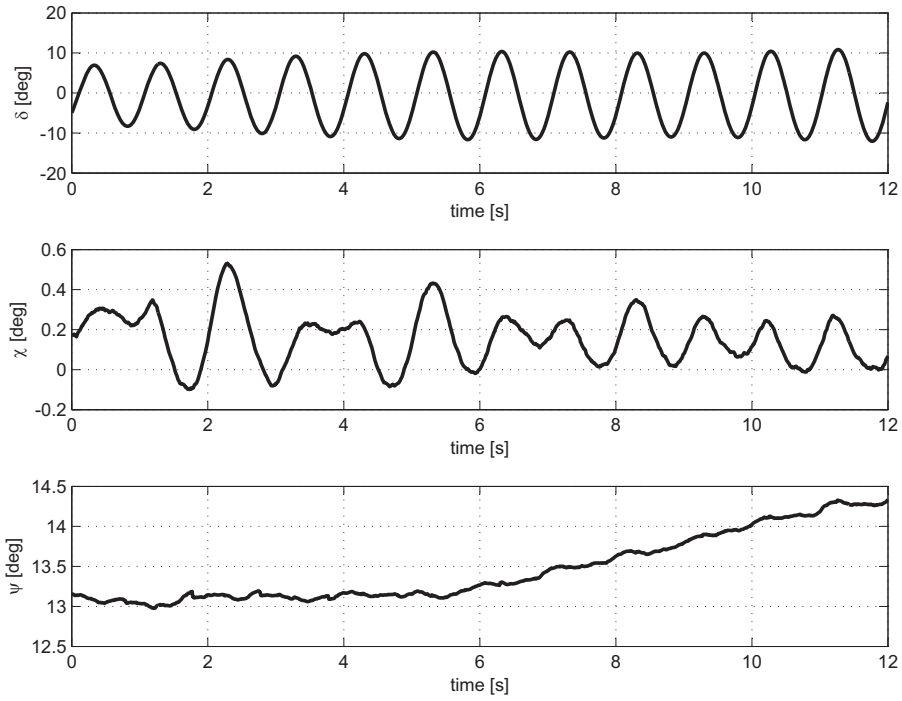

Figure 7.13. The Euler angles of the float with the ISWEC converter switched off.

7.6 Main test

The first flume test has been performed in the rated conditions[2] and then, to assess the system performances out of the rated condition, a series of tests has been done varying the gyro angular velocity $\dot{\varphi}$.

7.6.1 Rated conditions

The system has been set with the rated parameters and the nominal wave is produced. After few minutes, the flume and ISWEC reach the equilibrium: as shown in figure 7.21, since the ISWEC is almost still due to the action of T_δ, ISWEC behaves like a wall as wide as the flume and thus reflecting all the incoming waves.

[2]Cfg. A, refer to paragraph 3.4 for details.

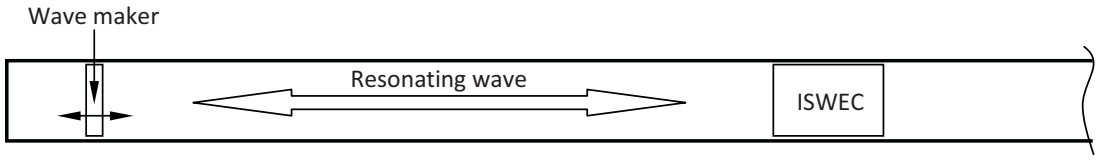

Figure 7.14. Resonating wave.

The reflected waves come back to the wave maker and, depending on the phase between reflected wave and wave maker, they can be reflected once more towards the ISWEC in addition to the generated wave. This generates a kind of 'beating' phenomenon, leading to waves bigger than the set amplitude and overtopping the buoy. In order to don't damage the sensors (in this configuration not completely watertight), the amplitude has been reduced to 70 mm. Figures 7.15 and 7.16 show the real wave as the ISWEC works.

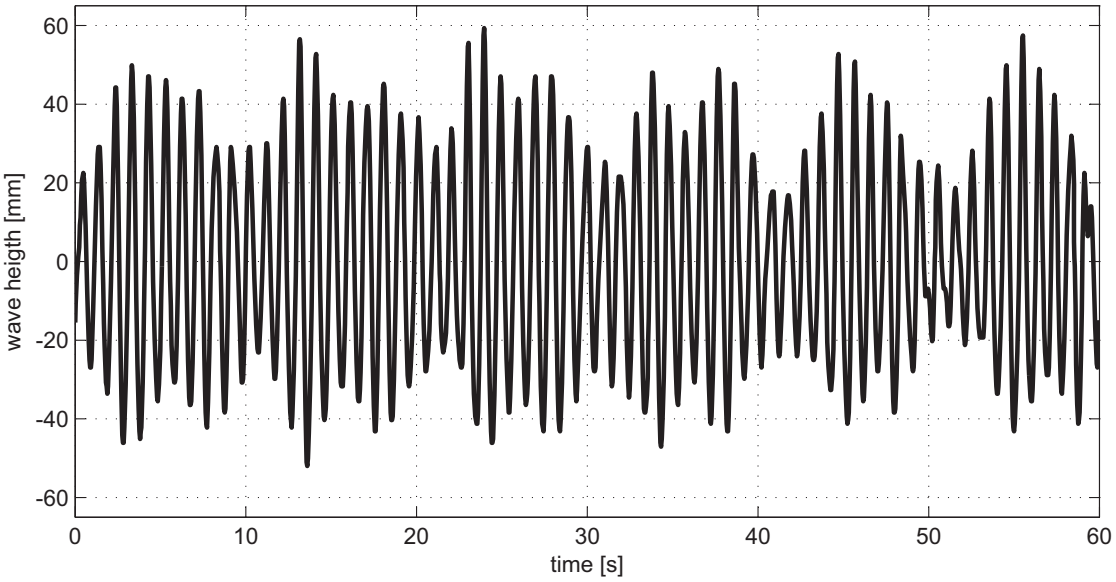

Figure 7.15. Time plot of the wave height with the gyroscope running at 2000 rpm.

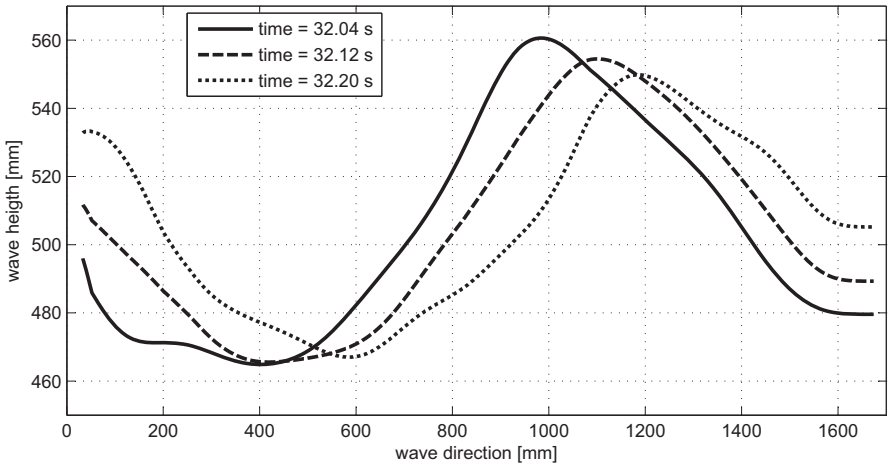

Figure 7.16. Wave height plot with the gyroscope running at 2000 rpm.

7.6.2 Wave power evaluation

The wave power density has been evaluated by elaborating the time series coming from the image processing of the camera recording. Figure 7.17 shows a sample frame from the video recording.

Figure 7.17. A shot from the camera record.

The wave signal in this case is the sampled time history of the wave height (taken in the middle of the window and subtracted of the mean value).

The wave power analysis has been carried out by managing these sampled data in the frequency domain [37].

The autocorrelation function R_{xx} of the signal $x(t)$ is defined as:

$$R_{xx}(\tau) = E[x(t) \cdot x(t+\tau)] \tag{7.1}$$

Where $x(t)$ is a stationary random process and $E[\cdot]$ represents the expected value. The *power spectral density function* is defined as the Fourier Transform of R_{xx}.

$$S_{xx}(\omega) = \int_{-\infty}^{\infty} R_{xx}(\tau) e^{-\jmath\omega\tau} d\tau \tag{7.2}$$

The power spectral density function states that the average power of the signal is decomposed in the frequency domain, in fact:

$$Var(x(t)) = \sigma_x^2 = \int_{-\infty}^{\infty} S_{xx}(f) df \tag{7.3}$$

The nth moment of such power spectral density function is defined as follows.

$$m_n = \int_0^{\infty} f^n S_{xx}(f) \mathrm{d}f \tag{7.4}$$

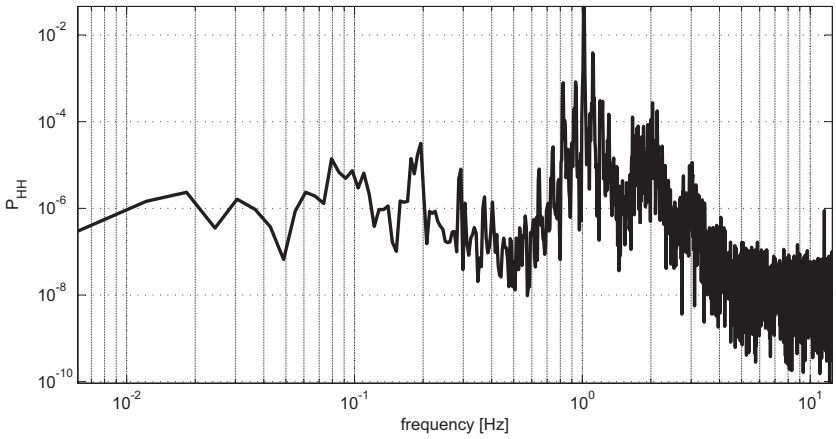

Figure 7.18. Wave height power spectral density. The main peak is on the spectral line at the frequency 1.022 Hz, coherent with the 1.0194 Hz set on the flume controller.

The significant wave height H_s, the wave energy period T_e and the wave power

density P_D are evaluated as follows [10][3].

$$H_s = 4\sqrt{m_0} = 4\sqrt{6.609 \cdot 10^{-4}} = 102.8mm \tag{7.5}$$

$$T_e = \frac{m_{-1}}{m_0} = \frac{6.478 \cdot 10^{-4}}{6.609 \cdot 10^{-4}} = 0.981s \tag{7.6}$$

$$P_D = \frac{c}{16} T_e H_s^2 = \frac{7.87}{16} \cdot 0.981 \cdot 0.1208^2 = 4.997 \frac{W}{m} \simeq 5 \frac{W}{m} \tag{7.7}$$

Being the float 570 mm wide, the nominal incident power is $P_D \cdot W = 4.997 \cdot 0.57 = 2.85W$

7.6.3 Mechanical analysis

The float pitching angle δ is smaller than the $\pm 2deg$ desired and presents a low frequency 'beating' visible in the PSD in figure 7.19.

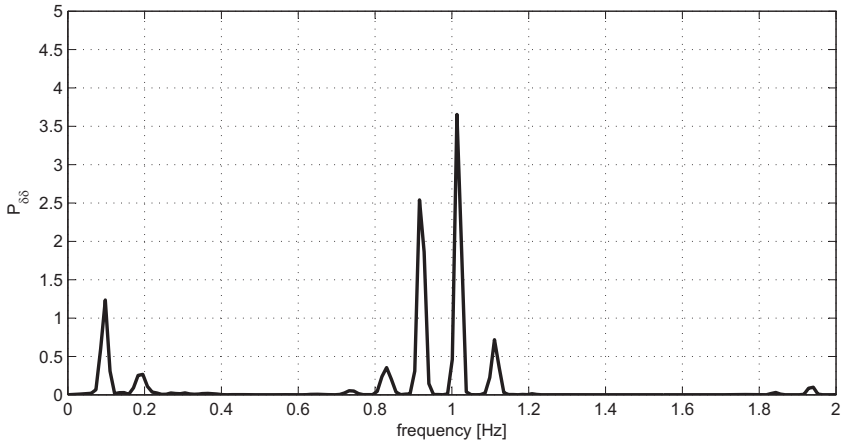

Figure 7.19. Float pitch power spectral density.

[3]The dispersion relationship from the Airy linear wave theory ($\omega^2 = gk \tanh(kd)$) links the wave period to the wave number. By evaluating the wave number with the deep water formula (a wave travels in deep water when the depth is bigger than half the wavelength: being the wave length in this case roughly 1.5 m and the water depth 505 mm, the wave is almost in deep water conditions) it results $k = \frac{2\pi}{\lambda} = \frac{4\pi^2}{gT_e^2} = 4.19$. By substituting this value in the dispersion relationship it is possible to iteratively converge to the real wave number assessed as $k = 4.011$, smaller than the deep water wave number of the 4.2%. Due to this small difference, in this work the deep water conditions are assumed: the estimated coefficient c in the 7.7 is therefore equal to $\frac{\rho g^2}{4\pi} = 7.87 \frac{kWs}{m^3}$.

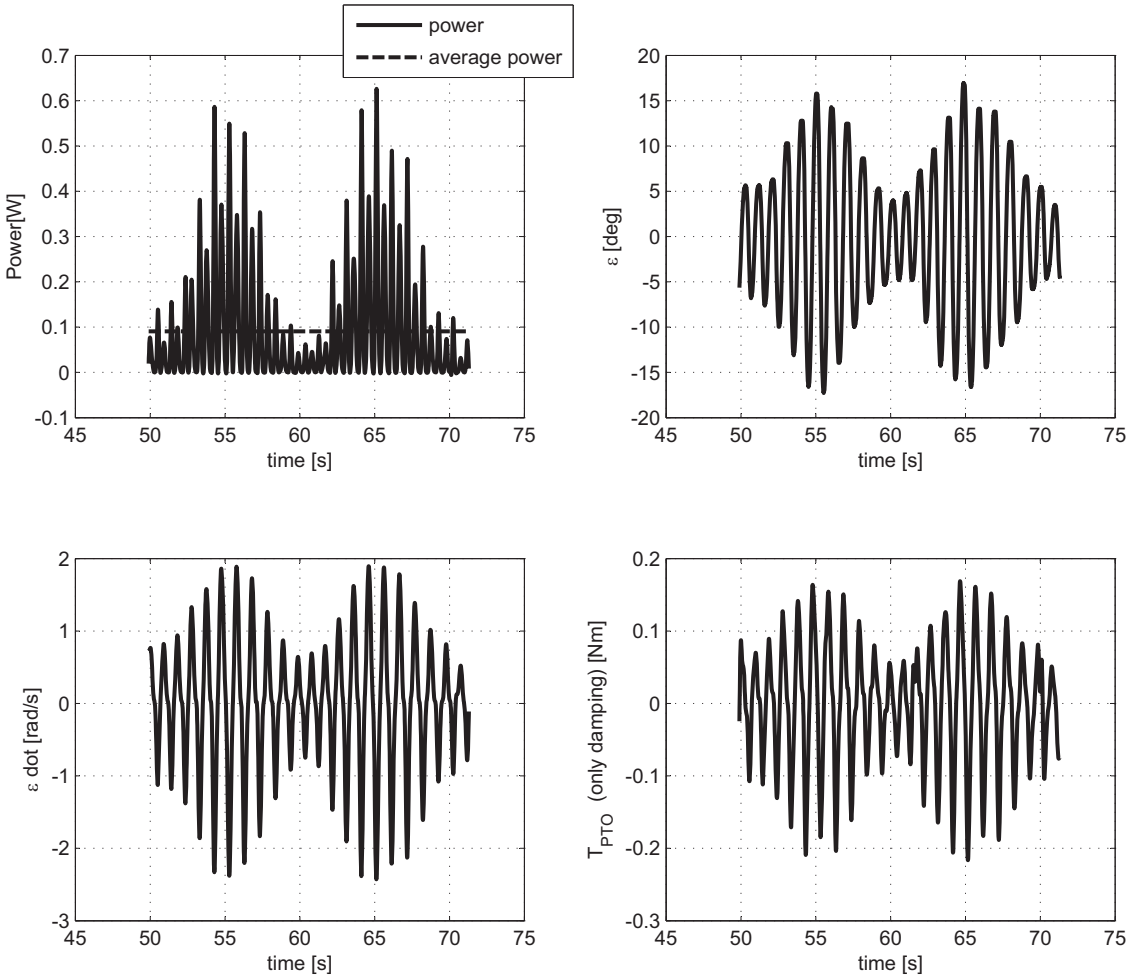

Figure 7.20. Time histories at 2000 rpm.

The analysis has been therefore carried out taking a 91.75 s time span corresponding to 90 wave periods and about 9 (8.998) cycles of the low frequency beating-like phenomenon. In this way it's possible to assess the average values of the acquired signals. Figures 7.20 and 7.21 show the time behavior of the system.

In this configuration the float is not able to transfer the wave energy to the system. The average power in input to the PTO is 0.08 W, and generally all the main quantities of the system are far from the desired values. In other words, due to the big value of $\dot{\varphi}$, a small velocity around ε is enough to create a large torque T_δ: T_δ and $\dot{\delta}$ are almost phased, so the effect of ISWEC on δ is the same as a large

damper[4]. Referring to the float we are experimenting, the 'damping factor' is too big and practically inhibits any motion along δ, impeding the power extraction.

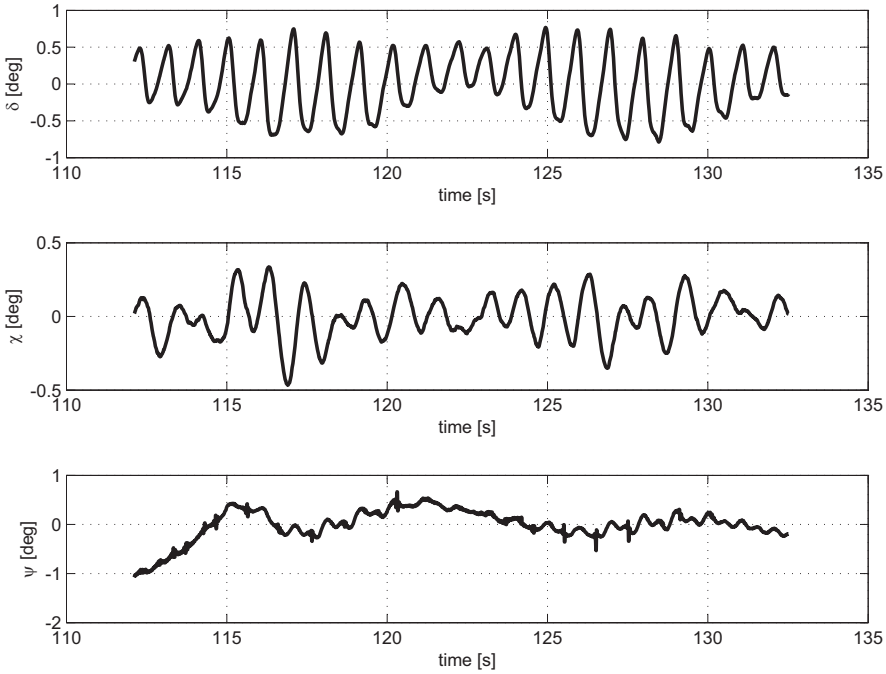

Figure 7.21. Float Euler angles in Cfg. A.

[4]The linearized equations (2.11) provide a quick view of the system interactions.

7.6.4 Reduction of the gyro speed

By reducing the angular velocity $\dot{\varphi}$, the damping action on the waves is reduced and, as (2.18) states, if the amplitude δ_0 increases more than the $\dot{\varphi}$ reduction, the amount of extracted power increases. Since the device tested in the rated conditions was found too stiff along the motion δ, the angular velocity $\dot{\varphi}$ has been reduced in five steps from 2000 rpm to 330 rpm. As shown in table 7.2 and figure 7.24, the reduction of $\dot{\varphi}$ allows the float to oscillate more freely, and since the gain on the amplitude of δ_0 is bigger than the reduction of $\dot{\varphi}$, the extracted power increases up to 0.89 W at 520 rpm. The last test at 330 rpm shows that in this case the power absorbed from the system diminishes because the small increase of δ (+17.2% on the rms value) can't compensate the -34% reduction of $\dot{\varphi}$.

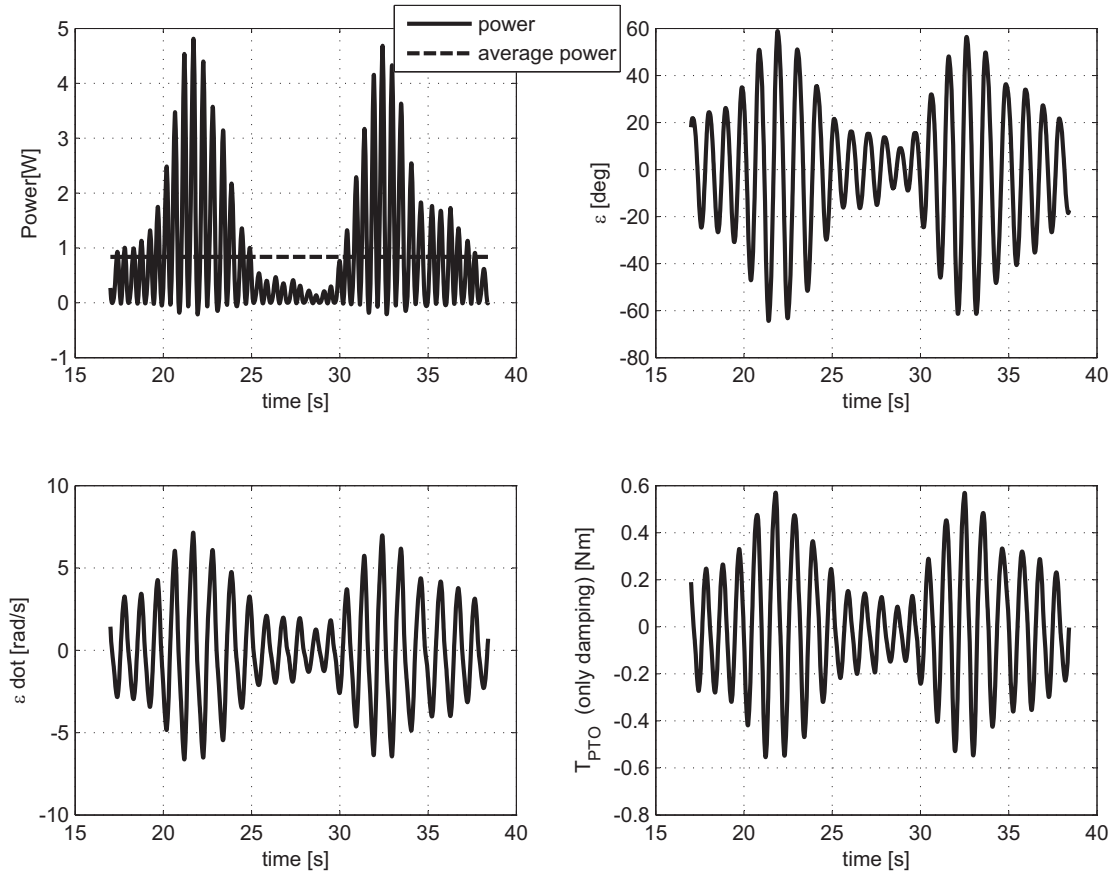

Figure 7.22. Time histories at $\dot{\varphi} = 520$ rpm.

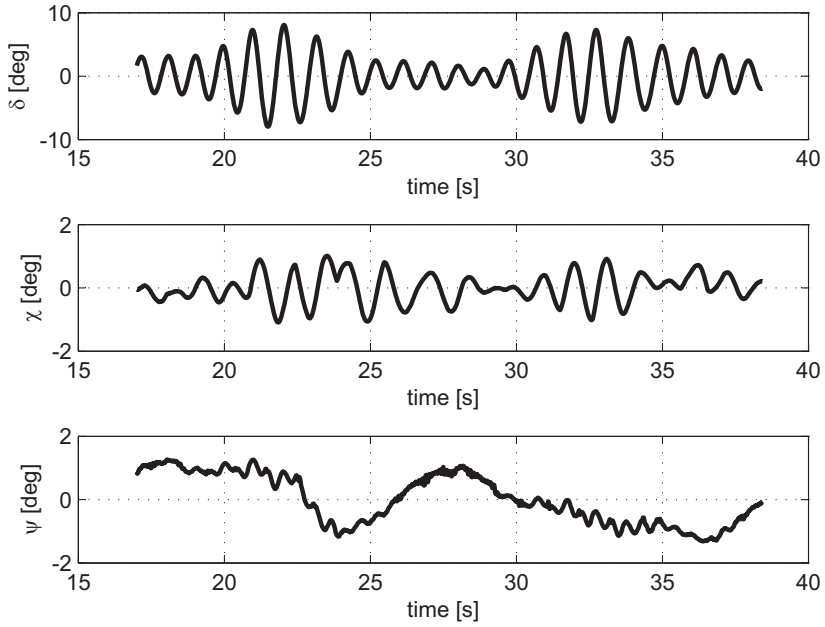

Figure 7.23. Float Euler angles with $\dot{\varphi} = 520$ rpm.

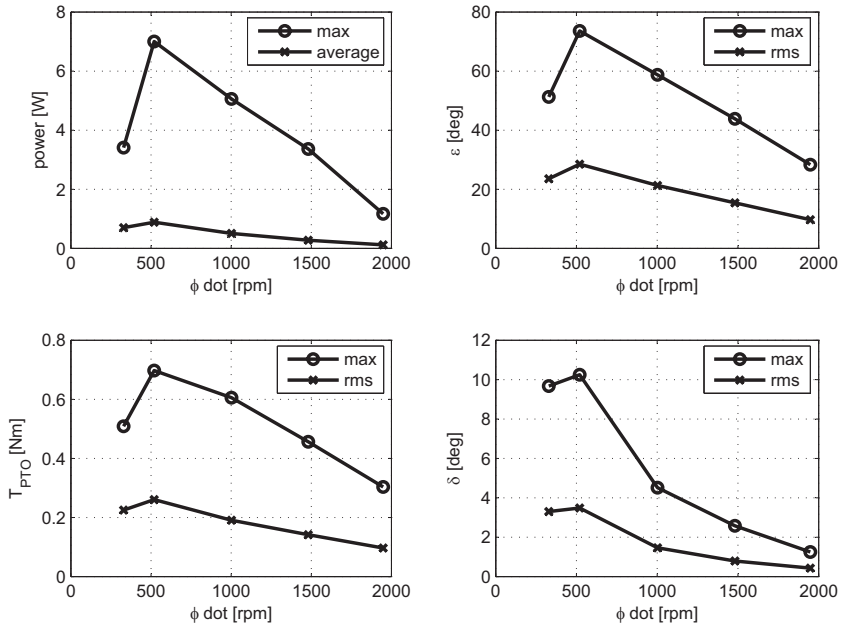

Figure 7.24. Influence of $\dot{\varphi}$ on the system.

$\dot{\varphi}$	[rpm]	330	520	1000	1480	1970
P_d -average-	[W]	0.7	0.89	0.51	0.28	0.11
P_d -max-	[W]	3.41	7	5.06	3.36	1.17
P_D -average-	[W/m]	6.59	7.21	6.54	5.53	4.997
P_R	[W]	3.76	4.11	3.73	3.15	2.85
RCW	[%]	18.6	21.6	13.6	8.7	3.6
$\hat{P}_d$ -average-	[W]	0.57	0.7	0.4	0.22	0.08
$\hat{P}_d$ -max-	[W]	2.71	5.61	4.05	2.71	0.95
ε -rms-	[deg]	23.57	28.49	21.31	15.4	9.7
ε -max-	[deg]	51.25	73.59	58.73	43.86	28.32
δ -rms-	[deg]	4.2	3.48	1.46	0.79	0.43
δ -max-	[deg]	9.67	10.25	4.51	2.58	1.25
χ -max-	[deg]	0.65	1.51	1.62	1.19	0.85
ψ -max-	[deg]	1.42	2.1	1.45	1.83	1.57
$\dot{\varphi}$ ripple	[deg]	0.98%	0.79%	0.46%	0.29%	0.27%

Table 7.2. Results of the analysis varying $\dot{\varphi}$.

7.7 Chapter remarks

The maximum relative capture width achieved from the device is the 21.6%, bigger than the 14.3% achieved in the wave tank in Edinburgh with a simplified float. However, the interesting outcome of the experimentation in the flume is that to absorb almost the 50% of the rated power a flywheel angular speed $\dot{\varphi}$ of only the 25% of the rated value is needed. This value has been achieved because in those conditions δ_0 is bigger than the ± 2 deg hypothesized. This means that the float can rock with a bigger amplitude and therefore, according to the (2.19), it absorbs the same power with a smaller angular momentum. In order to assess the real potential of the ISWEC prototype, in the next months it will be tested at the wave tank present in the University Federico II in Naples described in the next chapter.

The same wave tank will be used even to test a bigger device designed thanks to the outcomes of the experimentation performed both in the Edinburgh wave tank and in the flume in Torino.

Chapter 8

Design of a 1:8 scaled prototype

Using the results obtained in the wave tank at the University of Edinburgh and in the flume at the Department of Hydraulics of the Politecnico di Torino a bigger device has been designed for testing at the wave tank present at the University of Naples. The target of this chapter is to design a device working in the Naples wave tank with the biggest scale possible. The design process is going to finish by May 2010, the construction and dry test (on a purposedly built test rig similar to the wave simulation rig described in paragraph 5.1) by October 2010 and finally the tank tests are scheduled for December 2010. If the results are going to be satisfactory, the next step of the project will possibly be the full scale device or a device 1:2 scaled.

8.1 The wave tank

Figure 8.1. A view of the Naples wave tank.

The wave tank present at the University of Naples Federico II is composed of a tank 145 m long, 9 m wide and 4.5 m deep coupled with a wave generator and

completed with a sensorized overhead traveling crane to test models of keels moving with respect to the water. The tank can generate regular and irregular waves as shown in table 8.1.

Depth	4.2 m
Width	9 m
Length	145 m
Sinusoidal waves	
$\frac{H}{\lambda}$	$\frac{1}{100} \div \frac{1}{15}$
λ_{max}	9 m
Random waves	
Implementable Spectra	ITTC, ISSC, Pierson Moskowitz JONSWAP, Ochi

Table 8.1. Naples wave tank main features.

8.2 Design of the prototype

Using the longest regular wave the tank can generate, the largest achievable scale is determined: the maximum wavelength generable in the tank is 9 m, corresponding to a regular wave in deep water with period 2.40 s. The 9 m long wave is traveling in deep water conditions because the tank depth is 4.5 m, half the wavelength.

The location of Alghero, in the west coast of Sardinia, has one of the most powerful wave climate in the Mediterranean Sea with a power density of 13.1 kW/m [38]. The 2007 yearly average wave peak period (the period corresponding to the peak in the frequency spectrum) for the location is $T_p = 6.7$s[1]. The real waves in Alghero are not sinusoidal, but their main frequency is $\omega = 2\pi/T_p$[2]. So testing the device with regular waves at 2.4 s and comparing it with an equivalent sine wave at 6.7 s, leads to a Froude scaling of 1:7.8[3]. It has been decided to round this value to

[1]Data elaborated from www.idromare.it, accessed on June 2009, ISPRA - Istituto Superiore per la Protezione e la Ricerca Ambientale (the Italian Institute for Environmental Protection and Research).

[2]To pass from irregular waves to regular waves the peak period should be substituted with the energy period. However being the energy period not available directly from the ISPRA website and being its value not so different from the peak period in a typical sea spectra, in this work it has been decided to directly use the peak period for the regular waves analysis.

[3]There are mainly two ways to scale a WEC: according to Froude and therefore maintaining the ratio of inertia forces over gravitational forces constant or according to Reynolds maintaining the viscous forces over the inertia forces ratio constant. Since in a floating body the viscous effects are restrained in the boundary layer [39], the device is scaled to maintain the Froude number constant [40].

1:8, leading to a wavelength in the tank of 8.8 m corresponding to a period of 2.37 s. The scaled power density is 73.5 W/m and therefore the sinusoidal wave height achieving this value is 176 mm. According to table 8.1 at the 8.8 m wavelength the tank can generate waves high up to 590 mm: in order to explore a broader field with the tank tests, it has been decided to design the prototype to exploit a wave 300 mm high, making the device able to deal with the bigger power density of 213 W/m. In this chapter the 176 mm wave is called 'Cfg. A' and the 300 mm wave 'Cfg. B'.

Quantity	Scaling
Wave height and length	s
Wave period	$s^{0.5}$
Wave power density	$s^{2.5}$
Angular displacement	1
Mass	s^3
Inertia	s^5
Power	$s^{3.5}$
Angular velocity	$s^{-0.5}$

Table 8.2. Froude scaling.

The experimental tests on the flume showed a maximum relative capture width equal to the 21.6% with the gyro running at a quarter of the nominal speed. To design this new prototype a value of relative capture width equal to 20 % has been hypothesized. Furthermore, with the gyro running at a quarter of the nominal speed, $\delta_{0,rms}$ was 3.48 deg corresponding to an amplitude of a regular sine wave equal to 4.92 deg. In order to make an hypothesis on δ_0 and therefore make use of the design procedure, a comparison on the wave steepness (see paragraph 3.2 for further details) in the flume and in the Naples wave tank has been done.

$$\left\{ \begin{array}{c} \lambda_{s,flume} = \arctan \frac{\pi H}{\lambda} = \arctan \frac{\pi 0.07}{1.49} = 8.4 deg \\ \lambda_{s,Naples,Cfg.B} = \arctan \frac{\pi H}{\lambda} = \arctan \frac{\pi 0.3}{8.8} = 6.11 deg \end{array} \right\}$$

Being the wave steepness in the wave tank in Naples smaller than the nominal steepness in the flume, the δ_0 would probably be smaller than the δ_0 measured in the flume. In the hypothesis (to be verified a posteriori) that the behavior of the system is linear, the following relation can be written.

$$\delta_{0,Naples,Cfg.B} = \delta_{0,flume} \frac{\lambda_{s,Naples}}{\lambda_{s,flume}} = 4.92 \frac{6.11}{8.4} = 3.58 deg$$

This value is rounded up to $\delta_0 = 4 deg$.

With these assumptions and fixing the device width to 5 m in order to be far enough from the side walls of the wave tank, the linearized model allows to evaluate the required angular momentum for power extraction. The design process is done using Cfg. B since it's the most demanding working condition[4]. Table 8.3 summarizes the design process.

Assumptions
$\delta_0 = 4deg$
$\varepsilon_0 = 70deg$
RCW = 20%
Float width (W) = 5 m
Flywheel: $D_i/D_e = 0.9$, $h/D_e = 0.4$
Design procedure
$P_{d,res} = RCW \cdot P_D \cdot W = 213W$
$c = \frac{2P_{d,res}}{(\omega\varepsilon_0^2)} = 40.6\frac{Nm \cdot s}{rad}$
$J\dot{\varphi} = \sqrt{\frac{2cP_{d,res}}{\omega^2\delta_0^2}} = 710.6\frac{kgm^2 \cdot rad}{s}$
$T_{\delta 0} \simeq J\dot{\varphi}\dot{\varepsilon} \simeq 2300Nm$
$T_{\varepsilon 0} \simeq J\dot{\varphi}\dot{\delta} \simeq 132Nm$

Table 8.3. Design process.

8.3 Non linear simulation

The complete nonlinear model built in the Matlab/Simulink environment used in paragraph 3.4 has been used here to evaluate the real system performances. In figure 8.2 the power output of the linear and the non-linear models are compared.

[4]From the flume tests it seems the needed angular momentum to produce the desired power can be smaller than the one evaluated with this method. However in this new prototype it has been decided to implement the previously used procedure: if the needed angular momentum will be smaller than the designed one, the angular velocity will be reduced to match the float dynamics.

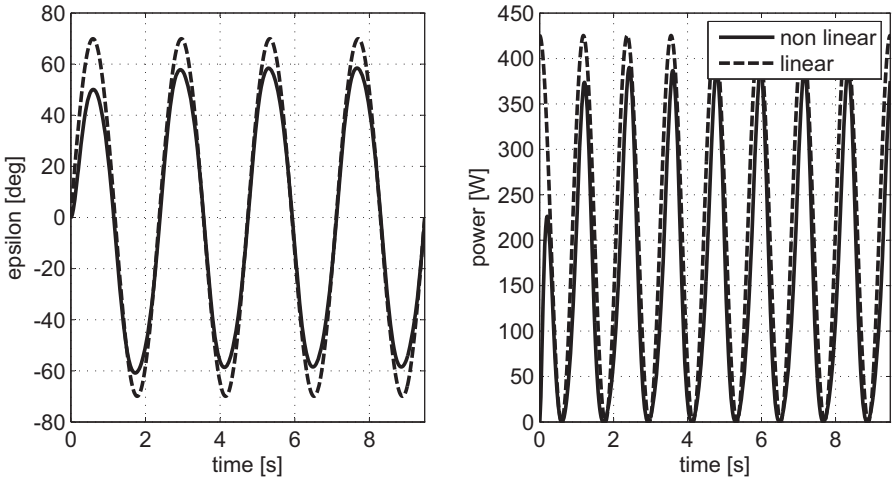

Figure 8.2. Comparison between linearized system and non-linear system.

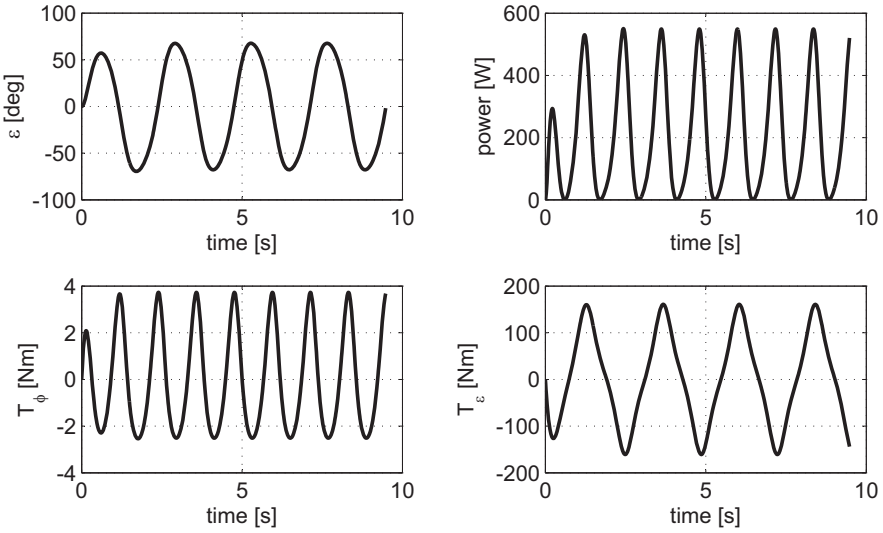

Figure 8.3. Non linear dynamic behavior of the system.

At the design point, the average power provided from the nonlinear model is not 213 W as desired, but 157.8 W (-25.9%). To increase the power output the amplitude ε_0 is increased to 70 deg by decreasing the damping, but the gain of power is not enough to reach 213W. The linear model is then used to find the new parameters asking a target power of $213 \cdot (1/(1 - 25.9\%)) = 287.5$ W and small

arrangements near the new configuration are made to have the system producing 213 W and oscillating at 70 deg (angular momentum = 871.8 $kgm^2 \cdot rad/s$ and damping coefficient 40.5 Nms/rad). Cfg. A is achieved reducing $\dot{\varphi}$ and changing the damping coefficient. The behavior of the system is summarized in Figure 8.3.

$J\dot{\varphi}$	871.8 kgm^2·rad/s
c	40.5 Nms/rad
P_d	214 W
T_ε	160 Nm
T_δ	2880 Nm

Table 8.4. Final system parameters.

8.4 Friction losses

In order to decide a proper $\dot{\varphi}$ and evaluate the inertia, some considerations on the power losses to maintain the flywheel in rotation have to be done. The two main power losses in the system are friction on the bearings and air drag. The design is carried out to maintain the sum of the two smaller than the 10% of the absorbed power in Cfg. B[5]. In a first approach the air drag losses and the bearing losses are set to the maximum limit of the 5% of the absorbed power each.

The flywheel inertia is condensed mainly in the external crown which dimensions are evaluated in function of $\dot{\varphi}$ imposing the form factors declared in Table 8.3. The following equations have been used to roughly evaluate the power loss for aerodynamic drag, treating the flywheel as a thin disc with external diameter D_e [41].

$$M_a = \rho_g \omega^2 r_0^5 C_m \tag{8.1}$$

$$\begin{aligned} lam: &\quad C_m = 3.87 \cdot Re^{-1/2} \\ turb: &\quad C_m = 0.146 \cdot Re^{-1/5} \end{aligned}$$

In the (8.1) ρ_g represents the air density, ω the flywheel angular velocity, r_0 the radius of the disc and C_m a coefficient function of the flow laminar or turbulent conditions. Figure 8.4 has been plotted with respect to $\dot{\varphi}$ by evaluating in each point the required inertia and calculating the air drag power loss using the (8.1). The procedure has been repeated for different air pressure values.

[5]The efficiency of the electric motor and the power electronics driving the gyroscope are neglected at this stage. They will be evaluated experimentally.

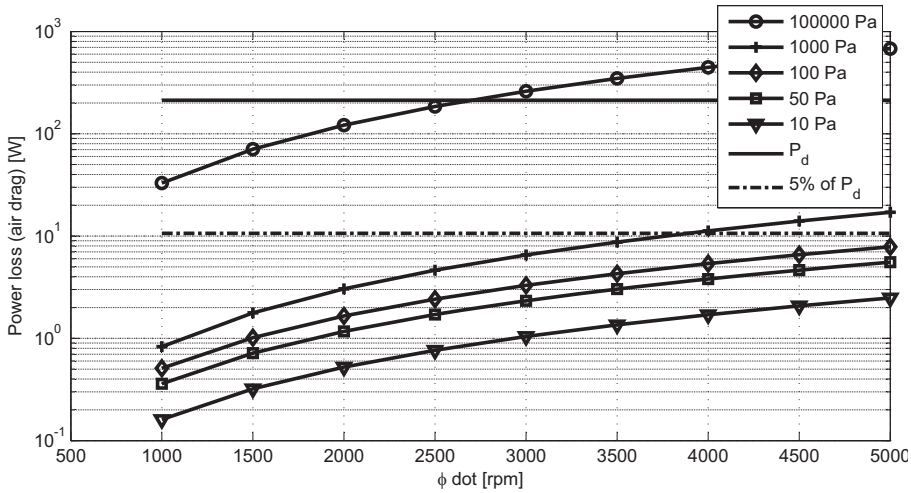

Figure 8.4. Power loss for aerodynamic drag with respect to $\dot{\varphi}$ and varying the pressure (absolute values) in the chamber.

Figure 8.4 highlights the absolute need for a vacuum chamber to lower the air drag. A value of 1000 Pa is relatively easy to obtain and it's cheaper to maintain with respect to lower pressure levels, allowing at the same time a small power consumption, even though only at low speed. To maintain the prototype as cheap as possible the prototype uses ball bearings (cost $10 \div 100$ €) instead of magnetic or hydrostatic bearings (cost > 10000 €). The bearings are chosen to obtain a minimum life of 1000 h when the system works in Cfg. B. The power consumption is evaluated through the SKF guidelines and it's a direct function of the forces on the bearing and of the angular speed. The two bearings will have seals to maintain the lubrication grease inside the bearing -for the sake of cheapness there is not a lubrication circuit. Since the friction model for the bearings with seals is not easy to implement in a Matlab for loop because of the several parameters involved, it has been decided to implement the simplified model reported beneath for bearings without seals. The axial forces are neglected too.

$$T_f = 0.5 \mu F_r d$$

Where T_f is the torque loss, μ is a coefficient equal to 0.0015 for ball bearings, F_r is the radial force on the bearing and d is the internal diameter of the bearing. The power loss evaluated with such a model is required to be smaller than the 5% of the rated power. A final verification on the real power loss on the bearings will be performed using the SKF calculator available on the SKF website www.skf.com. The radial forces on the bearing are function of T_δ, T_ε, the flywheel weight (evaluated as 1.5 the weight of the crown) and of the distance between the bearings. For each

configuration all the previous parameters have been calculated and averaged on a cycle to evaluate F_r[6]. Figure 8.7 shows the total power lost for air drag and on the bearings in function of $\dot{\varphi}$ and the distance between the bearings. The most suitable bearing for each condition has been chosen among the standards ball bearings within the dimensions of interest. The selected bearing are shown in table 8.5.

SKF catalog reference	Diameter [mm]	C [N]	C_0 [N]
6200	10	5070	2360
6201	12	6890	3100
6203	17	9560	4750
6204	20	15900	7800
6206	30	28100	16000

Table 8.5. Ball bearings considered in the losses estimation.

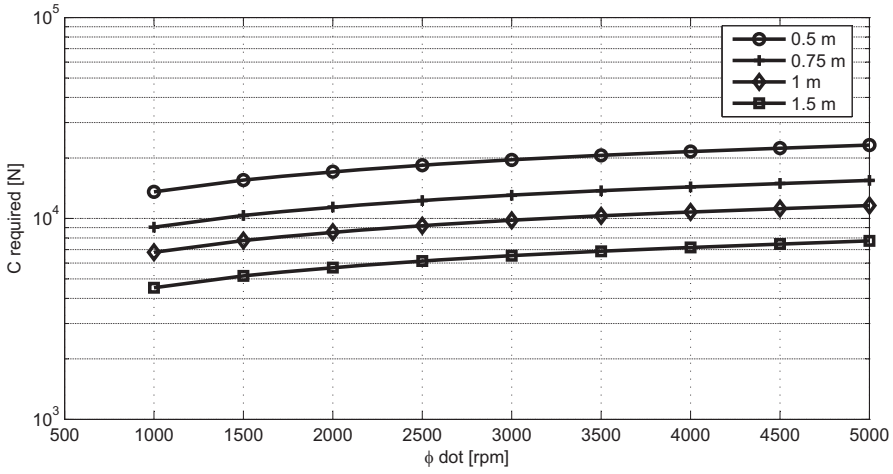

Figure 8.5. Dynamic load required from the bearings.

[6]A bearing life is proportional to $(\frac{C}{P})^3$, where C is the bearing dynamic load and P is the equivalent load (F_r in this case). So the 'average' F_r has been calculated as $((\frac{\int_0^T |F_r(t)|^3 dt}{T})^{\frac{1}{3}}$.

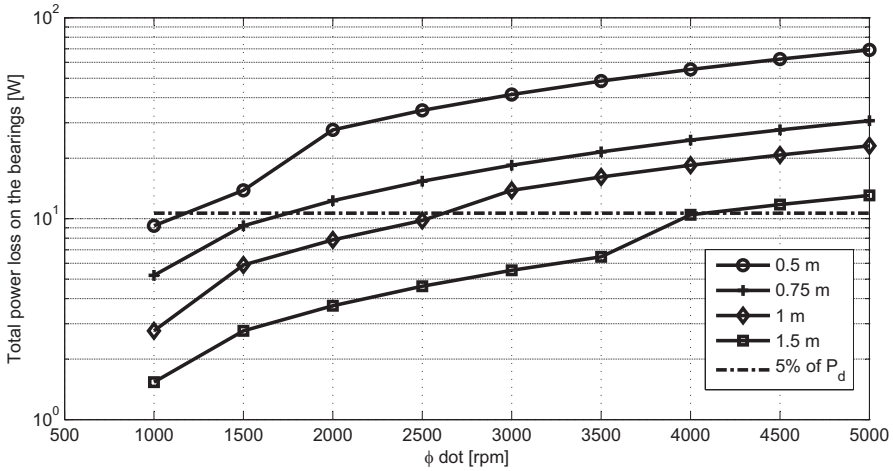

Figure 8.6. Power loss on the bearings.

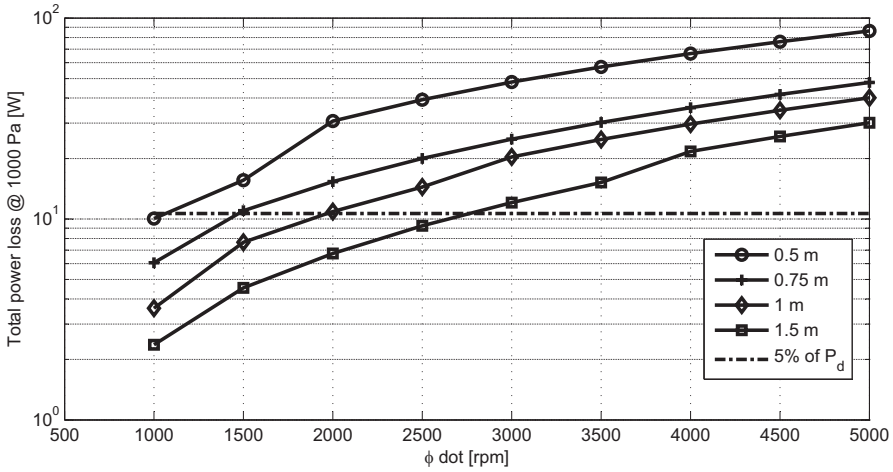

Figure 8.7. Total power loss (friction on the bearings and air drag at 1000 Pa abs).

From the solutions achieving the target power loss, the most suitable configuration holding down both the distance between the bearings and the inertia of the gyro has a flywheel with J = 5.55 kgm^2 and rotates at 1500 rpm with 6201 bearings spaced of 1 m. The total power lost for friction in this configuration is 7.98 W (2.18 W lost for air drag).

8.5 Engineered system

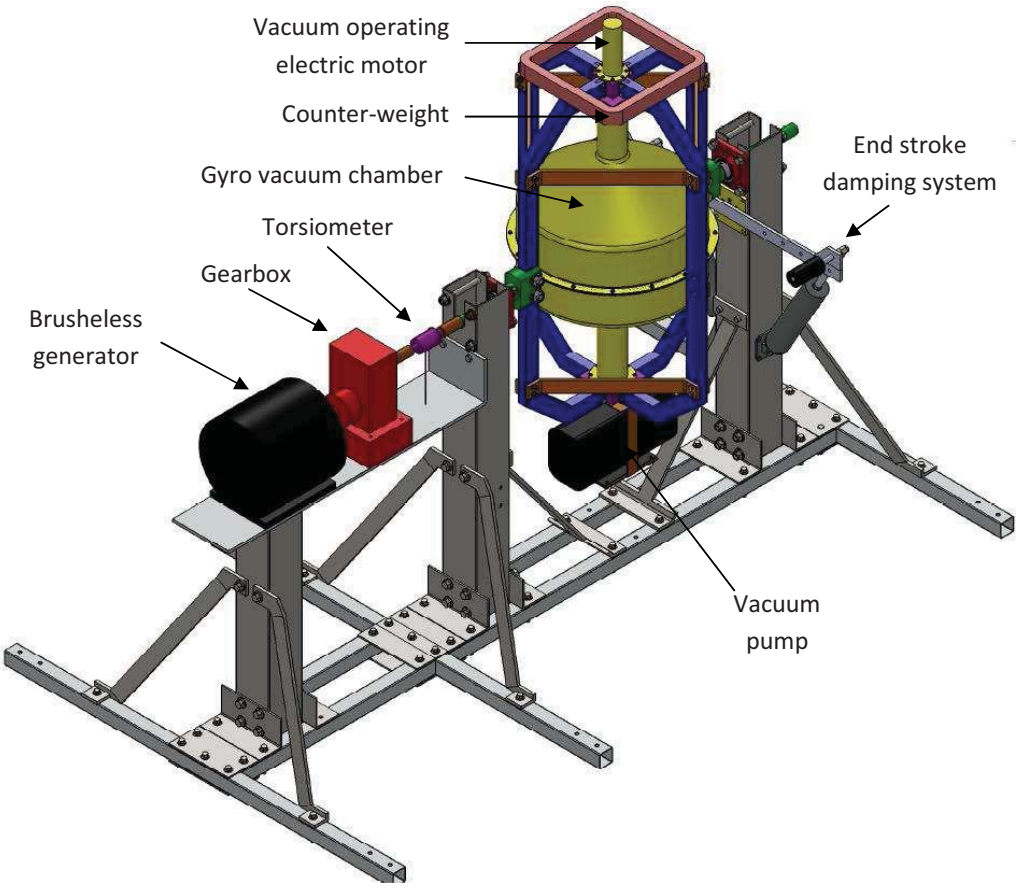

Figure 8.8. The prototype layout.

The system is then engineered as described in the next paragraphs[7] and the resulting layout is shown in figure 8.8.

[7]For a comprehensive description of the engineering process refer to [42] and [43]

8.5.1 Flywheel

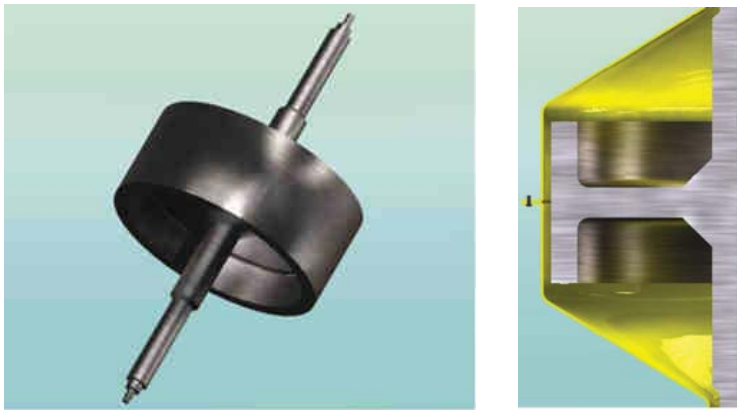

(a) Flywheel axonometry.

(b) Gyro cross section.

Figure 8.9. Gyro axonometry and cross section.

The final version of the flywheel is obtained with small arrangements to round off the configuration defined in the previous paragraph. The flywheel has the external diameter equal to 500 mm and the crown is 40 mm thick and 220 mm wide resulting in a total flywheel mass of 163 kg. An axonometry of the flywheel is shown in figure 8.9.

The flywheel is steel built (C60 UNI EN 10083) and it has been tested through a FEM model using the COSMSWorks tool of SolidWorks. The simulation demonstrated that the chosen geometry achieves a static factor of safety greater equal to 3.6 and a fatigue factor of safety greater than 3 in the most demanding conditions[8]. The FEM code showed even that the external border of the flywheel moves radially of a maximum of 0.048 mm. Being 10 mm the clearance between the flywheel and the air-tight case, there are no risk of unwanted contacts.

8.5.2 Air-tight case

The air-tight case is composed of two shells built in a 3 mm thick steel sheet. The two shells are joined in the middle through a series of bolts and the air-tightness is granted by a double O-ring running along the junction. The whole structure has

[8]The maximum stress (Von Mises) is 124 MPa localized in the 70 mm diameter flywheel shaft. For a dimension smaller than 100 mm the C60 steel has $R_{p02} = 450$ MPa and a fatigue limit estimated through the Fuchs rule $\sigma_{d-1} = 0.5\sigma_r = 0.5 \cdot 750 = 375MPa$. The external crown is almost unloaded having a maximum stress of 11.8 MPa.

been tested through the SolidWorks COSMOSMotion code to evaluate the stress state under the pressure difference between the inside (1000 Pa) and the outside (100000 Pa): the maximum stress is 28.7 MPa and the maximum deformation is 0.04 mm.

Figure 8.10. Half air-tight case.

8.5.3 End stroke

Two dampers to limit the angular stroke around ε have been inserted. They are composed of a damping cylinder mounted with a lever arm with respect to the ε axes: when the system goes over $\varepsilon = \pm 75 deg$ the black rubber pad intercepts the external structure allowing the damper to brake the system.

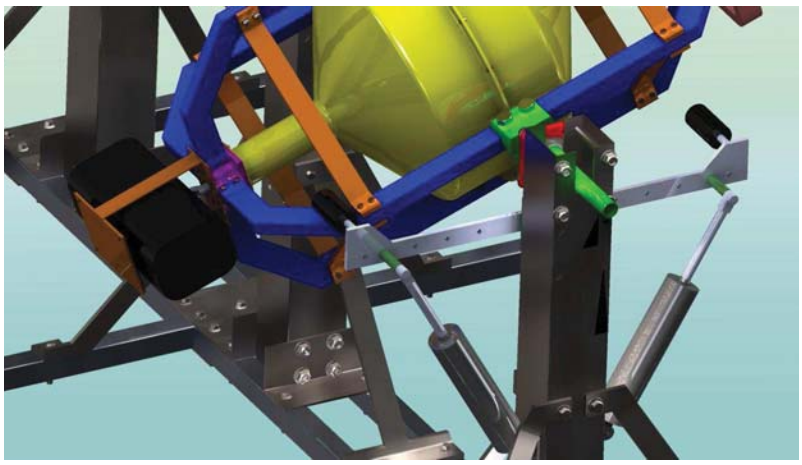

Figure 8.11. End strokes damper in action.

8.5.4 Bearings

The bearing mounting scheme envisages the use of two ball bearings provided with seals and the upper bearing supporting the whole axial load due to gravity. Due to the relevant axial load (1230 N average on a cycle), the 12 mm chosen bearing is no more suitable for the application. The next bearing in table 8.5 is chosen, the 6203-2Z version with seals is selected, it is verified to last over 1000 h (1090 h) and a power loss equal to 12.2 W is evaluated through the SKF online Calculator. The grease used in the calculation is the LESA 2, suitable for low friction torques applications and the working temperature was supposed equal to 30° Celsius. The lower bearing consumption is evaluated in the same way at 6.44 W. The sum of the losses to maintain the flywheel in rotation is 20.82 W, a value smaller than 21.3 W, the 10% of the absorbed power. So the goal of maintaining the power losses under the 10% of the absorbed power is achieved at the design stage.

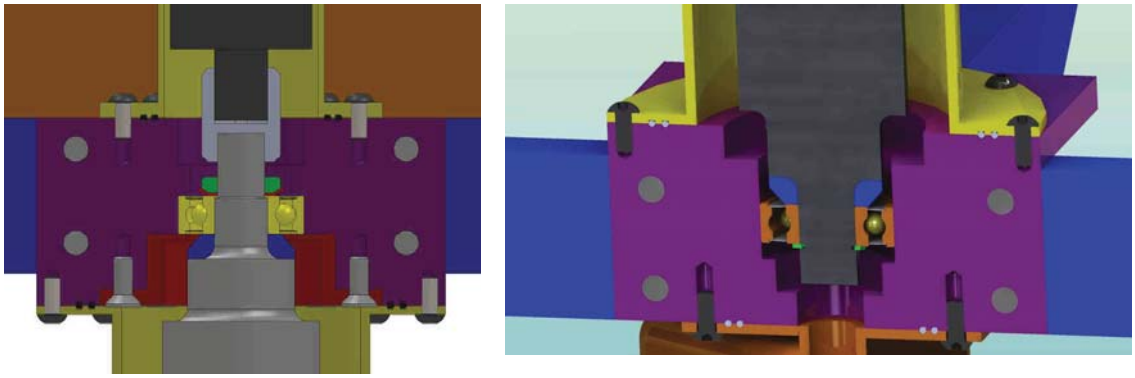

Figure 8.12. Flywheel bearings: on the left the upper bearing, on the right the lower bearing.

The two bearings allowing the whole platform to rotate around ε are of the type shown in figure 8.13. The bearing internal diameter is the relatively big value of 40 mm allowing this way the construction of a hollow shaft to let the wires pass through (supplies for the vacuum pump and the flywheel motor, signals from the hall sensors and the encoder of the flywheel motor and the vacuometer). This kind of bearing comes with the housing, allowing therefore a quick and easy placement on the system. Due to their small angular velocity, these bearings induce a power loss of 0.14 W each.

Figure 8.13. ε bearings (SKF code: FY 40 TR).

8.5.5 Electric motor

The electric motor driving the flywheel is chosen in order to accelerate the flywheel from 0 to 1500 rpm in about 5 minutes without being overloaded. Therefore if the flywheel is supposed to be brought to the rated speed with a constant acceleration ramp, the minimum rated torque of the motor will be:

$$T_{\varphi,startup} = J\ddot{\varphi} = 5.7 \cdot \frac{2\pi 1500}{60 \cdot 300} = 2.98Nm$$

One of the commercially available motors with the required parameters is the Parker SMB82 brushless motor, presenting rated speed 1600 rpm and rated torque 2.9 Nm. The SMB82 motor is able to work in the vacuum environment present inside the case and it is refrigerated with an aluminum heat sink adherent to the motor external case.

During the working time in Cfg. B if the flywheel is supposed to be driven at constant speed, the torque on the motor shaft presents an oscillating behavior with null mean value, as shown in figure 8.3. If this torque is applied to the inertia J, it leads to a velocity ripple of about ± 2.5 rpm on the 1500 rpm. This will be probably be comprised in the hysteresis of the controller, but nevertheless the use of a regenerative controller should be taken into account in order to avoid waste of power.

8.5.6 PTO

The PTO for this application is composed of a brushless generator coupled with a mechanical gearbox to increase the low angular velocity on the ε axes and therefore the efficiency of the brushless generator. After a search between the viable

solutions, the chosen solution is composed from a generator TML-210-150 produced by the company ETEL coupled to a S 401 3.8 gearbox produced by the Bonfiglioli Group[9]. According to the calculation made to evaluate windings losses, iron losses and mechanical losses, the PTO achieves a maximum efficiency of 73.2% in Cfg. A and 79.8% in Cfg. B.

8.5.7 Vacuum pump

The vacuum pump selected for this application is the Varian IDP-3 dry scroll pump. It is a light, compact and oil free pump capable of a peak pumping speed of 60 l/min and to reach pressures as low as 33 Pa, two orders of magnitude smaller than the 1000 Pa required. In order to avoid long tubes bringing the vacuum, in the proposed design it is attached to the bottom of the gyroscopic platform. A counterweight is put on the top of the platform to equilibrate the pump 9.5 kg mass. According to the Varian technical service, being the accelerations and the angular velocities relatively small, there are no working problems with this configuration. Furthermore the choice to suspend the pump on the gyro platform theoretically allows to investigate the device behavior when free to rotate around the ε axes (if the power supply is brought through sliding contacts and the end strokes removed).

Figure 8.14. The Varian vacuum pump.

[9]The ETEL company (website www.etel.ch) is well known in the wind energy field for supplying high efficiency generators. The Bonfiglioli Group (website www.bonfiglioli.it) is the major Italian builder of mechanical transmissions and the gearbox has been chosen with their Technical Assistance to achieve the maximum efficiency. The efficiency of the gearbox in these working conditions is not known, but it has been estimated at the 95%. However, before going to the tank, the PTO will be tested on a purposedly designed test rig to determine the real efficiency. For a detailed description of the choice of the PTO and the design of the test rig refer to [43].

8.5.8 Float

The float will have almost the same shape of the one used in the flume tests: a rounded fore, a sloped stern and two drifts to compensate T_ε. It is built using an internal aluminium structure covered with bended, riveted and glued aluminium sheets. This central body can be integrated with two side floats 1 m wide having the same keel shape except for the drifts: in this way a total width of 7 m is achieved allowing the device to harvest more incident power if needed (e.g. smaller waves conditions or relative capture width smaller than expected). The mooring system is the same used in the wave tank in Edinburgh: two mooring lines in the bow and one in the stern. The length of the float is 4.3 m, smaller than half the wavelength. The estimated mass of the float is about 150 kg, whereas the mass of the gyroscopic system is 440 kg, meaning the total mass is around 600 kg and a rough 40 mm nominal sink of the float.

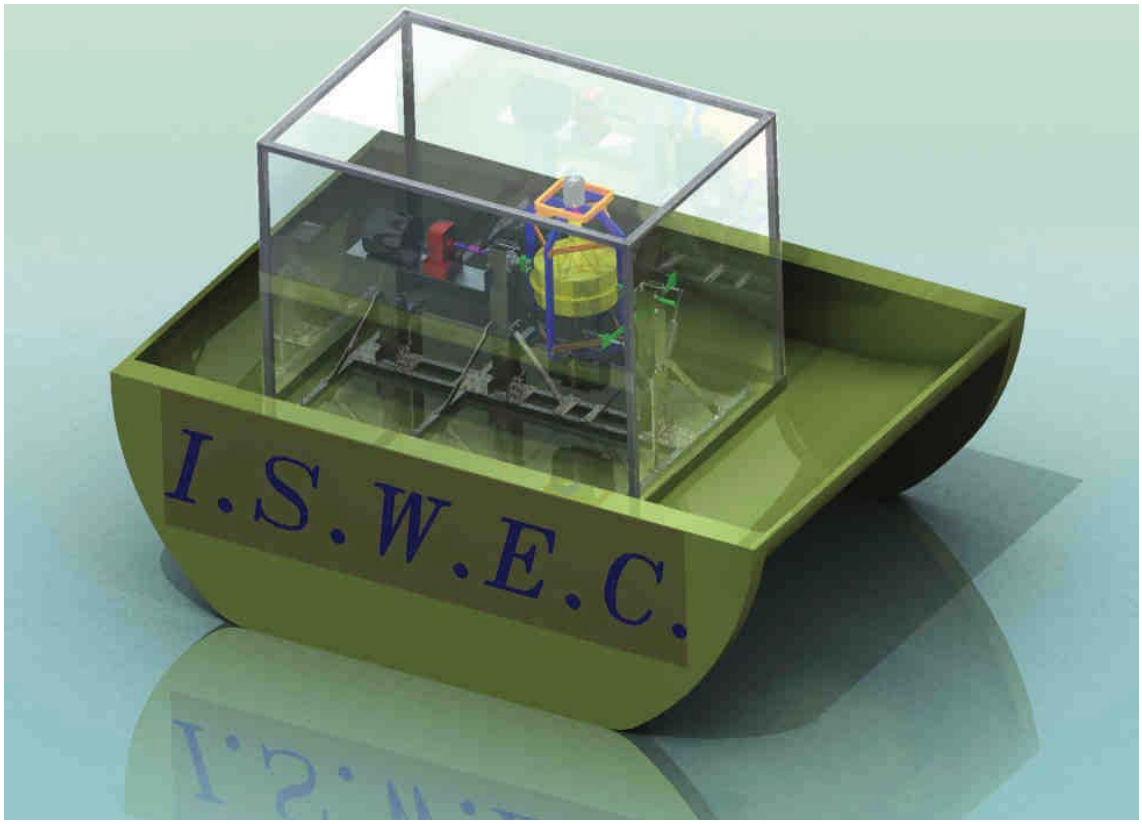

Figure 8.15. The prototype with the float.

8.6 Cfg. A

The system is designed to work in Cfg. B, but the Alghero site scaled at 1:8 is represented by Cfg. A, in which the power density is 73.5 W, the wave height is 176 mm and the wave period is the same as Cfg. B, 2.37 s. δ_0 is evaluated in the same way as for Cfg. B.

$$\delta_{0,Naples,Cfg.A} = \delta_{0,flume}\frac{\lambda_{s,Naples,Cfg.A}}{\lambda_{s,flume}} = 4.92\frac{3.6}{8.4} = 2.11deg$$

In the hypothesis to make the device oscillate at 70 deg, the angular momentum to catch the 20% of the incoming power is evaluated and so the damping coefficient and the torques on the PTO and the float along the pitching direction. Being the inertia evaluated previously, the new angular momentum is achieved by reducing $\dot{\varphi}$.

$J\dot{\varphi}$	584.3 $kgm^2 \cdot rad/s$
$\dot{\varphi}$	1005 rpm
c	13.5 Nms/rad
P_d	73.5 W
T_ε	53.2 Nm
T_δ	1860 Nm

Table 8.6. Working conditions in Cfg A.

Power losses in the new conditions are reported in table 8.7.

8.7 System efficiency

The power losses in the mechanical system can be summarized as follows.

1. friction on the bearing
2. friction due to air drag
3. PTO efficiency
4. vacuum pump power supply

In the next table the efficiency of the overall system working in Cfg. A and in Cfg. B is compared.

Type of loss		Cfg. A	Cfg. B
Upper bearing	[W]	7.93	12.2
Lower bearing	[W]	2.71	6.44
ε bearings	[W]	0.19	0.28
Air drag	[W]	0.97	2.18
PTO losses	[W]	19.7	43.02
Total	[W]	31.5	64.1
Absorbed power	[W]	73.5	213
Net power	[W]	42	148.9
Efficiency		57.1%	69.9%

Table 8.7. Efficiency evaluation.

Neglecting the power consumptions for sensors, data acquisition system and vacuum pump (whose consumption is function of the air leakages through the O-rings and will be assessed experimentally), the gyroscopic system overall efficiency is 69.9%. The main source of loss is the PTO which efficiency would be probably increased in the full scale device by using a purposedly designed electric generator. Furthermore experimental investigation is needed to assess the actual gearbox efficiency.

Chapter 9

The ISWEC project

In this chapter an overview of the ISWEC project going on at the Politecnico di Torino is given. Firstly a possible full scale system is analyzed scaling the prototype designed in the previous chapter to the actual dimensions. The resulting device is then compared with one of the Pelamis WECs deployed into the pilot plant in the western coast of Portugal [24]. Since one of the goals of the ISWEC project is to deploy a pilot device in the Mediterranean, a wave measurement station has been deployed to monitor the wave climate in the Isle of Pantelleria. The data coming from the station will allow a more accurate design of the full scale ISWEC. Finally, ISWEC is a unidirectional WEC needing a proper mooring system to weathervane and be always aligned towards the incoming waves. In the final part of the chapter a possible omnidirectional version of the ISWEC gyroscopic system is proposed.

9.1 The full scale system

Tables 9.1, 9.2 and 9.3 show the Froude scaling[1] of the prototype built for tank tests at the University of Naples.

[1]Refer to table 8.2 for details.

		Prototype	Full scale
P_d	[kW]	0.0735	106.4
$P_{d,effective}$	[kW]	0.042	61
$J\dot{\varphi}$	[kgm^2·rad/s]	584.3	6.77· 10^6
$\dot{\varphi}$	[rpm]	1005	355
c	[Nms/rad]	13.5	1.56· 10^6
T_ε	[Nm]	53.2	2.18· 10^6
T_δ	[Nm]	1860	7.62· 10^6
Crown stress	[MPa]	5.24	41
Wave height	[m]	0.176	1.41
Wave length	[m]	8.8	70.4
P_D	[kW/m]	0.0735	13.1

Table 9.1. Froude scaling to full scale (Cfg A).

Table 9.1 shows the full scale system working in Cfg. A, meaning in the year averages conditions present at the Alghero site[2]: $T_p = 6.7$ s and average power density 13.1 kW/m. The full scale device will produce, in the hypothesis of maintaining also the efficiency of the prototype, 61 kW. To catch this power, the required angular momentum is 6.77· 10^6 kgm^2·rad/s. Let's now analyze what happens by scaling Cfg. B.

		Prototype	Full scale
P_d	[kW]	0.214	310
$P_{d,effective}$	[kW]	0.149	216
$J\dot{\varphi}$	[kgm^2·rad/s]	871.8	1.01· 10^7
$\dot{\varphi}$	[rpm]	1500	530
c	[Nms/rad]	40.5	4.69· 10^6
T_ε	[Nm]	160	6.55· 10^6
T_δ	[Nm]	2880	1.18· 10^7
Crown stress	[MPa]	11.8	94.4
Wave height	[m]	0.3	2.4
Wave length	[m]	8.8	70.4
Wave period	[s]	2.37	6.7
P_D	[kW/m]	0.214	38.6

Table 9.2. Froude scaling to full scale (Cfg B).

In this configuration the required angular momentum is 1.01· 10^7 kgm^2·rad/s and

[2]refer to paragraph 8.2 for details.

the net power output is 216 kW. The full scale flywheel (brute scaling) is described in Table 9.3. Even if this configuration can be achieved structurally because of the relatively small mechanical stress induced in the crown, the huge mass of the flywheel (83.5 ton) can create problems in manufacturing and handling. Furthermore the configuration must be investigated to look for the cheapest way to obtain this huge angular momentum. This can involve to split the inertia in several subsystems with each a smaller inertia. If the number of subsystems is even, they can be counter-rotating to equilibrate the torque along the ε direction. Even a configuration with high speed carbon fiber or steel wires flywheels must be investigated.

Since Cfg. B brought to full scale involves a more powerful sea with respect to the yearly average of Alghero, it applies to a temporary state in Alghero or to the average of a more powerful site. In the next figures, the maps reporting wave power density, mean period and significant wave height shows that around the world there are several locations with the required wave features. Furthermore in a considerable number of locations, the wave climate is more powerful than the hypothesized in Cfg. B full scale (see also figures 1.2 and 1.3).

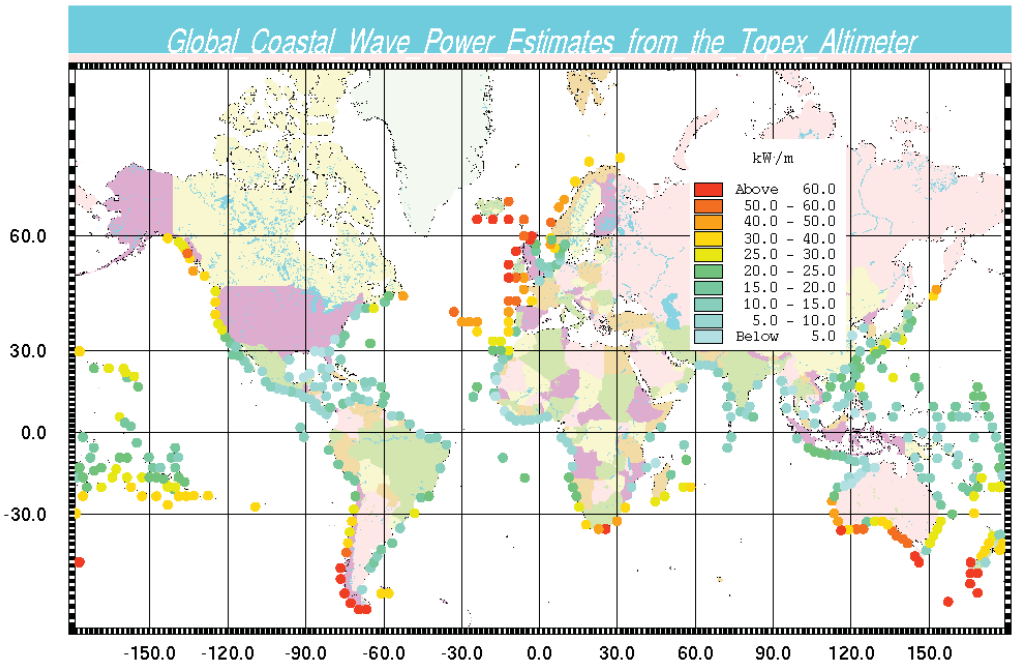

Figure 9.1. Yearly average power density.

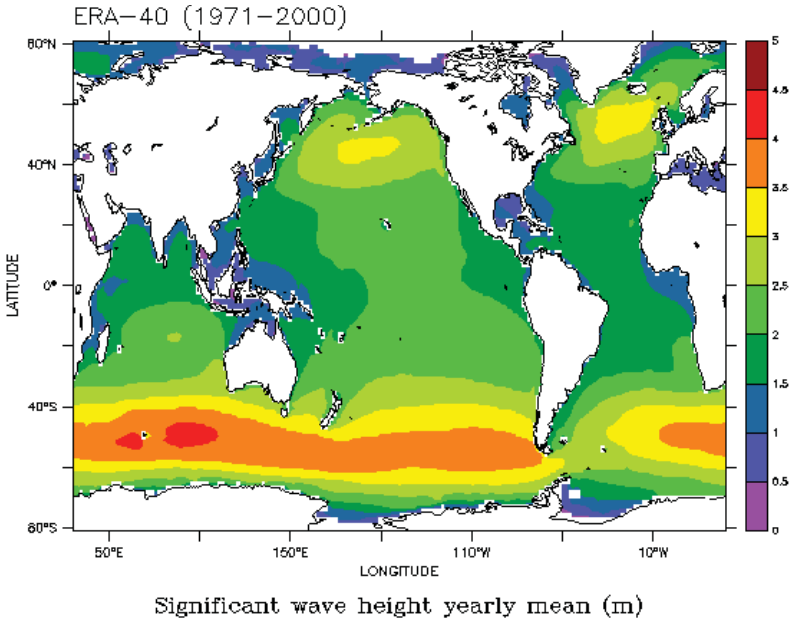

Figure 9.2. Yearly average significant wave height.

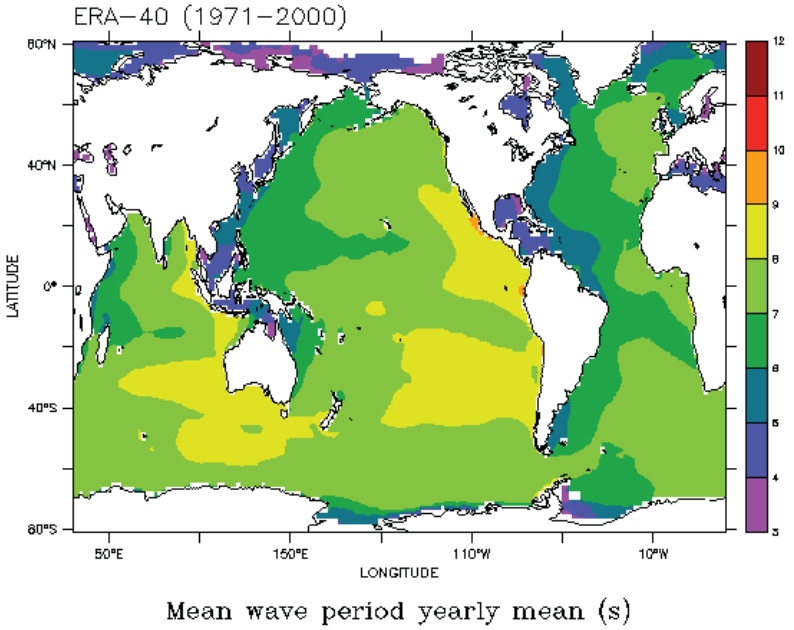

Figure 9.3. Yearly average mean period.

		Prototype	full scale
diameter	[m]	0.5	4
mass	[kg]	163	83500
J	$[kgm^2]$	5.55	$1.82 \cdot 10^5$

Table 9.3. Gyroscope scaling.

9.2 Benchmarking

Table 9.4 shows a comparison between the full scale ISWEC (brute scaling from Cfg. B) and the Pelamis WEC. Apart from the angular momentum ISWEC needs to create the gyroscopic effects, the overall performances are comparable. The Pelamis WEC claims a rated power of 750 kW when the wave power density of the incident wave is 55 kW/m, whereas ISWEC produces 216 kW at 38.6 kW/m wave power density. In the hypothesis the performances of ISWEC are proportional to the power density, the ISWEC produces 308 kW at 55 kW/m. With this new value two coefficient are evaluated to determine the power density of the devices with respect to the mass and the area. The power/mass ratio is almost the same for both the devices whereas the power/area is greatly in favor of the Pelamis. However these are nominal values which doesn't take into account the effective area usage, because the region perturbed from a WEC is bigger than its physical dimensions and its function of its geometry.

		ISWEC	Pelamis
Gyro		83.5 ton @ 530 rpm	-
Total mass	[ton]	300	700
Rated power	[kW]	216	750
Power density	[kW/m]	38.6	55
Power at 55 kW/m	[kW]	308	-
Width	[m]	40	3.5
Length	[m]	34	150
Surface usage	[m^2]	1360	525
power/mass	[kW/kg]	1.02	1.07
power/surface	[kW/m^2]	0.23	1.43

Table 9.4. Benchmarking.

The benchmarking previously described considers a scaling of the 1:8 ISWEC prototype that has been designed using conservative hypothesis over experimental data. The 1:8 prototype has yet to be tested and if it is going to behave as the small

prototype in the flume, a considerably smaller angular momentum can be required to produce the same power output. In this case the device would be considerably smaller and cheaper. The tank test scheduled for December 2010 will produce a more accurate evaluation of the ISWEC performances with the following primary goals:

- evaluation of the power output and the power losses and the determination of the overall efficiency
- evaluation of the pitching motion amplitude
- evaluation of the relative capture width

A particular care will be put even to:

- determine the suitability of the float shape
- determine the impact of the mooring lines on the float dynamics
- implement new control strategies
- assess the device behavior with irregular waves

9.3 A possible location for the pilot plant

The Italian Island of Pantelleria (36°50'0"N, 11°57'0"E) is midway between Sicily and Tunisia. The island is powered by a thermoelectric power station using Diesel fuel which is ship transported to the island. The fuel supply is difficult, expensive and unreliable. To contrast these disadvantages, the power station has been modified to accept power from renewable energy sources and a photovoltaic plant has been already installed.

In the past months contacts have been made to possibly install a wave power pilot plant in an area relatively close to the power station. An authorization has been granted to deploy a low environmental impact submerged stand-alone measurement station in the point shown in figure 9.4 at the depth of 16 m. That point has been chosen even because it is an existent mooring point for ships. See the Appendix for more maps of the measurement point.

The deployed measurement unit is composed of an AWAC system[3], a submerged wave climate sensor supplied by an accumulator giving to the unit a two months autonomy. The unit has been moored to the seabed in January 2010 from a scuba

[3]The AWAC is produced by the Nortek company www.nortek.no.

divers team. A scuba diver is going every two months to change the batteries and collect the wave data.

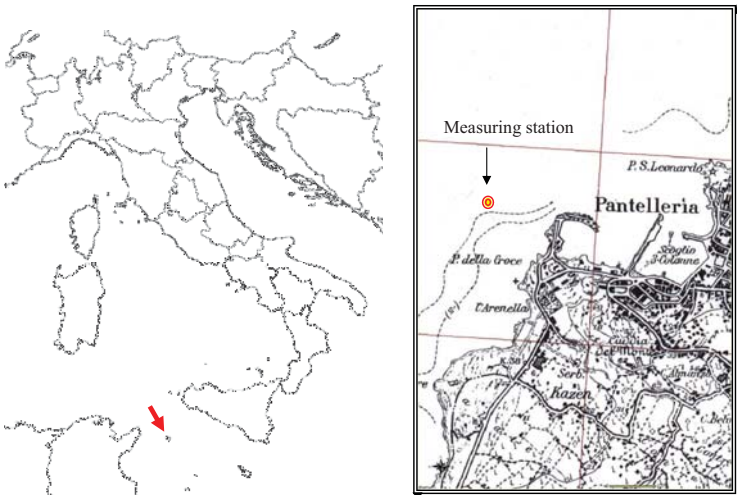

(a) Position of the Isle of Pantelleria on the Italian map (red harrow).

(b) The wave measurement station in the North-West corner of the Isle of Pantelleria.

Figure 9.4. Position of the measurement unit.

(a) AWAC.

(b) Stand-alone AWAC deployed (photomontage).

Figure 9.5. The AWAC measurement station.

The AWAC measurement unit measures pressure, wave orbital velocity and surface position to estimate wave height and wave period. The pressure is measured with a high resolution piezo-resistive element, the orbital velocity by a Doppler shift and the surface position with Acoustic Surface Tracking (AST).

9.4 The two degrees of freedom system

The device described in this Thesis is unidirectional: in order to work ISWEC must be aligned with the incoming wave. This cannot be a problem since the device with the two drifts and a mooring system allowing the device to weathervane can be auto-aligning. However at the Politecnico di Torino the omnidirectional gyroscopic system represented in figure 9.6 is under study.

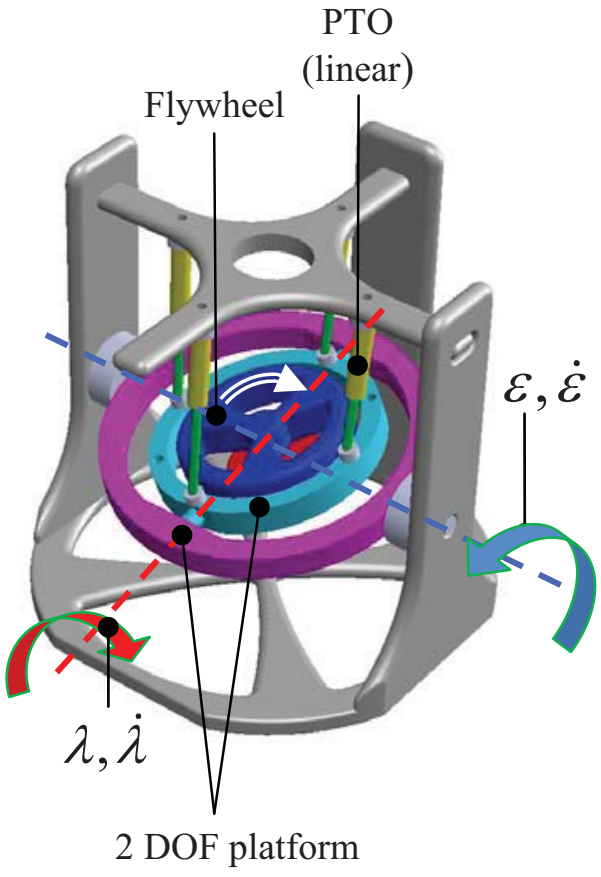

Figure 9.6. The two degrees of freedom device.

In this configuration the flywheel is carried on a gimbal. The gimbal allows the

gyro to precess with two degrees of freedom around its center of gravity. The PTO in the representation of Figure 9.6 are linear devices linked to the inner platform of the gimbal and the hull. The working principle of the device can be summarized in three main steps:

1. The incoming waves tilt the buoy (along any direction)
2. Due to the PTO stiffness and damping (in analogy to the 1 DOF system, refer to eq. (2.3)) a fraction of this rotation is transmitted to the inner platform of the gimbal perturbing the gyroscope.
3. Thanks to the inertial effect the gyro starts to precess. By damping the precession and restoring the initial condition, the PTOs produce energy.

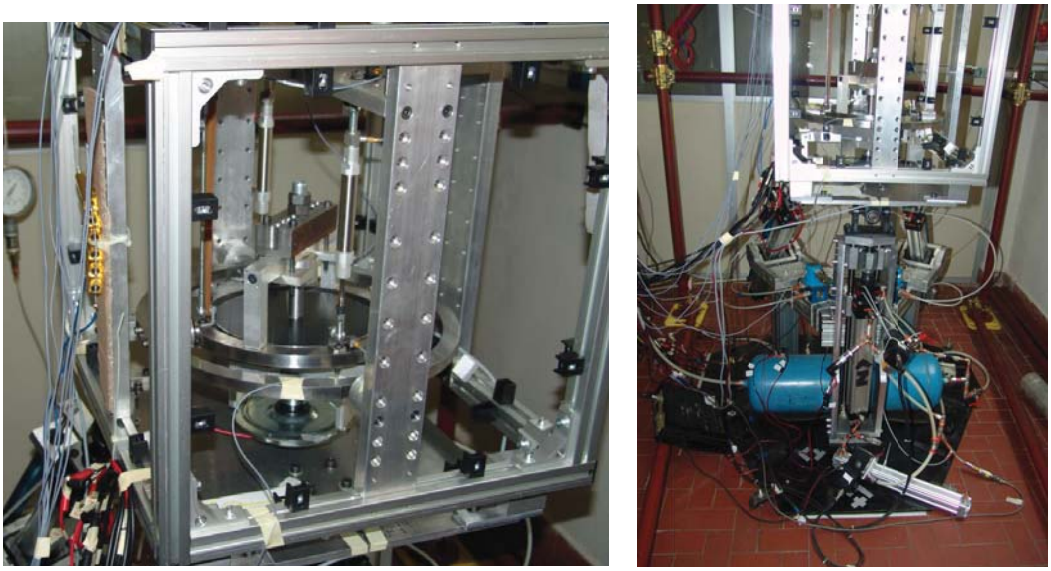

(a) The demonstrator itself.

(b) The demonstrator on the HPR platform.

Figure 9.7. The two degrees of freedom demonstrator.

The job of the PTOs is both to establish a mechanical link between the gyro and the hull and to damp the gimbal-hull relative motion. The PTOs can be either linear or rotational. In the second case they are coupled directly on the axis of motion to damp, their shaft on the mobile part and their carter on the still part. In this last configuration there are not restrains to the angles performed by the gimbal and the gyro can freely rotate around the two axis. The device described before is omni directional: the gimbal, if designed properly, does not have a preferential

direction of action and so there is not the need to orientate the buoy with respect to the wave.

A demonstration device has been built and some early tests have been performed using a HPR platform available at the Mechanical Department [44], [45], [46].

The two degrees of freedom device described previously is one of the possible answers to the need to absorb waves from different directions. However the new device is more complex and therefore more costly. Productivity and economic analysis are needed to understand if the omnidirectional device would be more effective than the one degree of freedom ISWEC.

Chapter 10

Economic scenarios

In this Chapter a preliminary economic analysis dealing with the industrialization of the ISWEC is carried out and the development of a company selling two types of products is considered. The first is a grid connected device, the second is a stand-alone device for powering on-site applications. The power rating of the devices are respectively 5 kW and 1 kW if deployed to the Alghero site. The goal is to offer energy to the end user at a cost smaller than 0.40 €/kWh, making the solution competitive with diesel generators, which are often used in small islands. The two products, 5 kW grid connected and 1kW stand-alone, will have different target markets:

1. The grid connected device will be used as a solution for power generation in sea places, joining the traditional or renewable sources, through the creation of 'Seafarm' consisting of a fleet of properly spaced and connected devices. In this case the ideal users are the small islands in the Mediterranean Sea.

2. The stand-alone device can be used:

   - in harbors (1200 in the Mediterranean, 7000 in the world) for signaling
   - in operation or decommissioning of offshore platforms (about 150 being dismantled each year worldwide, according to estimates of the next 10 years)
   - in the execution of the so-called 'motorways of the sea', which are estimated in 14000 km in the Mediterranean and where buoys will be needed to transmit signals every 20-30 km.

From the numerical point of view the 'Seafarm' seems to be the most attractive market. Only for Italy, there are more than 50 smaller islands where the cost of energy is very high. Moreover, including small and medium-sized islands out of Italy, we have 70 inhabited islands in Greek, 37 for Croatia and 26 pertaining to Turkey.

As we have seen in Chapter 1, so far there are no real competitors on the market with commercial solutions exploiting sea waves. In fact we witness the presence of demonstration prototypes. However, there is a wide range of substitute products, in particular, as mentioned, the solution has advantages over using photovoltaic and diesel generation. Vice versa it is not competitive in general, at least according to research conducted so far, compared with wind power or hydroelectric, to remain in renewables. Should however be noted that not all places, especially in the Mediterranean, are liable to create wind farms and even more the availability of sources for hydroelectric power is limited. The proposed solution has been developed instead to solve problems that other solutions leaving unresolved the seas like the Mediterranean. Almost all the systems currently being developed to generate energy from marine sources are manufactured and designed to exploit these characteristics so that they can be classified as ocean waves, characterized mostly by high periods and amplitudes, can be seen as this market is completely unsaturated and as currently there is no monopolistic forms showing sales volumes such that undermine the recent spread of technologies and/or first sales phase, as might be the ISWEC in the Mediterranean.

10.1 Energy scenario

The solutions proposed by the use of ISWEC are part of devices for power generation from renewable sources. At a very general level some observations supporting the conclusion that the market is extremely large and growing can be reported, especially given the growing demand for energy and new technologies for the production of electricity economically efficient and clean. It is also a market heavily influenced by the political strategies of various countries and supranational bodies like the European Union. As a general statement, energy is a key resource in global production system: presumably in the coming years we will see a sustained growth of the energy demand, considering the growth prospects of developing countries and countries that are undergoing the transition from economy planned to a market economy. The IEA, International Energy Agency estimates a global demand growth of 1.7% per year in the period between 2000 to 2030. Even more decisive is the estimated growth in demand for electricity: 2.4%. In 2000 the final consumption of electricity amounted to 1088 Gtep, against an overall consumption of energy of 6030 Gtep. Those values are expected to increase up to 1419 Gtep in 2010 against 7255 Gtep of global consumption. It is therefore easy to understand the benefits that would be obtained with more efficient and cleaner technologies, both to reduce the costs of producing goods and services and to reduce harmful emissions into the environment. Therefore, measures are going to be set for political and economic incentives for technological research and application of the technology itself, both

in terms of energy production from renewable sources with low emissions and in terms of the increase of energy generation from traditional fuels. In recent years some clean technologies are reaching levels of development making them competitive with traditional generation systems. The IEA estimates a growth rate of energy from renewable sources of 3.3%, excluding hydroelectric power (expected to grow by 1.6%), 2.4% growth of energy from natural gas and 4% growth from coal. This should lead to a total of 4.4% of energy produced from non-hydro renewable sources by 2030, compared to 1.6% in 2000. This scenario implies a higher power of 15000 GW, of which half are expected in developing countries. The new hydroelectric power is expected to reach about 400 GW and the total of other renewable sources to around 380 GW. Since 2020 is expected to attend a significant contribution to energy generated from fuel cells (100 GW in 2030). Among non-hydro renewables the role of solar is thought to be predominant in terms of growth (16% per year), but with a minimum contribution to the total (92 TWh produced in 2030). Wind will increase of 10% per year up to a total of 539 TWh in 2030 whereas geothermal and biomass will increase respectively of the 4.3% and the 4.2%. The ISWEC device will produce energy from waves, hitherto a little used but energy-intensive source, widespread throughout the globe. Currently several technology are in the demonstration phase, but wave power still lacks a reference, which is the case for wind power.

10.2 Market analysis

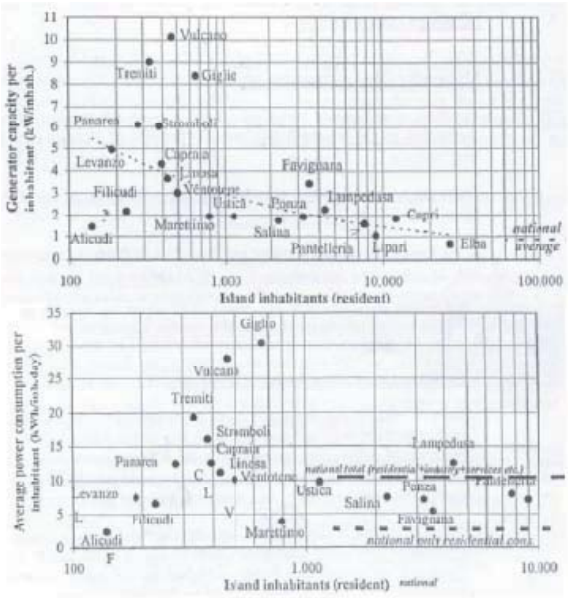

Figure 10.1. Power generation capacities and average consumption of the main Italian islands.

For the grid connected system, the market customers are represented by energy companies (utilities) and ESCO (Energy Service Companies). In Italy, according to the Database of the European Union, there are 51 ESCOs. In order to provide small renewable energy systems or hybrid, the ESCOs may be attractive partners (as complementary in terms of technical skills) and possible intermediates in the construction of plants for Public Administration, for island communities, for businesses and consortia. The five companies have imported more than a share of 74%. Among the utilities operating in the face of renewable energy potential customers of the company you mention EDENS (Edison Energie Speciali), ENEL Green Power, Falck Renewables, ERG-RENEW, ITALY ENDESA, ENECO TRADE, API, FRI-EL and E. ON ENERGY.

The market in which customers can operate the device ISWEC is mainly from the smaller islands, often unconnected to the national grid. In these areas it is necessary to meet their own energy needs. Currently the energy required is supplied by diesel generators supplying both diesel for electricity production, water heaters and boilers. This situation could change profoundly thanks to projects like the 'green island' with the goal to power archipelagos with renewable sources and, where possible, to allow a gradual transition to their total energy self-sufficiency. Given

the high seasonal demographic differences, the electrical load and thermal presents peak values are much higher than the yearly average. It is therefore necessary to oversize the system to ensure adequate capacity and reliability. This necessity is evident making sure that the average installed power per capita is much higher on smaller islands (1 to 10 kW per capita) than on the mainland (0.8 kW per capita), although generally there are no industrial installations. For these areas, the cost of energy varies between 0.30 and 0.44 €/kWh, depending on the accessibility of the site and size of the generators, in some smaller islands were recorded costs of 0.52 ÷ 0.67 €/kWh.

To estimate the potential market in the Mediterranean using these data, the following parameters are assumed:

- average population of small/medium-sized islands: 2500 inhabitants
- average per capita consumption: 6 kW/day
- provide the 10% share of renewable energy (representing the 20% of total)

A total annual consumption of about 20 GWh is therefore estimated.

For the stand-alone system, the market is mainly represented by manufacturers of flotation and signaling devices. For this type of market a product with compact size and developing the small power required for lanterns and marine radio systems is deemed suitable. A primary research identified as potential customers the following companies:

1. Oil Companies
2. Offshore engineering companies
3. Companies designing and/or building devices for harbors
4. Port Authorities
5. Public and private management companies

It was estimated that: Mediterranean ports are 1200 (7000 in the world), each of which shall be deemed necessary at least two buoys, then it is about 2400 for the Mediterranean and 14000 buoys for the world. Furthermore in the Mediterranean 107 offshore units operate (6500 offshore in the world), each of which shall be considered at least four buoys necessary leading to a need of about 428 for the Mediterranean and 26000 for the world. About 14000 km of motorways of the sea under construction in the coming years, corresponding to approximately 560 radio link systems required.

10.3 Expected demand

In order to have a first estimate of the energy produced from the 5 kW ISWEC device along a year, its performances were evaluated in the different wave climates occurring during the year. The 5 kW device was designed using the Alghero mean conditions[1] and its performances were evaluated with the following assumptions:

1. The wave climate is approximated with a regular wave carrying the same power of the real sea state
2. Sea states with peak period smaller than 3 s are not considered
3. Extracted power limited to the rated power (5 kW)

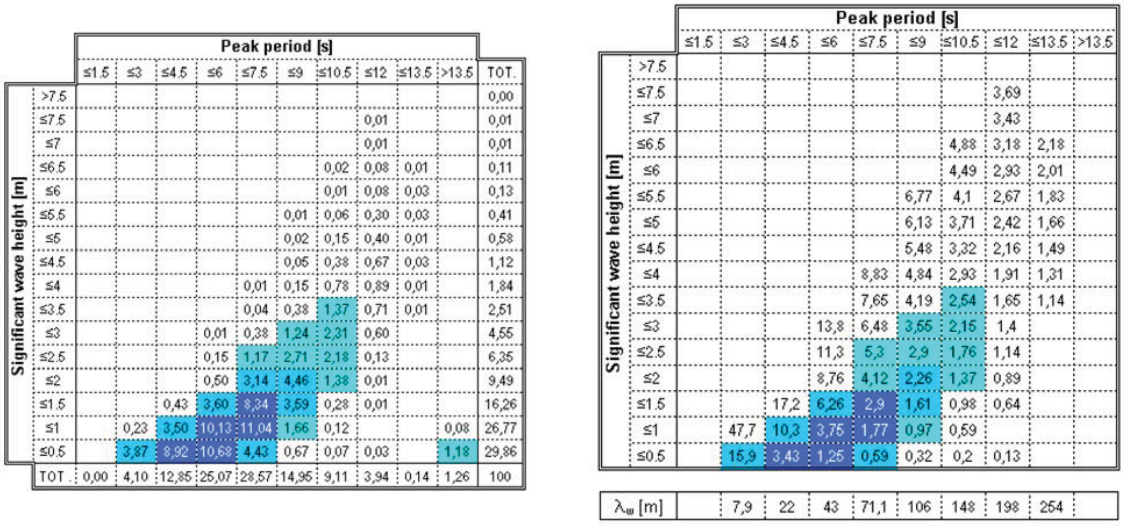

Significant wave height [m] \ Peak period [s]	≤1.5	≤3	≤4.5	≤6	≤7.5	≤9	≤10.5	≤12	≤13.5	>13.5	TOT.
>7.5											0,00
≤7.5								0,01			0,01
≤7								0,01			0,01
≤6.5							0,02	0,08	0,01		0,11
≤6							0,01	0,08	0,03		0,13
≤5.5						0,01	0,06	0,30	0,03		0,41
≤5						0,02	0,15	0,40	0,01		0,58
≤4.5						0,05	0,38	0,67	0,03		1,12
≤4					0,01	0,15	0,78	0,89	0,01		1,84
≤3.5					0,04	0,38	1,37	0,71	0,01		2,51
≤3				0,01	0,38	1,24	2,31	0,60			4,55
≤2.5				0,15	1,17	2,71	2,18	0,13			6,35
≤2				0,50	3,14	4,46	1,38	0,01			9,49
≤1.5			0,43	3,60	8,34	3,59	0,28	0,01			16,26
≤1		0,23	3,50	10,13	11,04	1,66	0,12			0,08	26,77
≤0.5		3,87	8,92	10,68	4,43	0,67	0,07	0,03		1,18	29,86
TOT	0,00	4,10	12,85	25,07	28,57	14,95	9,11	3,94	0,14	1,26	100

Significant wave height [m] \ Peak period [s]	≤1.5	≤3	≤4.5	≤6	≤7.5	≤9	≤10.5	≤12	≤13.5	>13.5
>7.5										
≤7.5								3,69		
≤7								3,43		
≤6.5							4,88	3,18	2,18	
≤6							4,49	2,93	2,01	
≤5.5						6,77	4,1	2,67	1,83	
≤5						6,13	3,71	2,42	1,66	
≤4.5						5,48	3,32	2,16	1,49	
≤4					8,83	4,84	2,93	1,91	1,31	
≤3.5					7,65	4,19	2,54	1,65	1,14	
≤3				13,8	6,48	3,55	2,15	1,4		
≤2.5				11,3	5,3	2,9	1,76	1,14		
≤2				8,76	4,12	2,26	1,37	0,89		
≤1.5			17,2	6,26	2,9	1,61	0,98	0,64		
≤1		47,7	10,3	3,75	1,77	0,97	0,59			
≤0.5		15,9	3,43	1,25	0,59	0,32	0,2	0,13		
λ_w [m]		7,9	22	43	71,1	106	148	198	254	

Figure 10.2. Scattering table of wave climate occurrences expressed in % on the left and scattering table of the input forcing function ($\lambda_0 \cdot \omega$) expressed in deg/s on the right.

The estimated annual production per device (statistics data on the occurrences of the sea of Alghero, 5 kW of average power) is about 22 MWh. Therefore to meet the demand hypothesized in the previous paragraph, the number of devices required is approximately 910.

For the stand-alone system it is estimated a replacement market of about 1/10 compared to the stocks listed in the previous paragraph. The market can therefore be estimated in 338 units for the Mediterranean and 4000 units for the world.

[1]Please refer to section 8.2 for details.

10.4 Marketing Plan

Politics of price

The most appropriate strategy is to choose a proper price of skimming: it must be such as to give the product a high business image and to attract consumers pioneers. To determine the price at which ISWEC will be sold to the end user a Mark-up Approach has used. The 1 kW stand-alone device has an estimated production cost of 12500 €and a Mark up 60% on the cost of components, assembly and testing. The 5 kW Grid Connected device will have a production cost of 30000 €and it will be sold at a price of 55000 €with a Mark-up of 83% only on components, assembly and testing. The price is inclusive of:

- preliminary study of the installation site (for ad hoc optimization of the device)
- verifying the correct operation
- any minor customization (to be carried out prior to installation of the device)
- warranty (and servicing, repair, replacement)
- ISWEC device.

In the case of the 5 kW device, the connection to local power line is not included in the price.

Advertising

The part of the advertising will be carried out by using contacts in universities and research centers, through market research, email, direct contacts (trade shows, conferences) and contacts through the partners. The channels will be privileged promotional trade shows and conferences. The communication policy mainly consists of:

- direct contact (commercial agents / clients)
- promotional activities in trade shows
- business consultancy
- contacts via Internet.

For the Internet channel a website where you can find all information about the characteristics of devices ISWEC will be created. The site will also be supported by a service contact and a mailing list for updates and information about the activities of the company. In the case of direct contact will take care of the sales staff through its agents. These implement the promotion by having presentations and demonstration

through the distribution of devices. As for trade shows, they play an important role in promoting and advertising of new technological solutions developed. Below there is a list of international events which will have a dedicated management attention.

- International Conference on Energy Systems and Technologies (14feb to 16feb 2011) Cairo www.afaqscientific.com/icest2011/
- Energy and Sustainability 2011 (11apr ÷ 13apr 2011) Alicante, Spain www.wessex.ac.uk/11-conferences/energy-2011.html
- GENERATES 2011 (11mag 13mag-2011) Madrid
- Coastal Management 2011: Innovative Coastal Zone Management: Sustainable Engineering for a Dynamic Coast (15nov - 16nov 2011) Belfast www.ice-coastalmanagement.com/

Distribution and sale

The distribution channel will be mainly a direct channel, therefore it will be a fixed cost. The company will target direct sales to customers through its commercial agents. The sales agents will ensure greater customer focus while increasing efficiency in the sales stage from the point of view of costs. The company will operate on commission and for the purchase. The customer can contact the office of the company via telephone, Internet or with a direct contact going to the company office.

To ensure success in sales the company will need to focus on the following points:

- Try to offer a strong value proposition
- Identify the correct market
- Make simple contact between companies and customers

These three elements will be the focus of sales activities conducted by the company and, above all to ease the contact with the market, it is necessary to specify the type of relationship between agent and customer for each product.

10.5 Operative plan

Product development

For about two years the company will focus almost entirely on R & D in order to develop both the product models, starting with the small size one in order to acquire the necessary experience to make the larger one, which is expected to give the largest

contribution in terms of turnover. In particular, for stand-alone device, the company will develop a prototype and perform the experiments in different fields of use in order to commercialize the final version by the third year. Meanwhile, the experience will be partly transferred to the development of the Grid Connected product for which the testing activities and formulation of technical specifications will allow the marketing by the 5th year. The R & D is designed for optimization of devices (reduced size and weight), improved energy efficiency and reducing production costs. The company will rely for product development, in case it becomes necessary and in addition to the expertise represented by the figures of designers and technical director, to the consulting partners and the resources of the Politecnico di Torino.

Manufacturing / supply chain

- Raw materials, WIP: The company, after receiving the purchase order by the customer, prepares a production order supplier. The company decides for itself the necessary raw materials supply and management and handling of semi-finished goods.

- Production policy: The company policy is to not work with a stock product, but to follow a logical order, the production function will be completely outsourced to the partner for production.

- Warehouse: As already mentioned in the previous paragraph, the company works with job orders and therefore it is not expected to work with a warehouse. The partner, within its structure will hold in stock a minimum supply of raw materials, components or finished products.

- Logistics and Transport: The logistic function for the supply of raw materials and components necessary for production is handled entirely by the partners. As regards the distribution of the device, the company simply provides at its production facility or the place of the partner, the devices ready for shipping according to Incoterms 'ex works'.

- Vendors and suppliers: The company has as its main supplier the company that deals with the production function. Regarding the choice of suppliers of individual components and raw materials, it allows freedom of choice and bargaining power to the partner. The company sales means relies on the following channels:

  – Corporate Website
  – Sales representatives

  Initially (end of second year) there will be a couple of sales agents for the sale of stand-alone device. This number will rise to 4 with the commercialization of

Grid Connected. These will refer to the figure of the CMO also excluded from the initial team of entrepreneurs. The company, in order to identify contacts and potential customers will use commercial consultants, more specifically it will use a consultant during the marketing of the device size and less after that two of them with the market introduction of the product of larger size.

- Technology: The company needs the following facilities to carry out its activities:
  - Tools and hardware inside the company will be divided into several offices, the staff of each of these will have a computer with Internet, telephone, fax and printer. For furniture we turn to a supplier close to the company headquarters.
  - Software: the company personnel will be supplied because the Microsoft Office package and, depending on the professional, a series of applications relevant to performing the task (program order management, complaints management, billing, and programs for numerical computation, etc.)
  - Telecommunications: the company uses the telephone channel and the Internet to maintain contact with figures such as company internal and external designers and commercial agents as customers and business partners.
- Financial systems
  - Accounting: Figure CFO overlap the position of supervisor of accounting and controller and also the post of head of policy financing. As for general tasks such as managing billing and payroll will be referred to an accountant.
  - Order management: Orders from customers via website and sales agents will be managed within the company by the figure of CMO which will run on the production order to the supplier partner. The partner takes care of the following levels of value chain: inbound logistics, production, outbound logistics.
  - Payments management: It is expected to conclude an agreement with a financial institution for giving customers payment by installments. It was then estimated the average delay for sales in one month, while supposedly two months of deferred payment providers.
- Customer service, warranty: The mechanical parts and its correct working are guaranteed for 5 years.

10.6 Implementation plan

The company will focus on R & D on ISWEC both Stand Alone (SA) and Grid Connected (GC) in order to evaluate and optimize its performances.

The next activity will target respectively:

- Manufacturing of the 1:8 scale prototype of the system
- Testing the prototype in Naples in the tank
- Re-engineering of both products (SA - GC)
- Manufacturing of the prototypes SA in real scale
- Manufacturing of the prototypes GC in real scale
- Re-engineering of future production processes.

At the end of tank tests, the company will proceed to sea trials, probably on the island of Pantelleria where a sea site of interest is already monitored by the Politecnico di Torino. At the port of Pantelleria a wave gauge is in fact installed. The experimental data obtained will be used to identify the correct design specifications of the full scale system. The company expects to finalize the development of stand-alone device within two years so the commercialization can begin in the third year. A more accurate analysis is performed through the Gantt chart highlighting the key stages of the development.

10.7 Financial Plan

A detailed financial plan has been arranged and its main points are below reported.

1. Definition of the expected turnover, EBIT, EBITDA, Return on Sales, ROI, ROE in the 5 years period
2. Evaluation of the cash flow and burn rate and definition of the two main stage of the development:
   (a) The first phase, lasting two years, does not provide sales, but development activities of the devices and initialize the corporate structure: the capital required for this phase is estimated at around 700000 €, considering the majority of activities funded
   (b) The second phase deals with the commercial launch and the beginning of the production: another 200000 €is estimated to be needed

3. Definition of variable costs, investments and profits.

One of the main outcomes of the financial analysis is the definition of the cost of energy. For the grid connected device we can account the following parameters:

- 55000 €as cost of the device
- 10000 €for installation of the device (considering a sea farm of at least 10 devices)
- 4000 €per device for permissions and installation site design
- Useful life of the device: 20 years
- Annual interest rate: 5.6%
- 4380 hours of operation per year (average 12 hours a day, 365 days a year)
- Average maintenance costs: 1650 €/year.

It comes that the energy produced will cost about 0.34 €/kWh, which can be considered cost-effective when compared with the energy costs incurred in small islands or the price resulting from the sum of green certificates (0.34€) and the hourly rate for electricity (more than 0.10 €).

In the stand-alone applications it is not so important the cost of electricity generation as the critical role of the specific application. In particular in the telecommunication devices along the motorways of the sea the requirement can't be met at lower costs because of the power levels required by the application.

Chapter 11

Conclusions

In this work the ISWEC device has been analyzed. ISWEC is a Wave Energy Converter using gyroscopic effects to transform sea waves power into electrical power.

In order to understand the device dynamics a study of the mechanical equations describing the gyroscopic system has been done. Since the resultant equations are relatively complex in a first approach they have been linearized to obtain a simplified system to quickly understand the behavior of the ISWEC. Thanks to a comparison with a complete non-linear numerical model of the gyroscopic system built in the SimMechanics environment, the linearized system proved to be reliable for rough estimation but, except for the working conditions implicating small oscillations around the ε axes, a non linear analysis is needed for an accurate evaluation of the system behavior. However the linearized system allowed to build a design tool able to identify the ISWEC physical dimensions directly from the wave parameters (through some assumptions on the float dynamics). This method has been used to design a small scale prototype with 2.2 W rated power and able to work with the nominal wave of the curved wave tank present at the University of Edinburgh (100 mm wave height and 1 s wave period). The output of the design tool has been checked using the nonlinear model and resulting in small corrections on the design to make the system working as wished.

The final version of the device has then been constructed and subjected to dry tests. The dry tests have been performed on a wave simulation rig built at the Mechanical Department of the Politecnico di Torino and the tests demonstrated the power extraction capabilities of the prototype and the effectiveness of the non-linear numerical model. The device was so ready for the tank tests at the University of Edinburgh. The wave tank tests were aimed to understand the float dynamics being the gyroscopic system behavior already verified through the dry tests. The float proved to be an important part of the device: the designed float shape was not able to transfer the wave actions on the gyroscopic system which in turn could not produce the desired power. The float width had to be increased from 230 mm to

1200 mm, about five times the initial width. With this new float, albeit composed mainly of a Divinycell slab, the ISWEC prototype was able to extract 2.06 W, a value very close to the 2.2 W rated power. However, since the real wave produced from the tank when ISWEC was working was slightly bigger than the design wave, the wave power density was bigger too and the achieved relative capture width was the relatively small value of 14.3%.

In order to improve the result, a purposely designed float shape has been built and another test campaign has been performed using the 600 mm wide flume present at the Hydraulics Department of the Politecnico di Torino. The outcomes of the test campaign showed that for the 570 mm wide float, the rated gyro speed (2000 rpm) damped too much the float pitching motion and therefore resulting in a smaller extraction of power. By decreasing the gyro speed to 500 rpm, the float pitching angle increased and the exctracted power too, reaching the maximum of 0.89 W corresponding to a relative capture width of 21.6%. Being 500 rpm the 25% of the rated value 2000 rpm and being the absorbed power proportional with $\dot{\varphi}$, the prototype designed in chapter 3 seems to be able to absorb about the double of its rated power.

The outcomes of the tank and flume tests have been used to design a bigger device scaled 1:8 with respect to the average values of the Italian site Alghero. This new prototype will be tested in the Naples wave tank in approximately December 2010. The new model has a rated power of 213 W and a float width of 5 m. The power density of the 300 mm high and 7.8 m long incoming wave is 213 W/m. In this project a particular care is placed in order to reduce the power losses for maintaining in rotation of the flywheel to less than the 10% of the produced power. The goal is achieved by making the flywheel to rotate in a vacuum (1000 Pa abs) chamber and using normal ball bearings. The whole system will have an efficiency of about 70%, this value being relatively small due to the low efficiency of the PTO used in the project (80%).

The 1:8 ISWEC prototype main quantities have been then scaled to the full dimensions and compared with the Pelamis WEC main parameters. The comparison shows that ISWEC has almost the same power/mass ratio of the Pelamis whereas the nominal area usage per unit of power is about 6 times bigger. However that comparison has to be rectified when the tank tests in Naples will be performed. In fact, the small prototype tested in the flume proved to be able to catch the same power with about half the angular momentum: if this relevant improvement will be verified on the 1:8 prototype model, the rated power of the device can be doubled with respect to the rated power declared in chapter 9 and the device would be immediately cheaper.

One of the advantages of the ISWEC respect to the Pelamis WEC and respect to most of the existing converters, is the absence of moving part working in sea water or spray. This makes the ISWEC a device intrinsically suitable for high reliability

and long MTBF. Furthermore the ISWEC can be literally switched off if the wave conditions are too dangerous for safe operations. In this case, by nulling the gyro angular speed, the device behaves as a dead body slack moored to the sea bed (like a wave measurement buoy) and increases its capabilities to storm surviving.

In the tenth chapter an economical analysis has been carried out to understand possible market scenarios. A market for both a grid connected and for a stand-alone system were evaluated. A company able to exploit those markets was designed in order to be as lean and quick as possible. Eventually an estimate of the cost of energy for a 5 kW rated power ISWEC was given at 0.34 €/kWh with a device life of 20 years.

Finally, to give a general overview of the ISWEC capabilities in terms of extractable power, here it is recalled equation (2.19) representing the absorbed power evaluated through the linear model.

$$P_d = \frac{1}{2}(J\dot{\varphi})\omega^2\delta_0\varepsilon_0$$

Where P_d is the absorbed power, ω the wave frequency, δ_0 the angle of pitching, ε_0 the angle of the PTO oscillation and $J\dot{\varphi}$ is the angular momentum of the gyro.

The typical wave period in the oceans is comprised between 6 and 10s, meaning the order of magnitude of ω^2 is 10^0 rad/s. The order of magnitude of δ_0 is of some degrees and therefore 10^{-1} rad, whereas ε_0, if the device is controlled as described in this Thesis, has order of 10^0 rad. That means that if there is the need to build a device with 100 kW of rated power, the needed angular momentum will be of the order of 10^6 kgm^2·rad/s.

Being P_d proportional to ω^2, the extractable power can be increased by deploying the device in seas with shorter wavelength and therefore shorter periods (the Mediterranean, in spite of its small power density, is one of those). Furthermore the float can be studied to be wave resonating and therefore increase the δ_0 contribution and several strategies of control can be implemented to increase ε_0.

The large needed angular momentum can be split in several subsystems or achieved using high speed flywheels in carbon fiber or steel wires. These solutions need to be investigated. The proper choice, in absence of technical problems, would be decided on economical basis.

However the tests in the wave tank in Naples will help to evaluate more accurately the required angular momentum, a key factor in the development of ISWEC.

Appendix A

Datasheets

A.1 Small scale Prototype

Planetary Gearhead GP 42 C ∅42 mm, 3 - 15 Nm

Ceramic Version

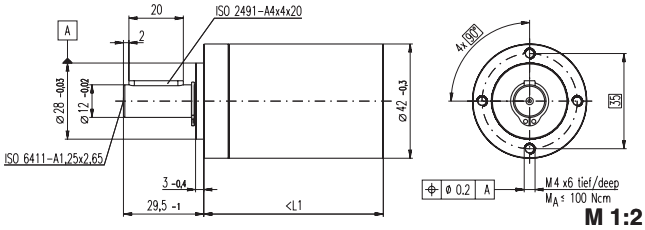

Technical Data

Planetary Gearhead	straight teeth
Output shaft	stainless steel
Bearing at output	preloaded ball bearings
Radial play, 12 mm from flange	max. 0.06 mm
Axial play at axial load	< 5 N 0 mm
	> 5 N max. 0.3 mm
Max. permissible axial load	150 N
Max. permissible force for press fits	300 N
Sense of rotation, drive to output	=
Recommended input speed	< 8000 rpm
Recommended temperature range	-20 ... +100°C
Extended area as option	-35 ... +100°C
Number of stages	1 2 3 4
Max. radial load, 12 mm from flange	120 N 150 N 150 N 150 N

Stock program
Standard program
Special program (on request)

			Order Number									
			203113	203115	203119	203120	203124	203129	203128	203133	203137	203141
Gearhead Data												
1	Reduction		3.5 : 1	12 : 1	26 : 1	43 : 1	81 : 1	156 : 1	150 : 1	285 : 1	441 : 1	756 : 1
2	Reduction absolute		$^{7}/_{2}$	$^{49}/_{4}$	26	$^{343}/_{8}$	$^{2197}/_{27}$	156	$^{2401}/_{16}$	$^{15379}/_{54}$	441	756
3	Mass inertia	gcm²	14	15	9.1	15	9.4	9.1	15	15	14	14
4	Max. motor shaft diameter	mm	10	10	8	10	8	8	10	10	10	10
	Order Number		**203114**	**203116**		203121	203125		203130	**203134**	203138	**203142**
1	Reduction		4.3 : 1	15 : 1		53 : 1	91 : 1		186 : 1	319 : 1	488 : 1	936 : 1
2	Reduction absolute		$^{13}/_{3}$	$^{91}/_{6}$		$^{637}/_{12}$	91		$^{4459}/_{24}$	$^{637}/_{2}$	$^{4394}/_{9}$	936
3	Mass inertia	gcm²	9.1	15		15	15		15	15	9.4	9.1
4	Max. motor shaft diameter	mm	8	10		10	10		10	10	8	8
	Order Number			203117		203122	**203126**		**203131**	203135	**203139**	
1	Reduction			19 : 1		66 : 1	113 : 1		230 : 1	353 :1	546 : 1	
2	Reduction absolute			$^{169}/_{9}$		$^{1183}/_{18}$	$^{338}/_{3}$		$^{8281}/_{36}$	$^{28561}/_{81}$	546	
3	Mass inertia	gcm²		9.4		15	9.4		15	9.4	14	
4	Max. motor shaft diameter	mm		8		10	8		10	8	10	
	Order Number			203118		**203123**	203127		203132	203136	203140	
1	Reduction			21 : 1		74 : 1	126 : 1		257 : 1	394 : 1	676 : 1	
2	Reduction absolute			21		$^{147}/_{2}$	126		$^{1029}/_{4}$	$^{1183}/_{3}$	676	
3	Mass inertia	gcm²		14		15	14		15	15	9.1	
4	Max. motor shaft diameter	mm		10		10	10		10	10	8	
5	Number of stages		1	2	2	3	3	3	4	4	4	4
6	Max. continuous torque	Nm	3.0	7.5	7.5	15.0	15.0	15.0	15.0	15.0	15.0	15.0
7	Intermittently permissible torque at gear output	Nm	4.5	11.3	11.3	22.5	22.5	22.5	22.5	22.5	22.5	22.5
8	Max. efficiency	%	90	81	81	72	72	72	64	64	64	64
9	Weight	g	260	360	360	460	460	460	560	560	560	560
10	Average backlash no load	°	0.3	0.4	0.4	0.5	0.5	0.5	0.5	0.5	0.5	0.5
11	Gearhead length L1	mm	40.9	55.4	55.4	69.9	69.9	69.9	84.4	84.4	84.4	84.4

EC 40 ∅40 mm, brushless, 120 Watt, CE approved

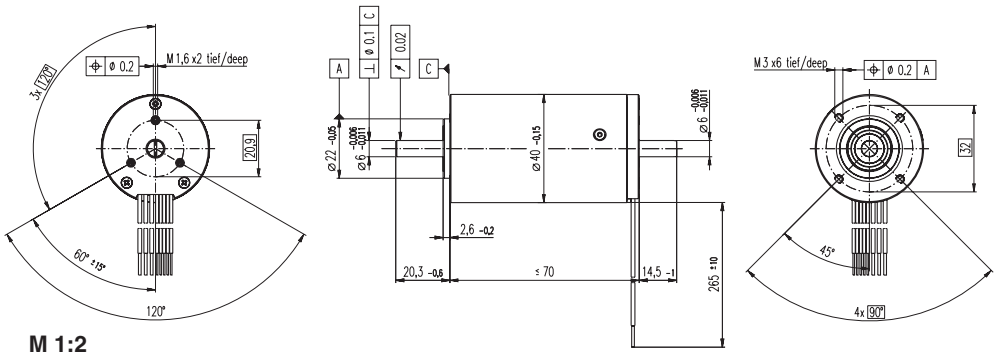

M 1:2

Stock program
Standard program
Special program (on request)

			Order Number													
			167176	167177	118894	118895	167178	167179	118896	118897	167180	118898	167181	167183	118899	118901
Motor Data																
	Values at nominal voltage															
1	Nominal voltage	V	12.0	18.0	21.0	30.0	24.0	36.0	42.0	48.0	48.0	48.0	48.0	48.0	48.0	48.0
2	No load speed	rpm	10300	12000	10400	11600	10300	9830	10400	7560	10300	5930	5420	3530	3110	2020
3	No load current	mA	886	754	515	426	443	275	258	139	222	97.8	86.2	48.6	41.3	24.4
4	Nominal speed	rpm	9050	10900	9240	10500	9160	8710	9290	6450	9190	4830	4290	2400	1990	893
5	Nominal torque (max. continuous torque)	mNm	107	113	116	120	120	123	122	127	123	130	126	127	129	129
6	Nominal current (max. continuous current)	A	10.4	8.62	6.46	5.24	5.78	3.76	3.40	2.22	2.96	1.77	1.57	1.03	0.920	0.599
7	Stall torque	mNm	985	1340	1150	1420	1210	1200	1280	940	1270	743	639	410	370	237
8	Starting current	A	89.2	94.4	60.1	57.9	55.0	34.6	33.5	15.7	28.8	9.72	7.65	3.21	2.56	1.07
9	Max. efficiency	%	81	83	83	84	83	83	84	82	84	81	80	77	76	72
	Characteristics															
10	Terminal resistance phase to phase	Ω	0.134	0.191	0.349	0.518	0.436	1.04	1.25	3.07	1.66	4.94	6.28	14.9	18.8	44.8
11	Terminal inductance phase to phase	mH	0.0266	0.0439	0.0797	0.132	0.106	0.263	0.319	0.788	0.425	1.28	1.52	3.56	4.57	10.7
12	Torque constant	mNm / A	11.0	14.2	19.1	24.6	22.1	34.7	38.2	60.1	44.1	76.4	83.5	128	145	221
13	Speed constant	rpm / V	865	673	500	389	433	275	250	159	216	125	114	74.8	66.0	43.2
14	Speed / torque gradient	rpm / mNm	10.5	9.05	9.13	8.20	8.55	8.26	8.20	8.12	8.16	8.07	8.59	8.76	8.56	8.75
15	Mechanical time constant	ms	9.39	8.06	8.13	7.30	7.61	7.35	7.30	7.22	7.26	7.18	7.64	7.79	7.62	7.78
16	Rotor inertia	gcm²	85.0	85.0	85.0	85.0	85.0	85.0	85.0	85.0	85.0	85.0	85.0	85.0	85.0	85.0

Specifications

Thermal data

17	Thermal resistance housing-ambient	3.2 K / W
18	Thermal resistance winding-housing	1.2 K / W
19	Thermal time constant winding	17.1 s
20	Thermal time constant motor	1050 s
21	Ambient temperature	-20 ... +100°C
22	Max. permissible winding temperature	+125°C

Mechanical data (preloaded ball bearings)

23	Max. permissible speed	18000 rpm
24	Axial play at axial load < 8 N	0 mm
	> 8 N	max. 0.14 mm
25	Radial play	preloaded
26	Max. axial load (dynamic)	10 N
27	Max. force for press fits (static)	170 N
	(static, shaft supported)	5000 N
28	Max. radial loading, 5 mm from flange	70 N

Other specifications

29	Number of pole pairs	1
30	Number of phases	3
31	Weight of motor	390 g

Values listed in the table are nominal.
Explanation of the figures on page 141.

Connection motor (Cable AWG 22)

red	Motor winding 1
black	Motor winding 2
white	Motor winding 3

Connection sensors (Cable AWG 26)[1)]

green	V_{Hall} 4.5 ... 24 VDC
blue	GND
red / grey	Hall sensor 1
black / grey	Hall sensor 2
white / grey	Hall sensor 3

Wiring diagram for Hall sensors see page 27

1) Not lead through in combination with resolver.

Operating Range

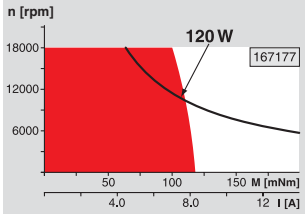

Comments

Continuous operation
In observation of above listed thermal resistance (lines 17 and 18) the maximum permissible winding temperature will be reached during continuous operation at 25°C ambient.
= Thermal limit.

Short term operation
The motor may be briefly overloaded (recurring).

Assigned power rating

maxon Modular System

Overview on page 16 - 21

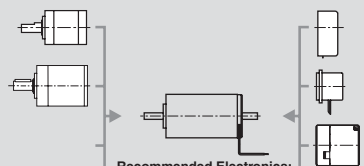

Planetary Gearhead
∅42 mm
3 - 15 Nm
Page 240

Planetary Gearhead
∅52 mm
4 - 30 Nm
Page 243

Encoder HED_5540
500 CPT,
3 channels
Page 269 / 271

Resolver Res 26
∅26 mm
10 V
Page 278

Brake AB 28
∅40 mm
24 VDC, 0.4 Nm
Page 316

Recommended Electronics:

DECS 50/5	Page 288
DEC 50/5	289
DECV 50/5	295
DEC 70/10	295
DES 50/5	296
DES 70/10	296
EPOS2 24/5	303
EPOS2 50/5	303
EPOS 70/10	303
EPOS P 24/5	306
Notes	**20**

maxon sensor

Encoder HEDL 5540, 500 CPT, 3 Channels, with Line Driver RS 422

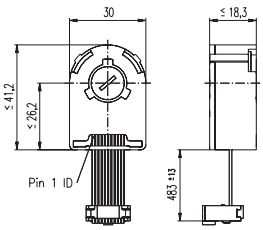

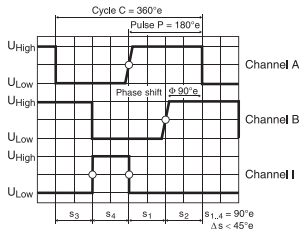

Stock program
Standard program
Special program (on request)

Order Number	110512	110514	110516
Type			
Counts per turn	500	500	500
Number of channels	3	3	3
Max. operating frequency (kHz)	100	100	100
Max. speed (rpm)	12000	12000	12000
Shaft diameter (mm)	3	4	6

GPM9

Peak Torque **130 Ncm**
Cont. Torque **13 Ncm**
Cont. Power **41 Watts**
Speed **<1 to 6000 rpm**

The Printed Motor Works *GP*M9 is a totally enclosed dc motor in an ultra slim pancake profile. This pancake motor can provide a cost effective servo capability. Using flat armature technology the motor is ideal for general purpose applications.

Motor Constants	Symbol	Unit	Value
Voltage	Ke	V/krpm	2.3
Torque	Kt	Ncm/Amp	2.2
Damping	Kd	Ncm/1000rpm	0.30
Friction	Tf	Ncm	1.2
Terminal Resistance	I	Ohm	1.1

Motor Ratings	Unit	Value
Voltage	Volts	14.5
Current	Amps	6.9
Torque	Ncm	13.1
Speed	RPM	3000
Power	Watts	41

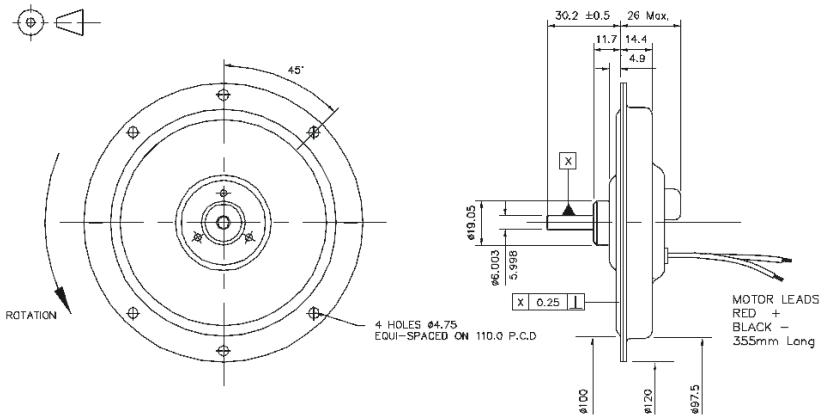

Sample design modifications

Shaft
Round shaft
Extra flats
Length variants
Cut gear
Other modifications

Brushes
Long life for continuous duty applications
Low resistance brushes for servo applications
High altitude
Vacuum

Extra
EMC suppression
Long leads
Connectors
Tri-rated cable
Rated for operation in 150°C ambient

ISO9001-2008

A.2 Naples prototype

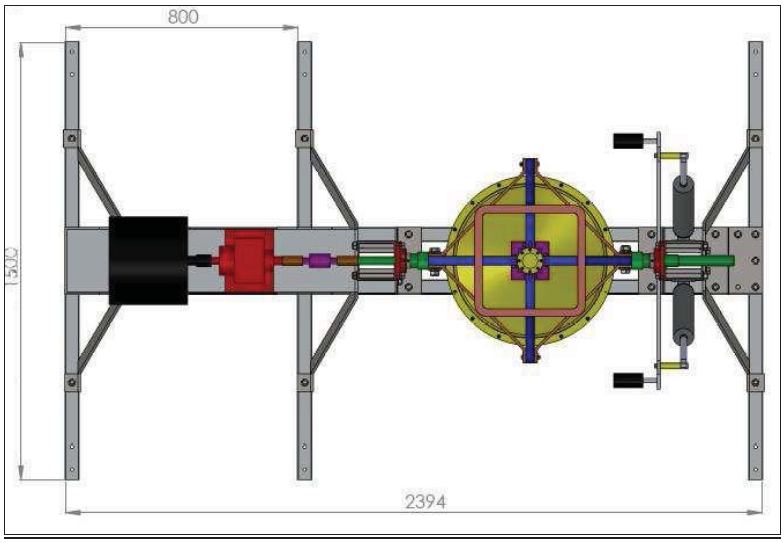

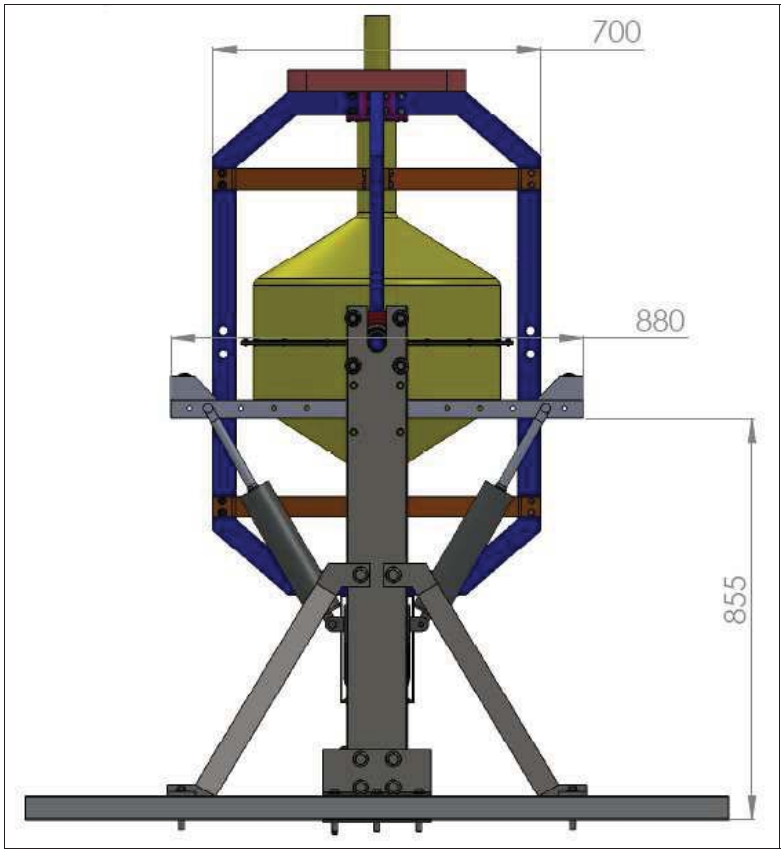

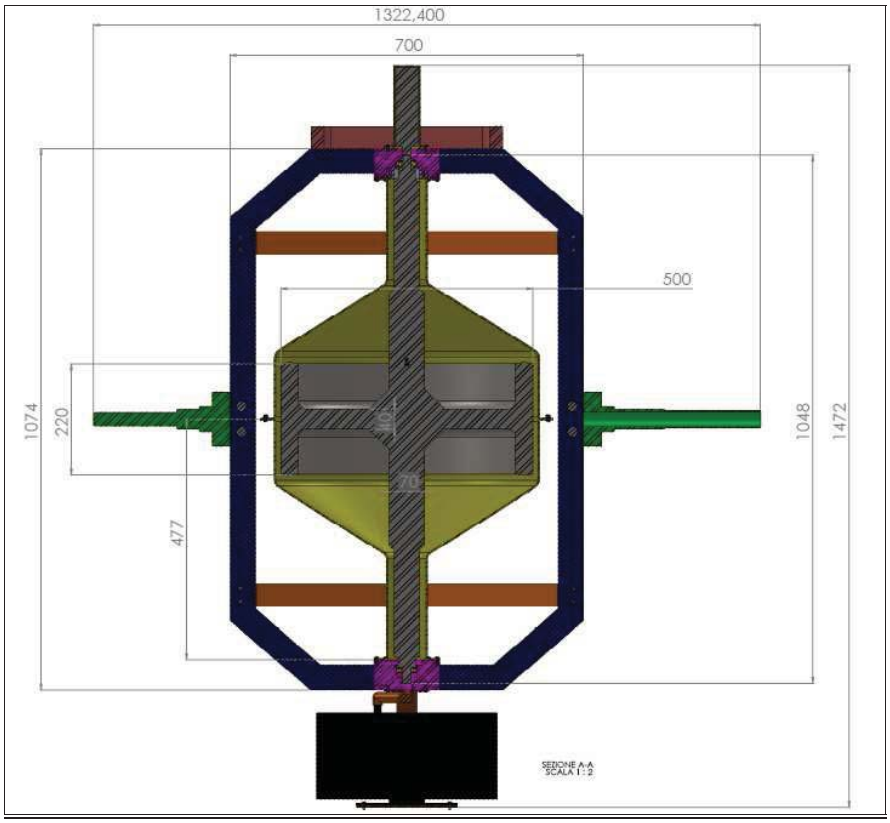
1322,400
700
500
1074
220
1048
1472
477
70
SEZIONE A-A
SCALA 1 : 2

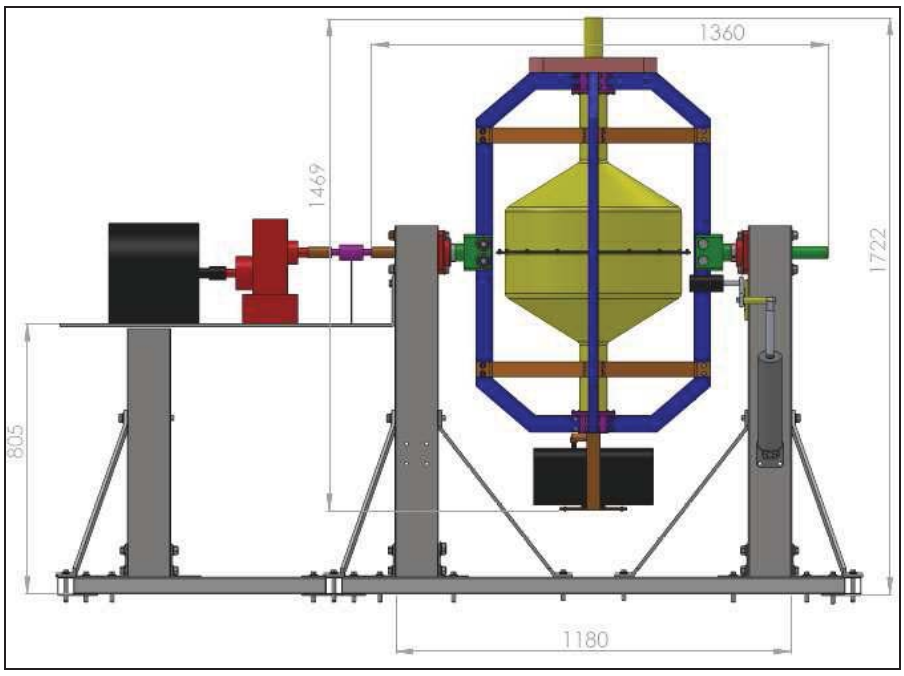
1360
1469
1722
805
1180

MOTION TECHNOLOGY

Standard

TORQUE MOTOR

TML0210-150

		Winding codes	3TBN	3UBS
PERFORMANCES		UNIT	FREE AIR CONVECTION	
Tp	Peak torque	Nm	672	
Tc	Continuous torque	Nm	98.3	95.8
Ts	Stall torque	Nm	73.9	71.9
Kt	Torque constant	Nm/Arms	16.9	12.7
Ku	Back EMF constant (*)	Vrms/(rad/s)	9.79	7.35
Km	Motor constant	Nm/ √ W	6.92	6.74
R20	Electrical resistance at 20°C (*)	Ohm	4	2.37
L1	Electrical inductance (*)	mH	22.9	12.9
Ip	Peak current	Arms	56.2	74.9
Ic	Continuous current	Arms	5.89	7.65
Is	Stall current	Arms	4.46	5.8
Pc	Max continuous power dissipation	W	286	286

	SPECIFICATIONS	UNIT	FREE AIR CONVECTION
Udc	Nominal input voltage	VDC	600
τ th	Thermal time constant	s	2800
Rth	Thermal resistance	K/W	0.333
2p	Number of poles	-	44
J	Rotor inertia	kgm²	4.5E-002
Mr	Rotor mass	kg	7.57
Ms	Stator mass	kg	14.1
Td	Max Detent torque (average to peak)	Nm	3.2
ns	Stall speed	rpm	0.0098
Δθw	Water temperature difference for Pc	K	--
qw	Minimum water flow for Δθw	l/min	--
Δpw	Max pressure drop at qw	bar	--

Notes: (*) terminal to terminal

Hypothesis and tolerances are in ETEL's Handbook

Ambiant Temperature = 20° Celsius, Inlet Water Temperature = 20° Celsius
Max Coil Temperature = 130 ° Celsius
Power with stator connected to a total surface of 0.3 m² and rotor to a total surface of 0.14 m²

Caution: Any use of the motor beyond rated speed could lead to hazardous voltage and serious injuries. ETEL cannot be held responsible if the previous recommandation is not strictly applied

T = f(n) for 3TBN

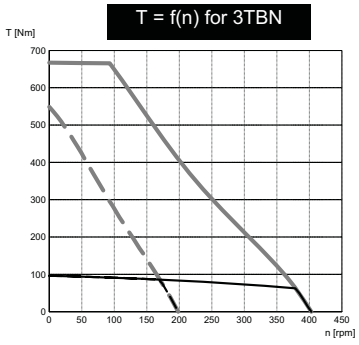

T = f(n) for 3UBS

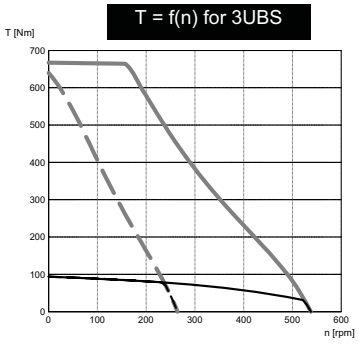

Peak Torque
Tp @ 600 VDC
Tp @ 300 VDC

Continuous Torque with air convection :
Tc @ 600 VDC
Tc @ 300 VDC

08.06.2007 Ver 2.1
ETEL SA
Zone industrielle - 2112 Môtiers - SWITZERLAND
Phone : +41 32 862 01 00
Fax : +41 32 862 01 01
E-mail : etel@etel.ch
http://www.etel.ch

MOTOR

Dimensions are in mm

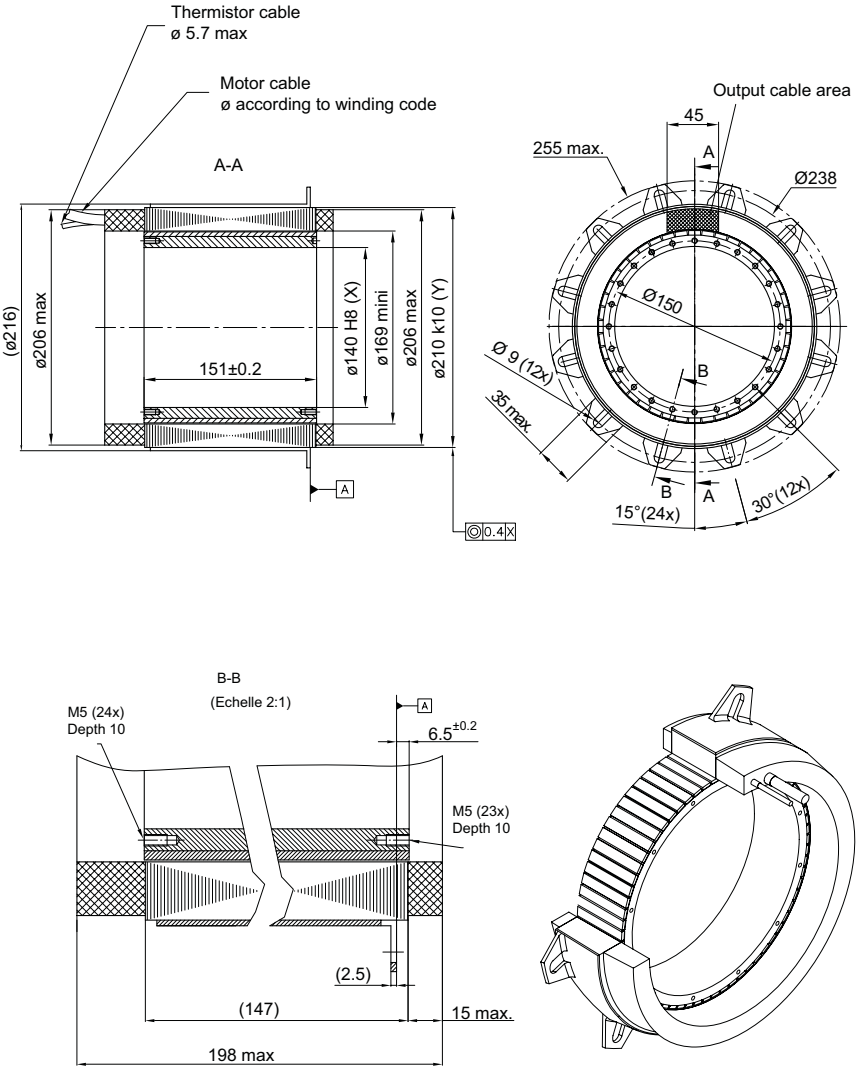

Note 1: Two configurations are available for the stator interface = one (current illustration) with lugs (ref. Face A) at the opposite side of the output cables and the other one with lugs on the same side of the output cables.

Note 2: Refer to the corresponding "Interface winding drawing" for more information about the output cable area

A.3 Pantelleria measurement station

NAUTICAL CHART 1:40000
source: Istituto Idrografico della Marina (Marine Hydrographic Institute), *Sheet* 241

ORTOFOTO
source: ORTOFOTO 2006, PNC

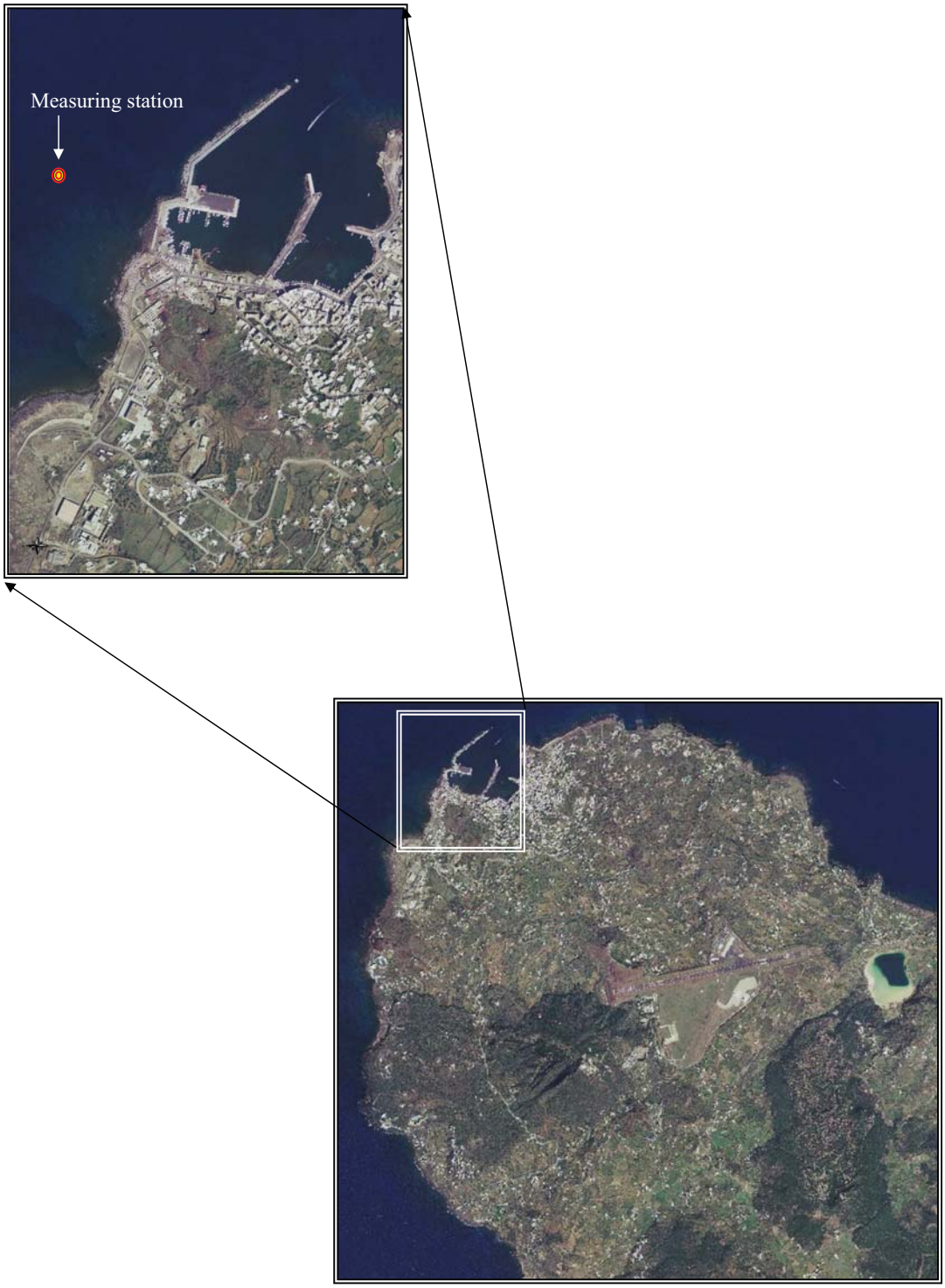

IGM 1:25000
source: Ministero dell'Ambiente e della Tutela del Territorio e del Mare
(Ministry for Environment and Territory and Sea)

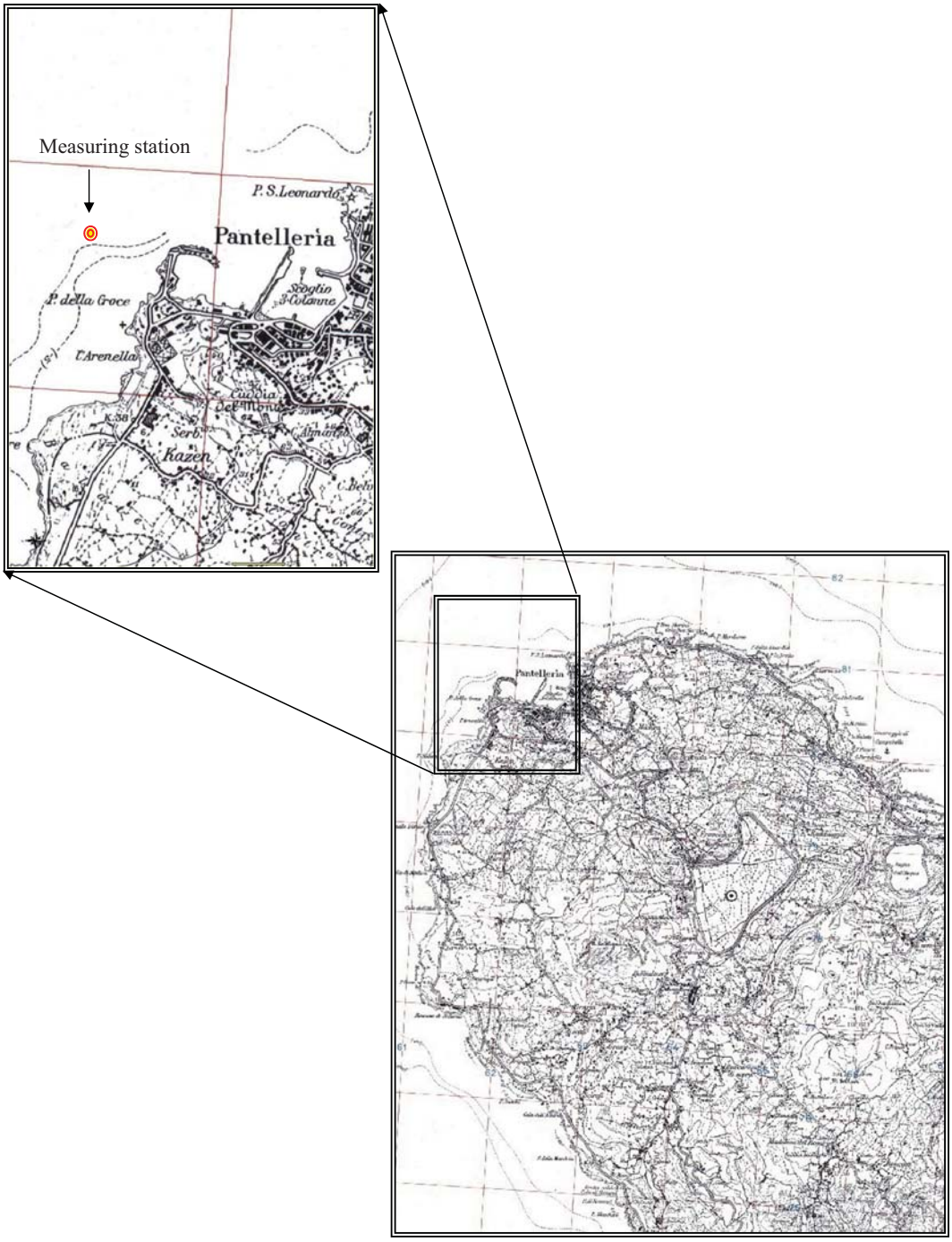

AWAC™

with Acoustic Surface Tracking (AST)

- ✓ **Wave height**
- ✓ **Wave direction**
- ✓ **Full current profile**

...all with a single instrument

The Nortek AWAC is a revolutionary instrument that gives you both a current profiler and a wave directional system in one unit. You can measure the current speed and direction in 1-m thick layers from the bottom to the surface and you can measure long waves, storm waves, short wind waves, or transient waves generated by local ship traffic.

The AWAC is designed as a coastal monitoring system. It is small, rugged, and suitable for multi-year operation in tough environments. It can be operated online or in stand-alone mode with an internal recorder and batteries.

The sensor is usually mounted in a frame on the bottom, protected from the harsh weather and passing ship traffic.

The mechanical design is all plastic and titanium to avoid corrosion. Online systems can be delivered with protected cables, interface units on shore, acoustic modems and backup batteries. In stand-alone use, the raw data are stored to the recorder, and power comes from an external battery pack. A variety of options are available to achieve your required combination of deployment length and sampling interval.

The AWAC software is used to configure the instrument for deployment, retrieve the data and convert all data files to ASCII, and view all the measured current profiles and wave data. In order to calculate the wave parameters, the non-graphical "Quickwave" software will generate ASCII files with all the interesting wave parameters, "Storm" gives you several graphical views of the processed data, and "SeaState" provides online information.

As the plotted time series indicates, both the AWAC's pressure and AST time series capture the long waves. The notable difference is that the AST is capable of measuring the shorter waves superimposed on the longer waves. The AST advantage becomes more relevant and clear as the deployment depths become greater.

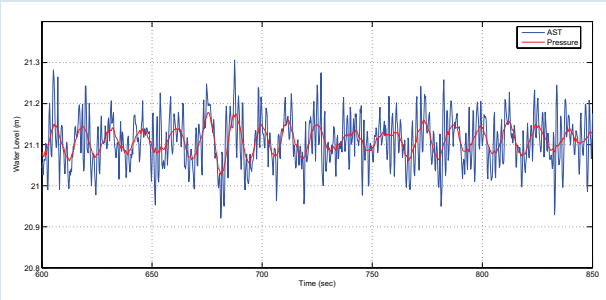

NORTEK AS

www.nortek.no

Specifications

System

Acoustic frequency	1MHz or 600kHz
Acoustic beams	4 beams, one vertical, three slanted at 25°
Operational modes	Stand-alone or online monitoring

Current Profile

Maximum range	30m (1MHz), 50m (600kHz) (depends on local conditions)
Depth cell size	0.4 – 4.0m (1MHz) 0.5 – 8.0m (600kHz)
Number of cells	Typical 20–40, max. 128
Maximum output rate	1s

Velocity measurements

Velocity range	±10m/s horizontal, ±5m/s along beam
Accuracy	1% of measured value ±0.5cm/s

Doppler uncertainty

Waves	3.5cm/s at 1Hz for 2m cells
Current profile	1cm/s (typical)

Wave measurements

Maximum depth	40m (1MHz), 60m (600kHz)
Data types	Pressure, one velocity cell along each slanted beam, AST
Sampling rate (output)	1Hz/2Hz standard, 2Hz /4Hz AST (1MHz), 1Hz standard, 2Hz AST (600kHz)
No. of samples per burst	512, 1024, or 2048

Wave estimates

Range	-20 to +20m
Accuracy/resolution (Hs)	<1% of measured value/1cm
Accuracy/resolution (Dir)	2° / 0.1°
Period range	0.5-30sec

Depth (m)	cut-off period (Hs)	cut-off period (dir.)
5	0.5 sec	1.5 sec
20	0.9 sec	3.1 sec
60	1.5 sec	5.5 sec

Sensors

Temperature	Thermistor embedded in housing
Range	–4°C to 40°C
Accuracy/ Resolution	0.1°C/0.01°C
Time constant	<10 min
Compass	Flux-gate with liquid tilt
Accuracy/Resolution	2°/0.1° for tilt <20°
Tilt	Liquid level
Accuracy/Resolution	0.2°/0.1°
Up or down	Automatic detect
Maximum tilt	30°
Pressure	Piezoresistive
Range	0–50m (standard)
Accuracy/Resolution	0.5% of full scale/ Better than 0.005% of full scale per sample

Transducer configurations

Standard	3 beams 120° apart, one at 0°
Asymmetric	3 beams 90° apart, one at 5°

Data Recording

Capacity (standard)	2 MB, expandable to 26/82/154MB
Profile record	Ncells×9 + 120
Wave record	Nsamples×24 + 46

Data Communication

I/O	RS232 or RS422
Baud rate	300–115200, inquire for 1MBit
User control	Handled via "AWAC" software, NIPtalk or ActiveX® controls

Power

DC input	9–16VDC
Peak current	2A
Power consumption	see AWAC software

Offshore Cable

The Nortek offshore cable can, when properly deployed, withstand tough conditions in the coastal zone. In RS422 configuration, cable communication can be achieved for distances up to 5km.

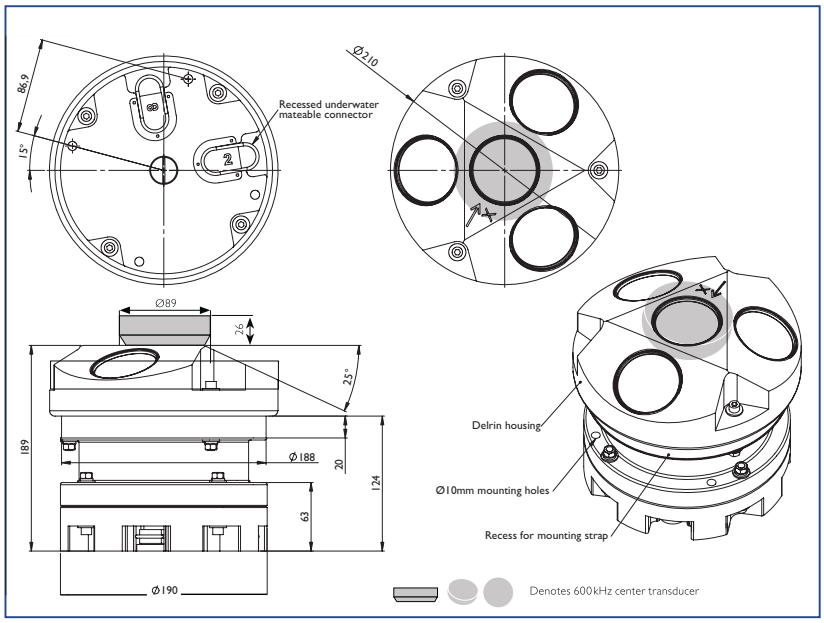

11.2006

References

[1] S. H. Salter, "Wave power," *Nature*, 1974.

[2] G. Boyle, Ed., *Renewable Energy - Power for a Sustainable Future*, 2nd ed.

[3] S. H. Antonio Luque, *Handbook of Photovoltaic science and engineering*. Wiley, 2003.

[4] J. Falnes, *Ocean waves and oscillating systems*. Cambridge: Cambridge University Press, 2002.

[5] I. R. Young, *Wind generated ocean waves*. Oxford: Elsevier, 1999.

[6] R. H. Stewart, *Introduction To Physical Oceanography*. Texas A & M University, 2007.

[7] . A. ARNTSEN, "Linear wave theory - part a," NTNU, Tech. Rep., 2000.

[8] *WAFO - A Matlab Toolbox for Analysis of Random Waves and Loads*, 2000.

[9] C. for Renewable Energy Sources (CRES), "Wave energy utilization in europe: current status and perspectives," Centre for Renewable Energy Sources (CRES), Tech. Rep., 2002.

[10] J. Cruz, Ed., *Ocean wave energy: current status and future perspectives*. Springer, 2008.

[11] A. Muetze and J. G. Vining, "Ocean wave energy conversion - a survey," *Proc. of ASME Conference Forty-First IAS Annual Meeting*, 2006.

[12] A. Clement, P. McCullen, A. Falcao, A. Fiorentino, F. Gardner, K. Hammarlund, G. Lemonis, T. Lewis, K. Nielsen, S. Petroncini, M. Pontes, P. Schild, B. O. Sjostrom, H. C. Srensen, and T. Thorpe, "Wave energy in europe: current status and perspectives," *Renewable and Sustainable Energy Reviews*, 2002.

[13] A. d. O. Falco, "Design and construction of the pico owc wave power plant," *Proc. of the 3rd European Wave Energy Conference*, 1998.

[14] F. Neumann, A. Brito-Melo, E. Didier, and A. Antnio Sarmento, "Pico owc recovery project: Recent activities and performance data," *Proc. of the 7th European Wave and Tidal Energy Conference*, 2007.

[15] I. Le Crom, A. Brito-Melo, F. Neumann, and A. Sarmento, "Numerical estimation of incident wave parameters based on the air pressure measurements in pico owc plant," *Proc. of the 8th European Wave and Tidal Energy Conference*, 2009.

[16] T. Heath, T. Whittaker, and C. Boake, "The design, construction and operation of the limpet wave energy converter (islay, scotland)," *Proc. of the Fourth Wave Energy Conference*, 2000.

[17] H. Polinder, M. E. C. Damen, and F. Gardner, "Linear pm generator system for wave energy conversion in the aws," *IEEE Transaction on Energy Conversion*, 2004.

[18] M. G. de Sousa Prado, F. Gardner, M. Damen, and H. Polinder, "Modelling and test results of the archimedes wave swing," *Proc. of the Institution of Mechanical Engineers, Part A: Journal of Power and Energy*, 2006.

[19] H. Polinder, M. A. Mueller, M. Scuotto, and M. G. de Sousa Prado, "Linear generator systems for wave energy conversion," *Proc. of the 7th European Wave and Tidal Energy Conference*, 2007.

[20] L. Hamilton, "Aws mk ii deployment, monitoring and evaluation of a prototype advanced wave energy device," AWS Ocean Energy Ltd, Tech. Rep., 2006.

[21] D. J. Pizer, C. Retzler, R. M. Henderson, F. L. Cowieson, M. G. Shaw, B. Dickens, and R. Hart, "Pelamis wec - recent advances in the numerical and experimental modelling programme," *Proc. of the 6th European Wave and Tidal Energy Conference*, 2005.

[22] R. Yemm, R. Henderson, and C. Taylor, "The opd pelamis wec: current status and onward programme," *Proc. of the 4th European Wave Energy Conference*, 2000.

[23] J. Cruz, Ed., *Ocean wave energy: current status and future perspectives*. Springer, 2008.

[24] AA.VV., "Pelamis p-750 wave energy converter," Pelamis Wave Power, Tech. Rep., 2010.

[25] S. H. Salter, D. C. Jeffrey, and J. R. M. Taylor, "The architecture of nodding duck wave power generators," *The Naval Architect*, 1976.

[26] J. Lucas, J. Cruz, S. H. Salter, J. R. M. Taylor, and I. Bryden, "Update on the modelling of a 1:33 scale model of a modified edinburgh duck wec," *Proc. of the 7th European Wave and Tidal Energy Conference*, 2007.

[27] J. Lucas, S. H. Salter, J. Cruz, J. R. M. Taylor, and I. Bryden, "Performance optimisation of a modified duck through optimal mass distribution," *Proc. of the 7th European Wave and Tidal Energy Conference*, 2007.

[28] S. H. Salter, "Recent progress on ducks," *IEE Proc.*, 1980.

[29] S. Salter, "The use of gyros as a reference frame in wave energy converters," *The 2nd International Symposium on Wave Energy Utilization*, 1982.

[30] ——, "Power conversion systems for ducks," *IEE Proc.*, 1979.

[31] G. Bracco, E. Giorcelli, and G. Mattiazzo, "One degree of freedom gyroscopic mechanism for wave energy converters," *Proc. of the ASME IDETC/CIE 2008*, 2008.

[32] ——, "Experimental testing on a one degree of freedom wave energy converter conceived for the mediterranean sea," *Proc. of the TMM 2008*, 2008.

[33] G. Bracco, E. Giorcelli, G. Mattiazzo, M. Pastorelli, and J. Taylor, "Iswec: design of a prototype model with a gyroscope," *Proc. of the ICCEP*, June 2009.

[34] J. R. M. Taylor, M. Rea, and D. J. Rogers, "The edinburgh curved tank," *Proc. of the 5th European Wave and Tidal Energy Conference*, 2003.

[35] G. S. Payne, J. R. M. Taylor, T. Bruce, and P. Parkin, "Assessment of boundary-element method for modelling a free-floating sloped wave energy device. part 2: Experimental validation," *Ocean Engineering*, 2007.

[36] A. Spadone, "Progetto e sviluppo di un banco hardware in the loop per l'analisi di sistemi fly by wire," Master's thesis, Politecnico di Torino, 2008.

[37] H. J. K. Shin, K., *Signal Processing for sound and vibration engineers.* Wiley, 2008.

[38] D. Vicinanza, L. Cappietti, and P. Contestabile, "Assessment of wave energy around italy," *Proc. of the 8th EWTEC*, September 2009.

[39] J. Newman, *Marine Hydrodynamics.* The MIT Press, 1977.

[40] G. Payne, "Guidance for experimental tank testing - draft," The University of Edinburgh, Tech. Rep., 23/09/2008.

[41] G. Genta, *Kinetic Energy Storage.* Butterworths, 1985.

[42] M. Beltrame and C. Botto, "Progettazione di un sistema giroscopico per la conversione dell'energia da moto ondoso," Master's thesis, Politecnico di Torino, 2010.

[43] S. G. Modena, "Sistemi elettromeccanici per la conversione dell'energia da moto ondoso," Master's thesis, Politecnico di Torino, 2010.

[44] G. Mattiazzo, S. Mauro, and S. Pastorelli, "A pneumatically actuated motion simulator," *Proc of the 12th World Congress in Mechanism and Machine Science*, 2007.

[45] G. Mattiazzo, S. Pastorelli, and M. Sorli, "Motion simulator with 3 d.o.f pneumatically actuated," *Proc of the Power Transmission and Motion Control Workshop*, 2005.

[46] S. Pastorelli and A. Battezzato, "Singularity analysis of a 3 degrees-of-freedom parallel manipulator," *Proc of the 5th International Workshop on Computational Kinematics CK2009*, 2009.

Attachment n° 2

SELECTION PANEL

On 13th May, 2010 Mr. Giovanni Bracco, in the Department of Mechanics of the Politecnico di Torino, has defended a thesis in Mechanics with the following title:

ISWEC: a gyroscopic Wave energy converter

The research object of the dissertation is: very well achieved

The methodology was assessed as: satisfactory

The research yielded interesting results and showed well developed critical thinking skills.

During the interview the candidate showed a deep and confident knowledge and a wide understanding of the problems dealt with.

The Board unanimously assessed the research work as very good and decided to award the **degree of Research Doctor** to the candidate:

Prof. Luigi Garibaldi (President)
Prof. Andrea Collina (Member)
Prof. Alessandro Rebora (Secretary)
Prof. Jamie Taylor (European Doctor)

Dr Fabrizio Scarpa, Eur-Ing, PhD, MRAeS, MInstP
Reader in Smart Structures
Department of Aerospace Engineering
Queens Building, University Walk
Bristol, BS8 1TR
Tel: +44 (0)117 3315306
Fax: +44 (0)117 9272771
f.scarpa@bristol.ac.uk
www.bristol.ac.uk/composites

04 May 2010

Dear Professor Giorcelli,

RE: Comments on PhD Thesis for European Doctorate – Candidate Giovanni Bracco

I have been asked to comment on the merit and level of the PhD Thesis titled: "ISWEC: A Gyroscopic Energy Converter", by Mr Giovanni Bracco from Politecnico of Torino, Italy.

The Inertial Sea Wave Energy Converter described in this work features some remarkable design features and originality, departing by the more established layouts like the Pelamis and Duck. The detailed nonlinear equations of motions of the system are illustrated in Chapter 2, and solved used a classical linearisation approach to identify the extractable power and the figures of merit of the device. For benchmark, a full nonlinear numerical model of the ODEs set is solved using a Simulink tool. A small-scale prototype for the Edinburgh water tank is presented in Chapter 3, with a detailed set of information related to the mechanical design, PTO, damper and electric motor. A parametric analysis of the device performance versus PTO, flywheel and incident wave frequency is illustrated in Chapter 4. The characteristics of the dry test, together with issues related to data acquisition and signal processing are described with thorough detail in Chapter 5. The wave and flume tests carried out at Edinburgh are featured in Chapters 6 and 7, while the design of the 1:8 prototype for the wave tank in Naples are illustrated in Chapter 8, with specific emphasis on the friction losses to be considered for the bearings design as an outcome of the nonlinear simulations. The originality of the ISWEC design proposed, together with the level of detail and analysis featured in this work put Mr Bracco endeavour at international level, between the best applied mechanics/machine design thesis I read as External Examiner this year. Moreover, the overall analysis tool used are robust, benchmarked and show the adequate robustness and confidence for a suitable high academic standard.

In summary, I am happy to recommend Mr Bracco's Thesis for an International/European Doctorate level.

Please do not hesitate to contact me in case of further queries.

Regards,

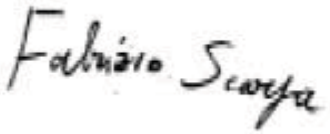

Fabrizio Scarpa

Institut de
Mathématiques de
Bordeaux

Bordeaux 4 Maggio 2010

Rapporto sulla tesi di dottorato dell'ingegner Giovanni Bracco intitolata "ISWEC: a Gyroscopic Wave Energy Converter"

Il documento di cui dispongo è composto di 132 pagine e si articola in 10 capitoli ed una appendice. Il documento è redatto in inglese e riguarda il progetto meccanico nonché la modellizzazione semplificata di un dispositivo per la conversione dell'energia del moto ondoso in energia elettrica.

L'organizzazione del documento è razionale, con una progressione della tematica tale da iniziare il lettore in modo completo al tema. La prima osservazione di rilievo è l'ampiezza della campagna di prove sperimentali realizzata: dalle prove su banco alle prove in scala via via maggiore in vasca. Questo solo aspetto sarebbe sufficiente a conferisce al presente lavoro una rilevanza tecnica tale da garantire l'attribuzione del titolo di dottore di ricerca in ingegneria meccanica. In aggiunta, è particolarmente da apprezzare il fatto che il lavoro sia stato condotto in collaborazione con più laboratori di ricerca, sia nazionali che internazionali.

Nel merito delle scelte tecniche, i risultati principali sembrano in linea con gli obiettivi di progetto proposto, benché l'efficienza del dispositivo si sia rivelata in alcuni casi inferiore, seppur di poco, alle aspettative. A questo proposito, lo studio parametrico delle prestazioni presentato nel capitolo 4 potrebbe essere ulteriormente sfruttato utilizzando metodi sistematici di ottimizzazione robusta, utili nel caso di un progetto multiobiettivo come in questo caso. In particolare, l'introduzione della nozione di forzante stocastica del sistema non lineare, permetterebbe, per esempio, di progettare per la massima efficienza del dispositivo nelle condizioni di mare peggiori.

Il testo della memoria è redatto con cura, sebbene alcuni refusi permangano ed il fraseggio risulti in alcuni casi intricato. E' comunque sicuramente commendevole il fatto di aver redatto il testo in inglese, con dei risultati globalmente soddisfacenti.

In conclusione questa tesi di dottorato dettaglia in modo chiaro e sintetico una mole importante di lavoro sperimentale dedicato ad un problema di grande attualità tecnologica. Inoltre, il candidato ha saputo integrare diversi laboratori di ricerca con risultati fruttuosi. Per tutti questi motivi esprimo un giudizio favorevole all'ottenimento del titolo di dottore di ricerca in ingegneria meccanica.

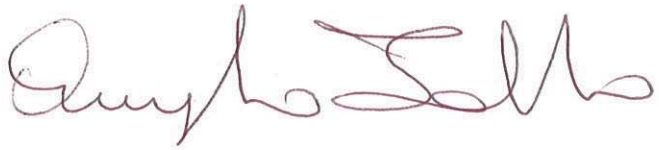

Angelo Iollo

Professore all' Institut de Mathématiques de Bordeaux - Université Bordeaux 1 et Institut National de Recherche en Informatique et Automatique